

A tumor-derived niche cell promotes tumor growth in medulloblastoma

Patrick Britten Ventura
Nogal, New Mexico

M.S., University of Oregon, 2012
B.S., University of New Mexico, 2007

A Dissertation presented to the Graduate Faculty
of the University of Virginia in Candidacy for the Degree of
Doctor of Philosophy

Department of Microbiology, Immunology and Cancer Biology

University of Virginia
May, 2015

ABSTRACT

Niche cells play critical roles in tumor initiation, progression, and metastasis. However, our understanding of niche establishment and function has been hampered by the complex cell composition in the tumor mass. Here we used a mouse genetic system called Mosaic Analysis with Double Markers (MADM) to analyze the tumor niche in medulloblastoma, taking advantage of the unequivocal GFP-labeling of tumor cells by the system. While tumor-infiltrating blood vessels and immune cells are free of GFP-labeling, surprisingly, astrocytes within tumors are all GFP+, suggesting that they are derived from tumor cells. Subsequent analysis confirmed the relationship between tumor cells and niche astrocytes in human medulloblastoma. Finally, tumor-derived astrocytes can support tumor cell survival and proliferation *in vitro* and coincide with tumor progression *in vivo*. In summary, our findings revealed a self-building niche in medulloblastoma, in which some tumor cells transdifferentiate into niche astrocytes that in turn support tumor growth.

ACKNOWLEDGEMENTS

The journey to become a scientist progresses through many stages, but training and mentorship are constant. I am gratefully indebted to my teachers in this journey thus far. First and foremost, I will be forever grateful for my thesis advisor Dr. Hui Zong. Hui has an infectious personality and a hunger for creative science that has and will always inspired me. He taught me to never argue with the reality of science and life, but instead question and probe it with creativity, rigor, and persistence. For this I am forever changed and grateful. I would also like to acknowledge mentors early in my career, Drs. LeeAnna Cunningham and Maggie Werner-Washbourne, whom inspired and encouraged me to continue in this journey. This journey has also progressed from the critique and advice of my committee members, both past and present. First, I sincerely thank Dr. Amy Bouton for all of her efforts to make me a better writer and scientist. I also thank Drs. Tom Parson, Jim Mandell, and David Wotton for their insights that brought this thesis to fruition. Furthermore, this journey would not have been possible without the support of so many former and current lab members, whom engaged in scientific discussions and are great friends, many thanks to you all! I must also thank my biggest cheerleaders, my family. To my parents, who have provided unconditional love and support through the years, I love you and dedicate this thesis to you. Last, to my best friend and partner in life Galo, I am so lucky and grateful to have you in my life. Your love and support through the ups and downs have made this journey possible, thank you!

TABLE OF CONTENTS

Abstract	i
Acknowledgements	ii
Table of Contents	iii
List of Figures	viii
List of Abbreviations	xii
Chapter 1 Introduction	1
1.1 Preface.....	1
1.2 Tumor Microenvironment	3
1.2.1 Carcinoma-associated Fibroblasts	6
1.2.2 Angiogenesis	7
1.2.3 Tumor-associated Macrophages and Other Myeloid Cells.....	9
1.3 Clinical aspects of medulloblastoma.....	12
1.4 Tumor niche cells in human medulloblastoma	16
1.5 Cerebellum development informs medulloblastoma etiology	22
1.5.1 Cerebellum development highlights importance of cell-cell interactions	22
1.5.2 Identifying the cell of origin in medulloblastoma using mouse genetic models	29
1.5.3 Modeling the clonal nature of cancer	31
1.5.4 MADM medulloblastoma model	38
1.6 Project Rationale.....	41

Chapter 2 Tumor cells build their own niche in medulloblastoma	44
Introduction	44
Results.....	51
2.1 The medulloblastoma tumor niche.....	51
2.1.1 Blood vessels	62
2.1.2 Tumor-associated macrophages.....	66
2.1.3 Oligodendrocyte precursor cells.....	69
2.1.4 Astrocytes	72
2.2 Multiple phenotypes confirm astrocytic transdifferentiation in MADM as well as in human tumors	78
2.2.1 Tumor astrocytes express mature astrocytic markers	78
2.2.2 Tumor astrocytes display similar functional phenotypes of mature astrocytes.....	81
2.2.3 Transdifferentiation is evident in human medulloblastoma	85
2.3 Fate-restricted GNPs can transdifferentiate after postnatal transformation.....	89
2.4 Tumor GNPs retain the transdifferentiation potential in secondary tumors.....	93
2.5 Tumor astrocytes do not display cancer stem cell features.....	97
2.6 Astrocytes correlate with mutant GNP proliferation in early mutant cell expansions	105

2.7 Cultured astrocytes promote proliferation and suppress death and differentiation of tumor GNPs	111
2.7.1 Normal astrocytes support wildtype GNP proliferation.....	111
2.7.2 Normal astrocytes support tumor GNP proliferation.....	114
2.7.3 Culture-derived tumor astrocytes support tumor GNP viability.	118
2.7.4 Testing whether astrocyte support is mediated through secreted factors or membrane-associated interactions	133
Discussion.....	140
2.D.1 MADM is a valuable tool to study tumor-niche interactions	143
2.D.2 Tumor GNP transdifferentiation generates true astrocytes.....	144
2.D.3 Astrocytes promote the growth and survival of tumor GNPs	148
2.D.4 Concluding remarks and perspectives: a self-building tumor niche reveals increased complexity in tumor development.....	149
Chapter 3 Perspectives	151
3.1 Does tumor GNP heterogeneity enable transdifferentiation?.....	151
3.1.1 Is tumor GNP transdifferentiation stochastic or determined?	151
3.1.2 Do dynamic transcription factor activities promote transdifferentiation?	157
3.2 Investigate tumor astrocyte support mechanisms in tumor development	164
3.2.1 Develop new genetic cell ablation transgenes to target tumor astrocytes	164

	vi
3.2.2 Molecular characterization of tumor astrocytes	170
3.3 Therapeutic implications	173
3.3.1 Designing anti-transdifferentiation therapies to target tumor astrocytes	172
 Chapter 4 Methods and Materials	 175
4.1 Mouse Lines.....	175
4.2 Tamoxifen Administration	175
4.3 BrdU Administration	176
4.4 Ganciclovir administration	176
4.5 Tissue Preparation	176
4.6 Tissue Immunofluorescence	177
4.7 Cell Culture Immunofluorescence	178
4.7.1 EdU labeling and Click-iT Detection	179
4.8 Imaging	179
4.9 Quantification & Statistics	180
4.9.1 Tumor astrocyte quantification throughout tumor development.....	180
4.9.2 <i>In vitro</i> quantification of proliferation, cell death, and differentiation in co-culture assay	180
4.10 Purification of Tumor GNPs and FACS purification of Aldh1L1-GFP astrocytes.....	181

4.10.1 Tissue Dissociation for tumor GNP purification and Aldh1L1-GFP cortex	181
4.10.2 Percoll gradient subfractionization for GNP purification	182
4.11 <i>In vitro</i> transdifferentiation of tumor GNPs into tumor astrocytes and co-culture	183
4.12 Fluorescence Activated Cell Sorting (FACS) of Aldh1L1-GFP astrocyte and culture conditions	184
4.13 Fluorescent In Situ Hybridization (FISH) of chromosome loci with immunofluorescence	185
4.14 Tumor cell orthograft.....	186
4.15 Quantitative real-time polymerase chain reaction (qPCR)	186
4.16 Antibodies for Immunofluorescence.....	188
 Appendix 1 Genetic ablation of tumor astrocytes to determine functional contribution to tumor niche dynamics	190
A.1 Overview of genetic techniques for cell ablation.....	190
A.2 Thymidine kinase-mediated astrocyte ablation	198
A.3 Diphtheria toxin-mediated astrocyte ablation	210
A.4 Intersectional approach with diphtheria toxin for astrocyte ablation	220
 Literature Cited.....	224

LIST OF FIGURES

Figure 1.1	General carcinoma tumor microenvironment	5
Figure 1.2	Classification of medulloblastoma subtypes.....	14
Figure 1.3	Human medulloblastoma niche cell types	20
Figure 1.4	Distinct lineages during cerebellum development	24
Figure 1.5	SHH signaling pathway	27
Figure 1.6	Clonal nature of cancer and reflective mouse models.....	34
Figure 1.7	MADM: Mosaic Analysis with Double Markers in Mice	36
Figure 1.8	MADM medulloblastoma model.....	39
Figure 2.1	Visualizing niche cells in medulloblastoma	49
Figure 2.2	Math1-Cre specifically targets granule neuron progenitors	54
Figure 2.3	MADM enables distinct visualization throughout tumor development.....	56
Figure 2.4	Two distinct physical regions in MADM medulloblastoma.....	58
Figure 2.5	Niche cells exist in both tumor regions.....	60
Figure 2.6	Blood vessels in tumor regions	64
Figure 2.7	Tumor-associated macrophages in tumor regions	67
Figure 2.8	Oligodendrocyte precursor cells in tumor regions	70
Figure 2.9	Astrocytes are derived from GNPs in tumor regions	74
Figure 2.10	Tumor astrocytes are consistently generated throughout tumor development.....	76
Figure 2.11	Tumor astrocytes express multiple astrocyte markers	79

Figure 2.12	Tumor astrocytes display similar functional phenotypes of canonical astrocytes.....	83
Figure 2.13	Transdifferentiation is evident in human medulloblastoma	86
Figure 2.14	Fate-restricted GNPs can transdifferentiate after postnatal transformation	91
Figure 2.15	Tumor GNPs retain the transdifferentiation potential in secondary tumors	95
Figure 2.16	Lineage tracing tumor astrocytes	99
Figure 2.17	<i>Glast</i> -CreER labels tumor astrocytes	101
Figure 2.18	Tumor astrocytes do not generate tumor GNPs.....	103
Figure 2.19	Astrocytes correlate with mutant GNP proliferation in early mutant cell expansions.....	107
Figure 2.20	Astrocyte presence varies in PNLs	109
Figure 2.30	Normal astrocytes support wildtype GNP proliferation <i>in vitro</i>	112
Figure 2.31	Normal astrocytes support tumor GNP proliferation <i>in vitro</i> ...	116
Figure 2.32	Experimental design for tumor astrocyte and tumor GNP co-culture.....	122
Figure 2.33	Culture-derived tumor astrocytes	124
Figure 2.34	Tumor GNPs were evenly distributed and proliferated when seeded on tumor astrocytes	126
Figure 2.35	Tumor astrocytes support tumor GNP proliferation and survival	128

Figure 2.36	Co-culture live imaging: Tumor GNPs migrate toward and proliferate on tumor astrocytes	130
Figure 2.37	Mode of astrocyte support is likely not through secreted factors.....	136
Figure 2.38	Testing whether astrocyte support is mediated through membrane-associated interaction	138
Figure 2.39	The MADM medulloblastoma tumor niche	141
Figure 3.1	Clonal analysis of tumor GNP transdifferentiation potential ...	155
Figure 3.2	Tumor GNPs and astrocytes express OLIG2	162
Figure 3.3	An inducible binary genetic ablation model to target tumor astrocytes	168
Figure A1.1	Genetic cell ablation models	195
Figure A1.2	GFAP-TK expression in the cerebellum and Bergmann glia ablation.....	202
Figure A1.3	GFAP-TK expression in tumor astrocytes	204
Figure A1.4	GFAP-TK tumor astrocyte ablation	206
Figure A1.5	GFAP-TK is misexpressed in tumor GNPs	208
Figure A1.6	Conditional knockout model with DT-A ^a ablation and reporter transgenes.....	214
Figure A1.7	Bergmann glia are resistant to DT-A ^a ablation	216
Figure A1.8	GFAP-tTA transgene is misexpressed in tumor	218
Figure A1.9	DT-A ^a does not ablate tumor astrocytes.....	222

Table 2.1 Quantification of FISH/IF signals between human tumor cells . 88

LIST OF ABBREVIATIONS

ACM = astrocyte-conditioned medium

ADP = adenosine diphosphate

ALDH1L1 = Aldehyde Dehydrogenase 1 Family, Member L1

BG = Bergmann glia

bFGF = basic fibroblast growth factor

bHLH = basic helix-loop-helix

BLBP = brain lipid binding protein

BRAF = V-raf murine sarcoma viral oncogene homolog B1

BrdU = 5-bromo-2'-deoxyuridine

CAF = carcinoma-associated fibroblast

CD34 = cluster of differentiation 34, Hematopoietic Progenitor Cell Antigen CD34

CD68 = cluster of differentiation 68, macrophage antigen CD68

ChIP-seq = chromatin immunoprecipitation followed by sequencing

CKO = conditional knockout

CML = chronic myeloid leukemia

Cre = Causes Recombination

CSC = cancer stem cell

CSF-1 = colony stimulating factor -1

CT = cycle threshold

DAPI = 4',6-diamidino-2-phenylindole

DIV = days *in vitro*

DNA = deoxyribonucleic acid

Dox = doxycycline

dpi = days post injection

DT-A, -B = diphtheria toxin A chain or B chain

DT-A^a = attenuated form of DT-A

DTR = diphtheria toxin receptor

E# = embryonic day #

ECM = extracellular matrix

EdU = 5-ethynyl-2'-deoxyuridine

EGL = external germinal layer

EMT = epithelial-to-mesenchymal transition

FACS = fluorescence-activated cell sorting

FISH = fluorescent *in situ* hybridization

GBM = glioblastoma

GCV = ganciclovir

GFAP = glial fibrillary acidic protein

GFP = green fluorescent protein

Glast = glutamate aspartate transporter

Gli = Glioma-associated oncogene homolog 1

GNP = granule neuron progenitor

GOI = gene-of-interest

HB-EGF = heparin-binding epidermal growth factor

HGF = hepatocyte growth factor

HIF-1 α = hypoxia inducible factor 1 alpha

IBA-1 = ionized calcium-binding adapter molecule 1

ID3 = inhibitor of differentiation 3

IGL = inner granule layer

INK4, ARF = cyclin-dependent kinase inhibitor 2A

Ki67 = marker of proliferation Ki67

LCA = large-cell anaplastic

LCM = laser capture microdissection

MADM = Mosaic Analysis with Double Markers

MAPK = mitogen-activated protein kinase

Math1 = mouse atonal homolog 1

MBEN = medulloblastoma with extensive nodularity

MDSC = myeloid-derived suppressor cells

ML = molecular layer

N-myc = Neuroblastoma MYC oncogene

NDS = normal donkey serum

NeuN = Neuronal Nuclei

NeuroD1 = neuronal differentiation 1

NOD-SCID = non-obese diabetic/severe combined immunodeficiency

NSC = neural stem cell

Olig2, 3 = oligodendrocyte lineage transcription factor 2, 3

OPC = oligodendrocyte precursor cells

P# = postnatal day #

p27^{Kip1} = cyclin-dependent kinase inhibitor 1B

PBS = phosphate buffered saline solution

PBT = PBS plus Triton-X 100

PCR = polymerase chain reaction

PDGFR α = platelet-derived growth factor alpha receptor

PDGF β = platelet-derived growth factor beta

PFA = paraformaldehyde

PN = Purkinje neuron

PNL = pre-neoplastic lesion

Ptch1 = Patched1

RFP = red fluorescent protein

RL = rhombic lip

RNA = ribonucleic acid

RT = room temperature

SEM = standard error of mean

SHH = Sonic hedgehog

siRNA = small interfering RNA

Smo = Smoothed

SuFu = Suppressor Of Fused Homolog

TAM = tumor-associated macrophages

tetO = tetracycline operator

TGF α = transforming growth factor alpha

TGF β = transforming growth factor beta

TGs = transgenes

TK = thymidine kinase

TP53, p53 = tumor protein 53

tTA = tetracycline transactivator

TuAstros = tumor “astrocyte-like” cells

Tuj1 = neuron-specific class III beta tubulin

VEGF = vascular endothelial growth factor

WM = white matter

WNT = Wingless-related integration site

Zic1 = Zic family member 1

Zic3 = Zic family member 3

Chapter One – Introduction

1.1 Preface

Dynamic cell-cell interactions ensure proper development and homeostasis of the body, while dysregulation of these interactions can cause excessive growth, leading to cancer. As a tumor grows and evolves over time, the tumor mass becomes a complex tissue comprised of not only cancerous cells, but also a variety of infiltrating non-mutant cells, commonly known as niche cells. Niche cells play an active role in malignancy by secreting growth factors and providing nutrients to sustain tumor growth (Hanahan and Weinberg, 2011). Importantly, tumor-niche interactions often mimic physiological cell-cell interactions during development and homeostasis. Therefore, studying the dynamics of cell-cell interactions in cancer environments could inform us about the nature of tumor-niche cell interactions and invoke novel approaches to disrupt these interactions.

Decades of cancer research have greatly improved therapeutic outcomes through earlier detection methods and increased therapeutic efficacy. Conventional therapies involve a regime of radiation and/or chemotherapy to eradicate proliferating cells, i.e. tumor cells. While prognoses vary greatly for tumor types following treatment, devastating side effects of these therapies and tumor relapse are common. To improve the efficacy of cancer treatments, research has focused on identifying unique mechanisms attributed to promoting tumor cell growth, which can then specifically targeted them. For example,

chronic myeloid leukemia (CML) results from a chromosome translocation that generates a mutant tyrosine kinase BCR-ABL responsible for hyperproliferation of leukemic cells (Ben-Neriah et al., 1986; de Klein et al., 1982; Lugo et al., 1990; Rowley, 1973). Research of BCR-ABL led to the development Gleevec, a small molecule inhibitor of BCR-ABL, which is now used to treat CML (Druker et al., 2001; 1996). Gleevec has afforded patients long-lasting benefits by controlling the extent of disease progression and improving the quality of life for patients. Additionally, therapies are being developed to disrupt niche cell contribution to tumor growth. In many cancers tumor cells can secrete growth factors to promote angiogenesis in order to vascularize the tumor tissue (Folkman, 2007). One of the first targeted therapies developed was Bevacizumab, a humanized antibody that recognizes a critical vascular growth factor and inhibits angiogenesis, leading to a reduction in tumor volume (Presta et al., 1997). Although initial tumor reduction is often seen with this drug, tumors often relapse, becoming metastatic and resistant over time (Ebos et al., 2009; Loges et al., 2009; Pàez-Ribes et al., 2009). These results highlight the evolutionary nature of tumor cells to adapt and grow, which likely involves evolving mechanisms between tumor and niche cells. Therefore, while investigating tumor cell signaling is paramount, attention should also focus on niche cell contributions throughout tumor development and treatment to direct future combinatorial treatment strategies.

In this chapter, I first review research focused on the tumor microenvironment, examining several well-studied niche cells in carcinoma and

how this knowledge has informed therapeutic design and future research considerations. Next, I provide an overview of medulloblastoma and its microenvironment from the perspective of normal cerebellum development to highlight similarities in cell-cell interactions that may influence tumor growth. To better understand how the tumor niche can be investigated with currently available tools, I review the concepts and caveats of existing medulloblastoma mouse models. In addition, I substantiate the development and use of a new genetic mosaic model of medulloblastoma with unique benefits for studying complex cellular environments in the tumor, which enables my research work presented in subsequent chapters of this thesis. Last, I provide the considerations and rationale for designing and implementing this thesis project.

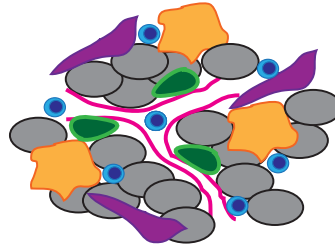
1.2 Tumor Microenvironment

Historical observations of tumor-niche cell interactions have inspired theories and resulted in a number of therapeutic advances. One of the first reports describing the tumor niche was published in 1863 by Rudolf Virchow, who noted the presence of leukocytes in malignant tissues (Balkwill and Mantovani, 2001). He hypothesized that this represented a potential link between chronic inflammation and cancer. Indeed, we now appreciate the significant contribution of inflammatory cells and cytokines to tumor growth and progression (Quail and Joyce, 2013). Early reports also described a dynamic vascular component in tumors, where grafted tumor tissues induced microvascular infiltration (Algire et

al., 1945). The concept of tumor angiogenesis was subsequently formalized by Judah Folkman (Folkman et al., 1971). Studies have evolved over time to greatly expand our knowledge of cell-cell interactions in the tumor niche, particularly in epithelial carcinomas. A general overview of known cell types and functions in these microenvironments is provided (Figure 1.1). While numerous cell types exist within the tumor microenvironment, I will focus in the next sections on three niche cells or cellular processes that have been therapeutically targeted: carcinoma-associated fibroblasts, angiogenesis, and tumor-associated macrophages and other myeloid cells.

Figure 1.1 General carcinoma tumor microenvironment

Carcinoma Tumor Microenvironment



Cell Type	Function	Cellular Target	Molecular Effectors
Tumor Cells 	Promote angiogenesis	Endothelial cells	VEGF
	Recruitment	TAMs	CSF-1, CCL-2, IL-6, IL-10
		CAFs	TGF β , FGF, PDGF
		MDSCs, Tregs	TGF β , CXCL5
Blood Vessels Endothelial cells 	Supports	Tumor cells	Oxygen and Nutrients
	Recruitment	Pericytes	PDGF β
Pericytes 	Supports	Endothelial Cells	ANG-1, VEGF for angiogenesis
			Vascular integrity
	Suppress	Endothelial Cells	Angiogenesis Vascular leakage
	Stromal Cells CAFs 	Promote growth	Tumor Cells
Promote metastasis		Tumor Cells	TGF β , HGF
Promote angiogenesis		Endothelial Cells	VEGF
Contribute to ECM			collagen, fibronectin
Innate Immune Cells TAMs, MDSCs 	Promote growth	Tumor Cells	EGF
	Promote invasion and migration	Tumor Cells	SDF-1, EGF, MMPs, TNF α
	Promote ECM degradation		MMPs, proteases
	Promote angiogenesis	Endothelial Cells	VEGF, FGF
	MDSCs - Suppress Immunoreveillance	Lymphocytes	arginase, reaction oxygen and nitrogen species
	Promote inflammation		TNF α , IL-1, IL-12
Adaptive Immune Cells T-cells, B-cells 	Immunosurveillance	Tumor cells, APCs	Survery MHC-I
	Cell killing	Tumor Cells	Perforin, granzymes, granulysin

Adapted from: Quail and Joyce, 2013; Balkwill and Mantovani, 2001.

1.2.1 Carcinoma-associated Fibroblasts

Fibroblasts in epithelial stroma contribute to tissue matrix composition and structure, which is necessary for tissue homeostasis and undergoes significant changes during injury repair. During wound healing, activated fibroblasts secrete extracellular matrix (ECM) components and growth factors to create a barrier and enable tissue reconstruction (Balkwill and Mantovani, 2001; Franco et al., 2010; Lu et al., 2012). In epithelial cancers, carcinoma-associated fibroblasts (CAFs) also secrete similar ECM and growth factors (Pietras and Östman, 2010; Quail and Joyce, 2013), and tumors have therefore been considered as ‘wounds that won’t heal’ (Dvorak, 1986). Additionally, CAFs help to promote metastasis by secreting growth factors that induce epithelial-to-mesenchymal transition (EMT), such as transforming growth factor beta (TGF β) and hepatocyte growth factor (HGF) (Balkwill and Mantovani, 2001; Quail and Joyce, 2013; Zhao et al., 2012).

One example of how CAF-tumor cell interactions can have profound effects on the tumor comes from studies showing that synergistic interactions between CAFs and tumors can confer tumor cells with an innate resistance to targeted therapies. In metastatic melanoma, 40-60% of tumors harbor oncogenic BRAF (BRAF, V-raf murine sarcoma viral oncogene homolog B1) mutations that result in a constitutively active MAPK (MAPK, mitogen-activated protein kinase) pathway to promote cell proliferation (Edlundh-Rose et al., 2006; Pollock and Meltzer, 2002). A small molecule inhibitor against mutant BRAF, Vemurafenib, was shown to be effective in ~50% patients with mutated BRAF, demonstrating

an intrinsic resistance of tumor cells in the non-responsive patients (Chapman et al., 2011). Could this innate resistance be conferred by the tumor microenvironment? One study found that fibroblasts secreted HGF when co-cultured with melanoma cells, which caused tumor cells to become resistant to the BRAF inhibitor. Indeed, when tumor samples were assessed for HGF expression there was a strong correlation between high HGF expression and resistance to the inhibitor. In a co-culture assay of tumor cells and CAFs, tumor cell resistance was overcome when an additional inhibitor was applied that targeted the HGF-cMet signaling cascade in the presence of the BRAF inhibitor (Straussman et al., 2013). Thus, combinatorial targeting of niche cell mechanisms that promote innate resistance could result in more effective treatment outcomes.

1.2.2 Angiogenesis

Tumor growth relies on a constant supply of nutrients and oxygen from the vascular system. As tumor tissue continues to expand, metabolic deprivation occurs because the new cells become positioned beyond the diffusion limits of nutrients and oxygen permeating from blood vessels. This hypoxic environment induces a transcriptional response in tumor cells, which results in the secretion of growth factors that stimulate angiogenesis. This initial step, termed the “angiogenic switch”, is driven by expression of the hypoxia inducible factor 1 alpha (HIF-1 α) transcription factor, which upregulates vascular endothelial growth

factor (VEGF) expression (Blouw et al., 2003; Ferrara, 2010; Hanahan and Folkman, 1996; Hoeben, 2004). VEGF induces endothelial cell proliferation and chemotaxis, whereby new capillaries sprout from existing vessels. As new capillaries are formed, stabilization and maturation must occur to prevent vascular leakage or hemorrhage. Pericytes are responsible for maintaining the integrity of blood vessels, are recruited by endothelial-derived platelet-derived growth factor beta (PDGF β) (Armulik et al., 2010; Lindahl, 1997; Sims, 1986). The primary role of pericytes is to stabilize vascular endothelial cells to maintain vessel integrity under physiological conditions. During tumor angiogenesis, pericytes are also recruited to newly formed vessels to maintain vascular integrity. The interactions between tumor vasculature and pericytes adds further complexity to tumor-niche interactions and provides additional therapeutic targets.

The dynamic interaction of pericytes and blood vessels can alter the therapeutic response to anti-angiogenic drugs. The clinically approved anti-VEGF-A antibody, Bevacizumab, is used to treat some cancers and can be quite effective at reducing angiogenesis and reducing tumor volume in humans and mouse models (Folkman, 2007; Quail and Joyce, 2013). However, despite initial tumor shrinkage, relapse often occurs in both mouse models and patients, and the tumor cells that grow out tend to be more invasive and metastatic (Burstein et al., 2008; Ebos et al., 2009; Loges et al., 2009; Mancuso et al., 2006; Pàez-Ribes et al., 2009). Interestingly, the surviving blood vessels had a high density of associated pericytes, which were hypothesized to suppress angiogenesis and

render the blood vessels resistant to therapy. Relapse was thought to occur because the remnant blood vessels provided a supportive niche for surrounding tumor cells (Dings et al., 2007; Mancuso et al., 2006; Willett et al., 2004; Zuniga et al., 2010). These studies highlight the dynamic nature of tumor-niche cell interactions, where specific mechanisms can be directly targeted to initially reduce tumor growth. However, secondary niche cell interactions may render the treatment incomplete, leading to relapse. Thus, investigating the potential of multi-modal therapeutic strategies that target multiple niche cell interactions could improve treatment efficacy.

1.2.3 Tumor-associated Macrophages (TAMs) and Other Myeloid Cells

In a process called immunosurveillance, the innate and adaptive immune systems constantly survey the body for foreign pathogens to prevent infections and maintain homeostasis. Early in cancer development, tumor cells can be recognized by the immune system as foreign and are often targeted for destruction. However, tumor cells evolve to become less immunogenic and to escape immunosurveillance (Swann and Smyth, 2007). For example, chemotactic molecules from tumor cells attract myeloid-derived suppressor cells (MDSCs), which in turn suppress leukocyte activation in the tumor by releasing arginase and reactive oxygen/nitrogen species (Gabrilovich and Nagaraj, 2009; Grivnenkov et al., 2010). Another example of beneficial immune cells in the tumors is the infiltration of macrophages, which secrete growth factors and

chemokines that support tumor cell growth and promote metastasis (Allavena et al., 2008; Grivennikov et al., 2010; Mantovani et al., 2002; Quail and Joyce, 2013; Sica et al., 2008). Initially, activated macrophages often interact with the tumor as “M1-polarized” protective/inflammatory cells that attack tumor cells. However, the tumor can induce polarization toward a tumor-supportive/immunosuppressive “M2- polarization state” through secretion of colony stimulating factor -1 (CSF-1) and other factors (Sica et al., 2008). In this way, tumor cells evolve to evade immune responses by attracting and manipulating innate immune cells to cause immunosuppression and promote tumor growth.

Current therapies aim to disrupt the immunosuppressive phenotype reinforced by TAMs. In an elegant study from Pyonteck *et al.*, the use of a novel CSF-1 receptor inhibitor against TAMs revealed a promising outcome in a glioblastoma (GBM) mouse model and in human GBM cells xenografted into mice (Pyonteck et al., 2013). Application of the inhibitor resulted in prolonged survival and regression of tumors due to macrophage-mediated phagocytosis of tumor cells. The inhibitor induced a “re-education” of TAMs from a tumor-supportive M2 state back to a host-protective M1 state. This study demonstrated that, by understanding the dynamics of niche cell phenotypic states, therapeutic strategies could be developed that move beyond simply targeting cells for elimination, but rather modify cellular behavior to become “anti-tumor.”

To summarize, investigating tumor-niche interactions has advanced our understanding of their contributions to tumor growth and therapeutic response. The unique response of niche cells to targeted treatments further reveals that we still have much to learn about their dynamic behaviors in tumorigenesis and relapse. Using new models and techniques, we can investigate niche cell populations from both a temporal and spatial perspective to reveal these dynamic contributions. In the following section, I will discuss a diverse tumor niche observed in human medulloblastoma. The function and origin of medulloblastoma niche cells have been poorly understood. However, the research described in this thesis elucidates the diversity of the medulloblastoma niche and uncovers the contribution of astrocytes in tumor growth.

1.3 Clinical aspects of medulloblastoma

Medulloblastoma is the most common pediatric brain cancer, which arises in the developing cerebellum. The majority of patients are under 10 years of age, but tumors can also present in adults. Standard treatment involves surgical resection of the tumor followed by intense regimes of radiation and chemotherapy. While a greater than five-year survival rate is observed in 60-70% of patients, the adverse effects of radiation and chemotherapy to the developing brain impart intellectual and neurological disabilities in patients (Louis et al., 2007). To develop new therapeutic strategies that have less adverse effects, research has focused on understanding the molecular mechanisms underlying the etiology of medulloblastoma.

Currently there are four molecularly defined subtypes of medulloblastoma: WNT group, SHH group, group 3, and group 4 (Figure 1.2) (Gibson et al., 2010; Gilbertson and Ellison, 2008; Northcott et al., 2012; Robinson et al., 2012). Each group was defined by mutations in specific signal pathways that was also related to a number of histopathological features. For example, in the sonic hedgehog (SHH) group, mutations are commonly found in the SHH receptor *Patched 1* (PTCH1) and the downstream effectors Smoothed (SMO) and Suppressor Of Fused Homolog (SUFU) (Figure 1.2). The SHH molecular signature was found in tumors histopathologically classified as desmoplastic/nodular, classic, large-cell anaplastic, or medulloblastoma with extensive nodularity (Louis et al., 2007; Northcott et al., 2012). There has been extensive research with mouse genetic

models of the SHH subtype to investigate molecular mechanisms driving tumor cell proliferation. Additional mutations have also been identified that can effect therapeutic response. For example, high-throughput sequencing of human medulloblastoma cohorts revealed mutations or deletions in the *TP53* locus that correlated with poorer prognosis (Zhukova et al., 2013). In this thesis I will use a mouse medulloblastoma model that mimics the SHH-group to study the establishment of the tumor niche.

Figure 1.2 Classification of medulloblastoma subtypes

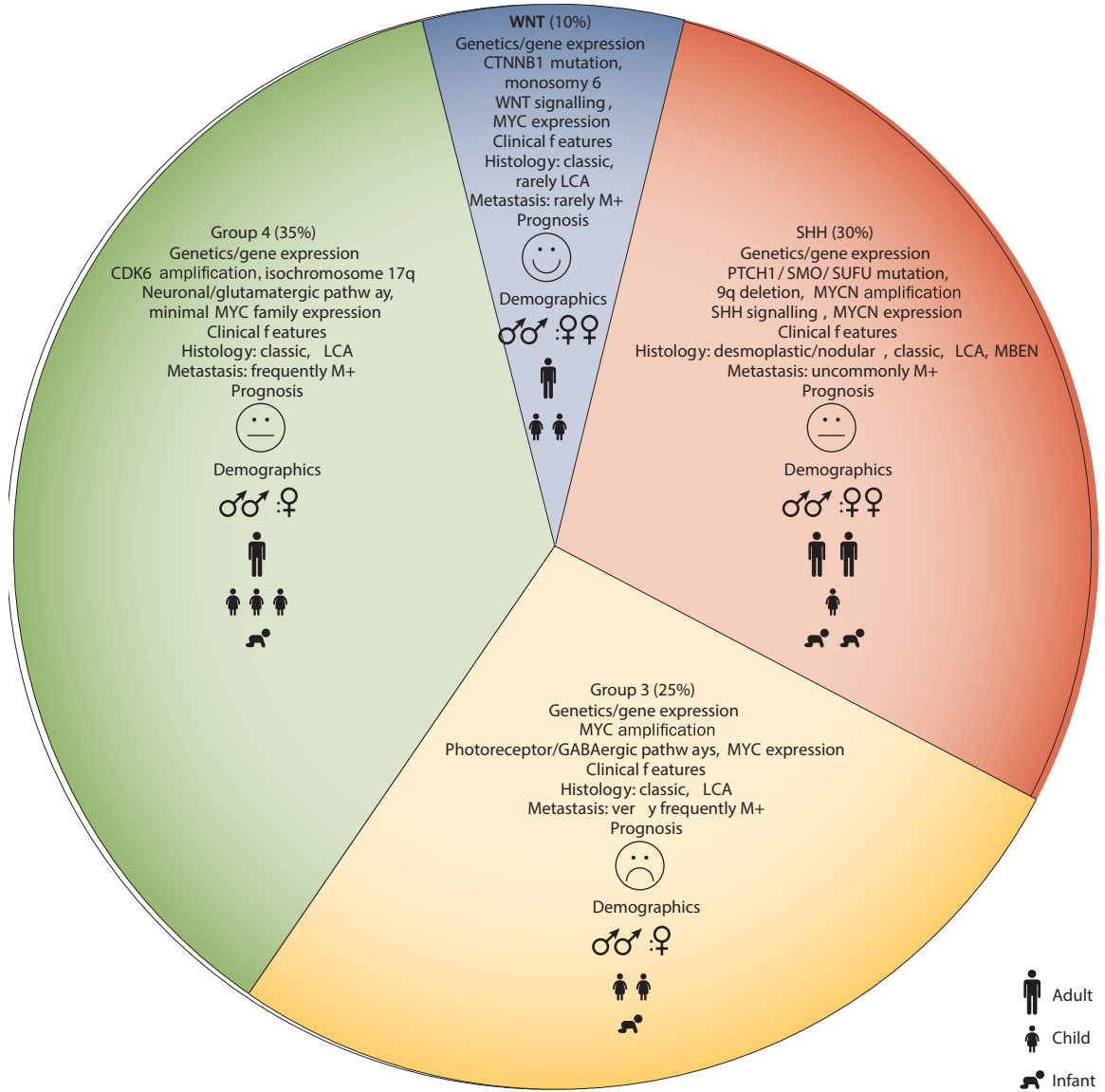


Figure 1.2 Classification of medulloblastoma subtypes.

Features of the four medulloblastoma subgroups. Pie chart illustrating the frequency, genetics, gene expression, clinical features, and demographics of the four subgroups of medulloblastoma.

[LCA= large-cell anaplastic; MBEN= medulloblastoma with extensive nodularity;

M+ = positive for metastasis at diagnosis; SHH= sonic hedgehog]

Adapted from (Northcott et al., 2012).

1.4 Tumor niche cells in human medulloblastoma

To better understand the putative cellular composition of the medulloblastoma tumor niche, I provide a brief overview of brain cell populations and their functions. The central nervous system, like all organ systems, relies on exquisite regulation of cellular interactions to maintain homeostasis. While the functional output of the brain is largely through a network of neuronal signaling, the maintenance of this neural network relies on glial cells. There are four major types of glial cells: astrocytes, oligodendrocyte precursor cells (OPCs), oligodendrocytes, and brain-specific immune cells, microglia. In addition to neurons and glial cells, the brain is highly vascularized with blood vessels that deliver oxygenated blood, glucose, and other nutrients needed for the high-energy demand of the brain. To better understand how these cells may contribute to the tumor niche, I will provide a brief overview of glia cell functions in homeostasis. The information provided is by no means exhaustive, but rather is meant to serve as reference point for relevant cell behaviors that may contribute to their role in the tumor niche.

Astrocytes are critical mediators of the blood-brain barrier and energy metabolism. Astrocytes outnumber neurons in many species, including man and mouse (Nedergaard et al., 2003). Astrocytes have two types of processes, those that contact blood vessels and others that wrap around entire neuronal synapses. Astrocytic endfeet that contact blood vessels are responsible for helping maintain the blood-brain barrier by secretion of factors, such as transforming growth factor

beta (TGF β) and basic fibroblast growth factor (bFGF), to induce endothelial cell tight junction formation and ensure junction integrity (Abbott et al., 2006). Astrocytes also play critical roles in metabolic regulation in the brain. Astrocytes regulate the rate of cerebral blood flow by release of vasodilators or constrictors depending on metabolic needs. Transporters present in the endfeet interfacing with vasculature mediate the flux of water and ions into the brain parenchyma. Astrocytes also uptake glucose, through glucose transporters, that is released into the parenchyma by endothelial cells and is subsequently metabolized through glycolysis. From glycolysis, lactate is generated and released from astrocytes for neuronal uptake. Glucose can also be shunted toward glycogenesis to generate glycogen that is stored as granules in astrocytes. Glycogen can then be metabolized for energy production when there is increased neuronal activity or during periods of hypoglycemia (Bélanger et al., 2011). Maintenance of the blood-brain barrier, regulation of blood flow, and energy metabolism are three aspects of astrocyte biology that could be important for the contribution to tumor growth.

Oligodendrocytes are responsible for the myelination of neuronal axons. Myelination is necessary to propagate action potentials over great distances with stealth speed. Oligodendrocytes ensheath axons with multiple sheets of myelin basic protein. Myelin sheets act as electrical insulators to prevent ionic dilution out of the axon membrane, which effectively pushes the ion concentration further down the axon toward a synapse (Baumann and Pham-Dinh, 2001).

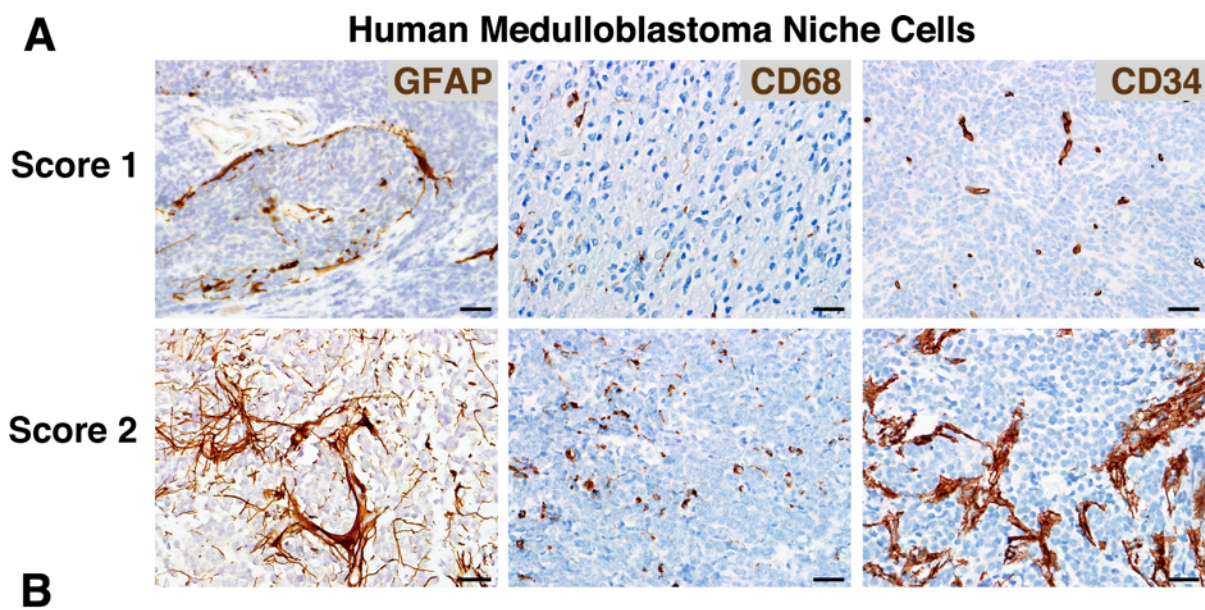
Oligodendrocytes are generated from oligodendrocyte precursor cells (OPCs) during development. However, OPC is almost a misnomer since this cell population remains in the brain parenchyma throughout the life of animal and is the most active proliferating cell population in the brain. OPCs constantly survey the brain tissue for injury and respond by proliferating to replace damaged oligodendrocytes (Kang et al., 2010).

Microglia are the resident immune cells in the brain. While all other glial cell types are derived from neural stem cells, microglia are derived from primitive myeloid progenitors in the yolk sac before embryonic day 8 (E8) in mice (Ginhoux et al., 2010). From E8-9.5 microglia populate the brain parenchyma where they remain for the rest of the animal's life (Ginhoux, 2013). Microglia constantly survey neurons, astrocytes, and blood vessels for distress signals and clear cellular debris or dying cells (Nimmerjahn et al., 2005). Under homeostatic conditions microglia self renew in the brain, but following injury monocytes from the blood can enter the brain and function in a similar capacity to microglia to protect against further damage (Ajami et al., 2007; Mildner et al., 2007).

A diverse cellular tumor niche in human medulloblastoma has been observed for over a century. Pathologists have extensively noted that tumors are highly vascularized and contain at least macrophages and astrocytes (Bailey and Cushing, 1925; Burger et al., 1987; Delpech et al., 1977; Eng and Rubinstein, 1978; Gilhuis et al., 2006; Mannoji et al., 1981a; Roggendorf et al., 1996a; Salsman et al., 2011; Wright, 1910). From a cohort of SHH-group tumors, we

observed varying degrees of blood vessel infiltration, composed of CD34-positive endothelial cells, in addition to CD68-positive macrophages and glial fibrillary acidic protein (GFAP) positive astrocytes (Figure 1.3A). Blood vessels were evident in all tumors (100%), while macrophages (95%) and astrocytes (69%) were present in the majority of tumors (Figure 1.3B). Both the function and origin of these niche cells in tumors are not well understood. In this thesis, I will further investigate the recruitment of these niche cells into the tumor and provide evidence toward a potential function of tumor astrocytes.

Figure 1.3 Human medulloblastoma niche cell types.



Score (0=none, 1=few, 2=many) (#score/#cases)	Astrocytes (GFAP)	Macrophages (CD68)	Blood vessels (CD34)
0	8/26	1/21	0/22
1	5/26	12/21	18/22
2	13/26	8/21	4/22
% tumors with cell type	69.23	95.23	100

Figure 1.3 Human medulloblastoma niche cell types.

(A) Tumor niche cells in human medulloblastoma samples include at least astrocytes (GFAP), macrophages (CD68), and blood vessels (CD34). There was a varying presence of niche cells in tumors from none (score= 0), to few (score=1), or many (score= 2). Scoring is based on qualitative pathological assessments.

(B) Quantification scoring tumor samples. GFAP+ astrocytes were present at varying degrees in 18 of 26 (69%) patient samples. CD68+ macrophages (20 of 21 cases, 95%) and CD34+ blood vessels were present in the majority of samples (22 of 22 cases, 100%).

Scale bars: A= 50 μ m.

Images and quantification courtesy of Dr. Fausto Rodriguez.

1.5 Cerebellum development informs medulloblastoma etiology

1.5.1 Cerebellum development highlights the importance of cell-cell interactions

To investigate tumor-niche cell interactions in medulloblastoma, knowledge of the tumor cell of origin is paramount to assess tumor-niche interactions. The first speculations for the cell of origin in medulloblastoma came from autopsies, which often revealed that tumors were predominantly located on the surface of the cerebellum (Bailey and Cushing, 1925). Histological characterization of cerebellum cyto-architecture began with Santiago Ramon y Cajal, who described a unique germinal zone on the surface of the developing cerebellum (Cajal et al., 1995; Folkman, 2007; Quail and Joyce, 2013; Roussel and Hatten, 2011). Cells in this germinal zone were hypothesized to be the cell of origin for tumor formation. From extensive studies characterizing cerebellum development these cells have been identified as granule neuron progenitors (GNPs) (Roussel and Hatten, 2011).

Cerebellum development is unique, as it is generated from 2 distinct germinal zones and the majority of histogenesis occurs postnatally. In contrast to the forebrain, which develops radially from a central germinal zone, the cerebellum initially develops radially but the majority of the tissue is generated from a second germinal zone on the outer surface of the tissue. It is at this site that the GNPs proliferate, differentiate, and migrate inward (Figure 1.4) (Roussel and Hatten, 2011). GNPs are derived from neural stem cells (NSCs) in the ventricular zone lining the fourth ventricle. NSCs also generate Purkinje neurons

(PN), other inhibitory neuron subtypes, and specialized astrocytes called Bergmann glia (BG). Beginning at embryonic day 13.5 (E13.5) in the mouse, a subset of neural stem cells (NSCs) transition through a structure called the rhombic lip (RL), the remnant lip of the closing neural tube (Alder et al., 1996; Dings et al., 2007; Willett et al., 2004; Zuniga et al., 2010). In the RL, transcriptional changes further induce NSCs to differentiate into GNPs. GNPs continually express the basic helix-loop-helix (bHLH) transcription factor, *Math1*, which restricts their differentiation potential (Ben-Arie et al., 1997; Machold et al., 2011). Therefore, GNPs are considered unipotent and under physiological conditions only differentiate into granule neurons (Alder et al., 1996; Machold and Fishell, 2005; Wang et al., 2005). From E13.5 to postnatal day 0 (P0), GNPs migrate outward from the RL along the surface of the cerebellum primordium, where they undergo exponential proliferation.

Figure 1.4 Distinct lineages during cerebellum development.

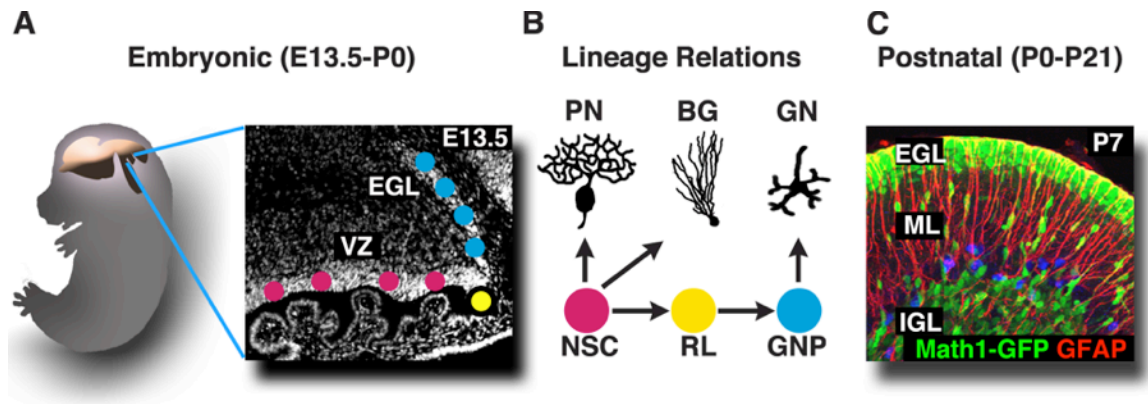


Figure 1.4 Distinct lineages during cerebellum development.

A) Neural stem cells (NSCs) lining the fourth ventricle (magenta) transition through the rhombic lip (RL) and are further specified (yellow) to become unipotent granule neuron progenitors (blue, GNPs) that migrate to surface of the cerebellum.

B) Lineage diagram indicate NSCs give rise to Purkinje neurons, other inhibitory neurons, and Bergmann glia/astrocytes (BG). Some NSCs transition through the RL to become GNPs that differentiate strictly into granule neurons (GN).

C) During postnatal development, Math1+ GNPs in the external germinal layer (EGL) differentiate and migrate inward along GFAP+ BG fibers in the molecular layer (ML) to their final destination in the inner granule layer (IGL) of the cerebellum.

Postnatal proliferation of GNPs is induced by the mitogenic growth factor, Sonic hedgehog (SHH) (Wechsler-Reya and Scott, 1999). Purkinje neurons secrete SHH in a graded fashion, being highest in the external germinal layer (EGL) (Figure 1.4C), where it activates the signaling cascade in GNPs resulting in proliferation. The receptor for SHH, Patched 1 (Ptch1), inhibits the G-coupled transmembrane protein Smoothed (Smo) when SHH is absent. The target of Smo is the transcription factor, Gli, which is sequestered in the cytoplasm by Suppressor-of-Fuse (SuFu). When SHH binds to Ptch1, inhibition of Smo is released which enables dissociation of SUFU from Gli. Gli can then translocate to the nucleus and promote transcription of various genes, including proliferation-promoting genes like N-myc (Kenney, 2003; Wilson and Chuang, 2010). Mutations in *Ptch1*, *Smo*, and *SuFu* have been linked to GNP hyperproliferation and medulloblastoma formation (Figure 1.5) (Goodrich et al., 1997; Pietsch et al., 1997; Taylor et al., 2002; Xie et al., 1998).

Figure 1.5 SHH signaling pathway

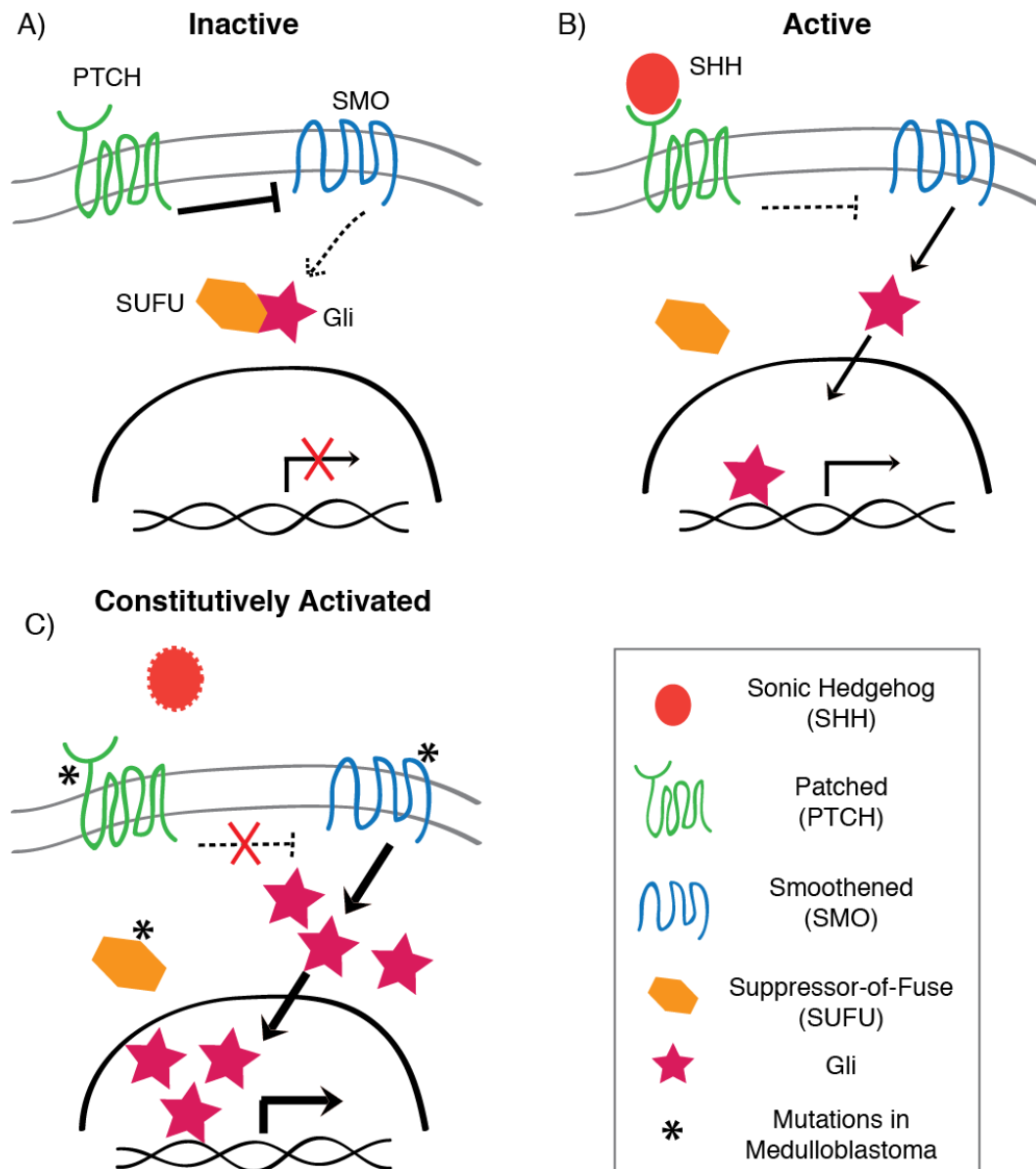


Figure 1.5 SHH signaling pathway

A) SHH pathway is inactive in the absence of SHH bound to the Ptch receptor, which negatively regulates the transmembrane protein Smo. The transcription factor Gli is sequestered in the cytoplasm by SUFU, which prevents Gli proteolysis.

B) SHH bound to Ptch derepresses Smo, which becomes active and dissociates SUFU from Gli. Gli translocates to the nucleus and promotes transcription of target genes, such as N-myc.

C) Mutations in different proteins of the pathway (asterisks) cause hyperproliferation. Ptch loss of function allows constitutive Smo-mediated phosphorylation of Gli. Activating mutations in Smo bypass Ptch regulation, resulting in constitutive Gli phosphorylation. Mutations in Sufu render it unable to sequester Gli in the cytoplasm and consequently Gli can accumulate in the nucleus to promote transcription.

Differentiation and migration of GNPs occur quickly and under strict control. Following a number of symmetric divisions in the EGL, GNPs upregulate the cyclin-dependent kinase inhibitor p27^{Kip1} to exit the cell cycle (Ayrault et al., 2009). Differentiation of granule neurons results from upregulation of the NeuroD1, Zic1, and Zic3 transcription factors (Aruga, 2004; Miyata et al., 1999; Pan et al., 2009). Immature granule neurons migrate inward along Bergmann glia (BG) fibers in the molecular layer (ML) (Figure 1.4C). This neuron-glia interaction is essential for proper localization of granule neurons to the inner granule layer (IGL) (Figure 1.4C). The essential role of this interaction was demonstrated by genetic ablation of BG during development. Because the transgene encoding thymidine kinase (TK) is specifically expressed in BG, temporal application of the TK substrate ganciclovir selectively killed BG by inhibiting DNA replication (Delaney et al., 1996a). The loss of BG resulted in halted migration of immature granule neurons into the IGL and subsequent cell death, which highlights the importance of this cell-cell interaction. Overall, these elegant developmental studies have shown how the cerebellum is developed and structurally engineered through spatio-temporal interactions of multiple cell types.

1.5.2 Identifying the cell of origin in medulloblastoma using mouse genetic models

The first mouse genetic model of medulloblastoma was a targeted disruption of the *Ptch1* gene. Targeting *Ptch1* was informed from mapping

mutations in patients with Gorlin syndrome, who are predisposed for basal cell carcinomas and medulloblastoma (Goodrich et al., 1997; Pietsch et al., 1997). The *Ptch1* heterozygous mice developed medulloblastoma at a penetrance of 15-20%, similar to Gorlin patients. Pathologically tumors arising spontaneously from *Ptch1*^{+/-} were typically classified as the desmoplastic subtype, which represent 20-30% of all medulloblastoma (Ellison et al., 2006; Northcott et al., 2012).

Additional mutations in tumor suppressor genes (TSG) have been identified from human medulloblastoma samples. Two commonly mutated TSG are *TP53* and *INK4a-ARF* (Ellison, 2002; Frank et al., 2004). Recently, Zhukova *et al.* reported a strong correlation between *TP53* mutations and a lower survival probability in patients compared to a better prognosis when *TP53* was not mutated (Zhukova et al., 2013). To further investigate the role of these TSGs in medulloblastoma, Wetmore *et al.* studied the effect of TSG loss in *Ptch*^{+/-} mouse models (Wetmore et al., 2001). They found somatic homozygous loss of *p53* in *Ptch*^{+/-} mice, but not *ARF*, significantly increased the tumor penetrance to ~95% from 20% in *Ptch*^{+/-} only mice. Furthermore, there was a significant decrease in the latency of tumor formation down to 12 weeks in double mutants compared to 30 weeks in single mutant *Ptch*^{+/-} mice (Wetmore et al., 2001). The effect of *p53* loss in the mouse medulloblastoma model reflects the poor prognosis seen in human medulloblastoma patients with mutated *TP53* (Zhukova et al., 2013). However, these early models did not distinguish the cell of origin for tumorigenesis, as the mutations were somatic in nature. It is important to

identify the cell of origin in order to better understand the tumor etiology and identify relevant cell-cell interactions in the tumor niche.

From previous observations, it was evident that tumors initiated on the surface of the cerebellum, prompting the hypothesis that a cell of origin for medulloblastoma were GNPs (Goodrich et al., 1997; Uziel et al., 2005). It was definitively proven that GNPs could serve as a cell of origin, since GNP-specific *Math1-Cre*-mediated inactivation of *Ptch* or activation of *Smo* consistently led to the formation of medulloblastoma with the desmoplastic phenotype (Marino et al., 2000; Schüller et al., 2008; Yang et al., 2008).

1.5.3 Modeling the clonal nature of cancer

In 1976 Peter Nowell elegantly postulated that cancers arose largely through clonal evolution as an expansion of mutant cells that withstood negative selection pressures (Figure 1.6A) (Nowell, 1976). This hypothesis has been strongly supported with advances in next-generation sequencing and more advanced computational modeling systems (Greaves and Maley, 2012). Given that cancers are clonal in nature, it is possible that interactions with the microenvironment could influence the course of transformation from early neoplasia to late malignancy. Therefore, to investigate niche interactions during certain stages of transformation, it is necessary to use mouse models that mimic clonal evolution (Figure 1.6B). Conventional knockout mouse models may not fully represent this clonal process, as whole populations of cells are singularly

transformed, and therefore could misrepresent true tumor-niche dynamics during clonal tumor formation. To address this concern, our group has developed a clonal model of medulloblastoma with Mosaic Analysis with Double Markers (MADM) in mice (Henner et al., 2013; Zong et al., 2005). MADM tumors progress in a clonal fashion from a small number of mutant GNPs that are permanently labeled with green fluorescent protein (GFP). These are surrounded by non-mutant GNPs, thus more closely mimicking how most human cancers are thought to develop.

The MADM system was generated to study clonal behaviors of sparse mutant versus wildtype cells in the same tissue using permanent fluorescent labeling. This system enables lineage analysis and the ability to observe differential cell behaviors between cell types (Zong et al., 2005). This genetic mosaic system is an ideal tool to study the clonal nature of human cancer in mice (Liu et al., 2011), as well as to study tumor-niche interactions by distinct visualization of labeled mutant cells. The genetic design of MADM includes two reciprocal chimeric cassettes, whereby the green fluorescent protein (*GFP*) and red fluorescent protein (*RFP*) genes are interrupted with loxP sites and the N-terminal and C-terminal halves of the genes are separated to generate chimeric alleles in the same chromosome (Figure 1.7). In the presence of a cell-type specific Cre-recombinase, intrachromosomal recombination of the chimeric cassettes can occur at low frequency when the cell undergoes division and the chromosomes are duplicated during S-phase. If recombination occurs and the

recombined chromosomes are segregated in either a X- or Z-pattern into daughter cells, this will impart the two daughter cells with either an intact *GFP* gene, an intact *RFP* gene, both *GFP* and *RFP* genes, or neither gene, producing a green, red, yellow or colorless phenotype, respectively. If a mutant allele of a gene-of-interest (GOI) is present telomeric to the cassette, it is linked to the fluorescent gene half of the MADM cassette on the same allelic side. For example, if the mutant allele is linked to the GFP-half, then upon Cre-mediated recombination and chromosomal segregation (X-patterned) into two daughter cells, it would result in the green cell being homozygous-mutant for the GOI and the red sister cell being wildtype for the GOI. The sibling wildtype cell serves as an internal control to analyze the green mutant cell behavior. If instead Z-segregation occurs, then one of the daughter cells would be identical to the mother cell (colorless and heterozygous for the mutated GOI), while the other daughter cell would be yellow due to intact *GFP* and *RFP* genes and also heterozygous for the GOI (Figure 1.7) (Zong et al., 2005). The sparse generation of related clones, distinguished by distinct and permanent labeling, provides a powerful tool to observe the very early stages of tumor development with high-resolution and assess tumor-niche interactions.

Figure 1.6 Clonal nature of cancer and reflective mouse models.

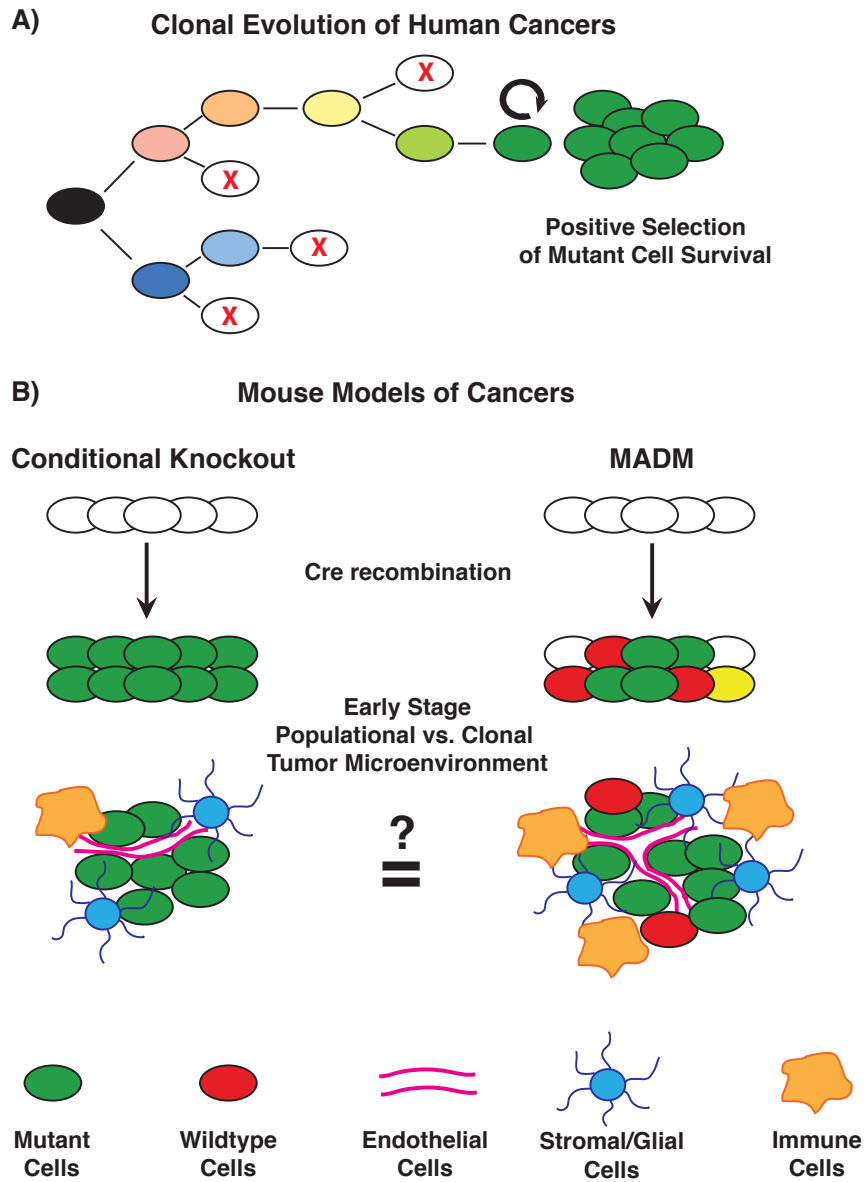


Figure 1.6 Clonal nature of cancer and reflective mouse models.

A) Tumors develop from clonal evolution of mutated cells. Accumulation of mutations and adaptations in individual mutant cells enable positive selection of tumor cells that eventually die (X) or survive and become tumorigenic.

B) Mouse genetic models of cancers: conditional knockout in whole cell populations versus clonal induction with MADM. In early tumor development, the tumor microenvironment could have differential effects in populational- vs. clonal-derived tumors.

Figure 1.7 MADM: Mosaic Analysis with Double Markers in Mice

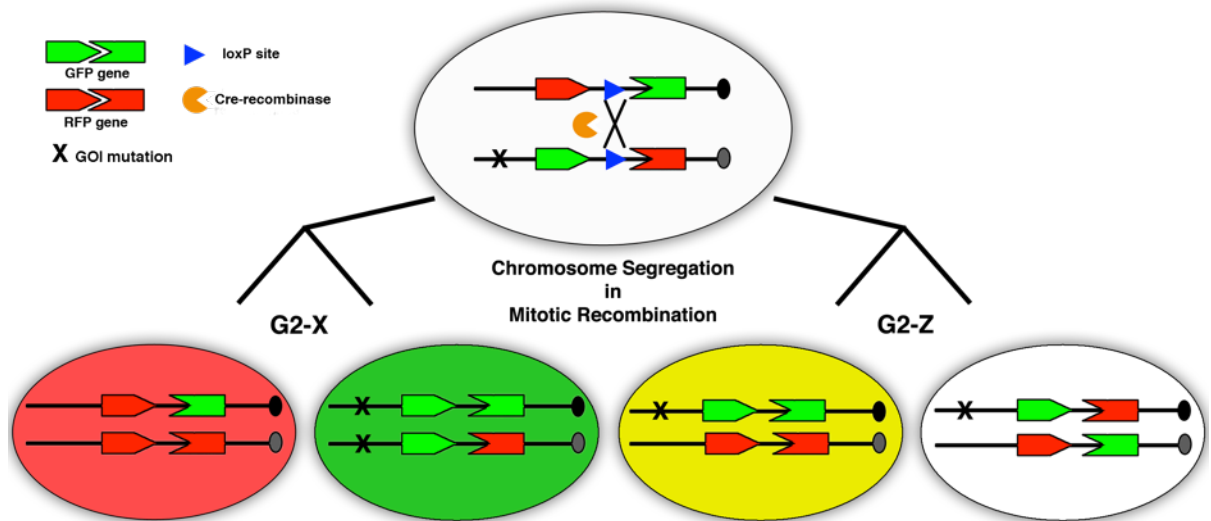


Figure 1.7 MADM: Mosaic Analysis with Double Markers in Mice

MADM is comprised of two chimeric fluorescent protein cassettes separated by a loxP site on both alleles in a chromosome. When Cre-recombinase is present, it can mediate intrachromosomal recombination between loxP sites of MADM cassettes at a low frequency upon cell division (when the large colorless mother cell divides to generate two daughter cells). Duplicated chromosomes, which have undergone recombination, will segregate into two daughter cells following a G2-X or G2-Z pattern. In a G2-X chromosome segregation pattern, one daughter cell will receive an intact *RFP* allele and the other allele is still chimeric, which permanently labels this cell lineage RFP+. The sister cell will receive an intact *GFP* allele and is permanently GFP+. In G2-Z segregation, one daughter cell receives both intact *RFP* and *GFP* alleles, resulting in one cell being permanently marked as yellow, while the sister cell that has both chimeric alleles is colorless. To assess gene function of heterozygous, homozygous mutant, or wildtype alleles in a cell population within the same tissue, a mutant form of a gene of interest (GOI) is incorporated telomeric to the MADM cassettes. When the mutant gene is linked with the *GFP* half of the cassette, then following G2-X recombination, both mutant alleles segregate into GFP+ cells while RFP+ sister cells serve as wildtype controls. In G2-Z recombination both daughter cells are heterozygous for the mutant gene.

1.5.4 MADM medulloblastoma model

To develop the MADM medulloblastoma model (Figure 1.8), a null allele of *p53* was incorporated telomeric to the cassette, enabling the study of *p53*-mutant cells with MADM labeling. To sensitize mice toward medulloblastoma formation a null allele of *Ptch1* (somatic genotype is now *Ptch+/-*) was bred into *MADM_p53+/-* mice to model desmoplastic SHH-subtype (Goodrich et al., 1997). Previous studies identified GNPs as a cell of origin for the SHH-subtype of medulloblastoma, therefore *Math1-Cre* was also bred into *MADM_p53+/- ;Ptch1+/-* mice to induce recombination in the GNP lineage (Schüller et al., 2008; Yang et al., 2008). Following *Math1-Cre* mediated recombination and mitotic X-chromosomal segregation, green mutant (*p53-/- ; Ptch+/-*) and red wildtype (*p53+/+ ; Ptch+/-*) GNPs are generated. Red GNPs are expected to undergo normal neuronal differentiation, while green mutant GNPs could not only differentiate into neurons but also become tumorigenic and eventually lead to tumor formation (Figure 1-7). The permanent fluorescent labeling of the tumor cells enables the determination of tumor GNP lineage and colorless tumor niche cells.

Figure 1.8 MADM medulloblastoma model.

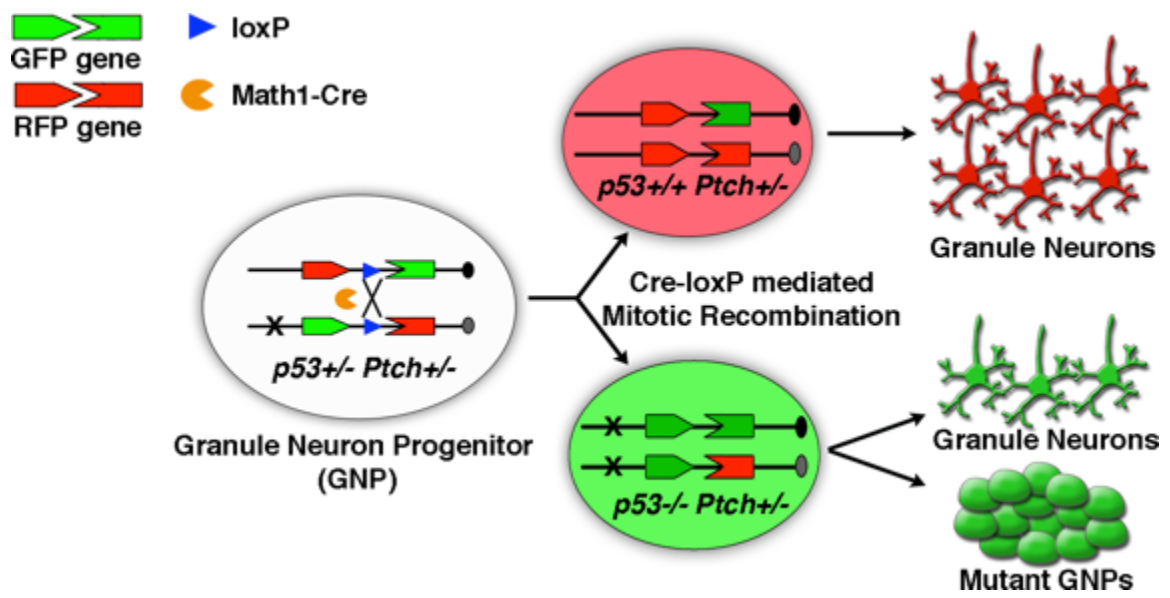


Figure 1.8 MADM medulloblastoma model.

From colorless *Ptch* and *p53* heterozygous GNPs, GNP-specific *Math1-Cre* expression will generate green *Ptch*^{+/-}; *p53*^{-/-} GNPs and red *Ptch*^{+/-}; *p53*^{+/+} GNPs. While red and most green GNPs differentiate into granule neurons, one or a few green GNPs eventually transform, leading to medulloblastoma.

1.6 Project Rationale

The burgeoning tumor microenvironment field has shed light on the complexity and importance of tumor-niche cell interactions. Therapies designed to target components of the microenvironment have shown promise in combination with other established therapies. Additionally, targeted therapies may also help alleviate side effects of traditional treatments, which is extremely important for pediatric patients whose bodies are still developing and treatment can interfere with normal development, leaving patients impaired for the rest of their lives.

Medulloblastoma has been thoroughly studied on a genomic level, where classic pathological classifications have been reinforced by distinct gene signatures from large cohorts of human samples (Gibson et al., 2010; Gilbertson and Ellison, 2008; Northcott et al., 2012; Robinson et al., 2012). These gene signatures implicate several developmental pathways that have instructed molecular studies, thus identifying key growth regulatory mechanisms. Several drugs have been developed to target molecules in the SHH-driven tumor cells (MacDonald et al., 2013). However, like other anti-cancer drugs, severe side effects have been observed due to off-target effects in other developing tissues of young patients (Packer and Vezina, 2008). While researchers constantly seek to refine therapies that target tumor cell mechanisms, a complementary approach should focus on unique cell-cell interactions in the tumor microenvironment that contribute to tumor growth and possibly resistance and relapse.

A diverse tumor niche in human medulloblastoma has been observed for many years, yet an in-depth understanding of the contributions of cells within the tumor microenvironment is incomplete. Pathological analyses over the past 100 years have identified many distinct cell populations in brain tumors, including blood vessels, immune cells, and brain-specific astrocytes (Bailey and Cushing, 1925; Barnard and Pambakian, 1980; Blouw et al., 2003; Delpech et al., 1977; Eng and Rubinstein, 1978; Ferrara, 2010; Grizzi et al., 2008; Hoeben, 2004; Huber et al., 2001; Mannoji et al., 1981b; Morantz et al., 1979; Roggendorf et al., 1996b; Rossi et al., 1991; Sica et al., 2008). However, the origin and function of these non-tumor niche cells has largely been speculative. By using mouse models that enable temporal and spatial analysis throughout tumor development, with distinct identification and tracing from a cell of origin, it should be possible to investigate tumor-niche interactions that will advance development of niche-targeted therapies.

Development of the MADM medulloblastoma model enables careful cellular dissection of the tumor microenvironment. This model allows examination of niche establishment at all stages of tumor development, with the expectation that tumor cells will be GFP+, while the associated niche cells would be colorless. Using the model described above, we found that endothelial and immune cells in the medulloblastoma were GFP-negative. Surprisingly, all astrocytes found in the tumor mass were GFP+. This suggested that the astrocytes had trans-differentiated from tumor GNP, rather than being recruited from surrounding

brain tissue. Characterization of this trans-differentiation event is the basis of this thesis project. First, I assessed the frequency and distribution of trans-differentiation throughout all tumor stages. Second, I determined the astrocytic nature of these cells in relation to normal astrocyte marker and morphological phenotypes. Third, I addressed whether this trans-differentiation was a common feature in human medulloblastoma. Fourth, I considered whether trans-differentiation was an intrinsic feature of tumor GNPs or whether external influences contributed to the process. Also, since astrocytic features are commonly associated with brain cancer stem cells, I also addressed whether tumor astrocytes displayed cancer stem cell properties. Finally, I developed a unique co-culture assay to determine putative functions of tumor astrocytes for tumor GNP growth. The findings presented in this thesis provide the first comprehensive analysis of medulloblastoma tumor-niche components and reveal a unique and functional trans-differentiation event that creates a self-building tumor niche.

Chapter 2 Tumor cells build their own niche in medulloblastoma*

**This chapter is adapted from Ventura et al, 2015 (submission to Cell in May 2015).*

Introduction

Interactions between distinct cell types ensure normal embryonic development and adult tissue homeostasis. Such interactions are also important in human diseases, particularly tumor-niche interactions in cancer. Rather than simply over-proliferating on their own, tumor cells often coerce surrounding cells to form a supportive niche. Niche support from blood vessels provides nutrients and oxygen to sustain tumor growth and tumor cells express molecules to dampen anti-tumor immune responses (Hanahan and Weinberg, 2011). For example, hypoxic tumor cells upregulate the transcription factor HIF1 α , which promotes VEGF secretion to promote angiogenesis (Plate et al., 1992; Pugh and Ratcliffe, 2003; Shweiki et al., 1992). Tumor cells can also create an immunosuppressive microenvironment by expressing PD-L1 and B7, which bind to PD-1 and CTLA-4 on T cells, respectively, to dampen cytotoxic T cell responses (Dong et al., 2002; Leach et al., 1996; Mellman et al., 2011). Encouragingly, therapeutic targeting of these niche factors has shown significant clinical benefits for cancer patients. Anti-angiogenic drugs (bevacizumab) reduce tumor vascularization, depriving tumor cells of essential nutrients (Bergers and Hanahan, 2008). In addition, immunomodulatory antibodies against PD-1 (BMS-

936558) and CTLA4 (ipilimumab) help restore immune responses against tumor cells (Peggs et al., 2006; Topalian et al., 2012). These initial successes call for expanded studies on tumor-niche communications to identify additional mechanisms for effective cancer therapy.

While our knowledge of tumor niche interactions is largely afforded by vast studies of the tumor microenvironment in carcinomas, as highlighted in Chapter One, our understanding of tumor niche interactions in brain cancers is still evolving. Medulloblastoma is the most common pediatric brain tumor arising in the cerebellum (Gilbertson and Ellison, 2008). Even though some tumors respond well to conventional radiation and chemotherapy, side effects to the developing brain often lead to lifetime learning disabilities in young patients. Among multiple subtypes of medulloblastoma, a great portion, especially the desmoplastic subtype, originates from granule neuron progenitors (GNPs) (Gibson et al., 2010; Goodrich et al., 1997; Pietsch et al., 1997; Schüller et al., 2008; Yang et al., 2008). The unique lineage development and regulation of GNP expansion during cerebellar development serves as a platform to study cellular processes underlying tumor niche interactions.

As proper development relies on robust signaling control and cellular interactions, similar mechanisms in the tumor niche may promote tumorigenesis. Interestingly, pathological analyses over the past 100 years have revealed multiple cell types within human medulloblastoma, including blood vessels, immune cells, and astrocytes (Bailey and Cushing, 1925; Burger et al., 1987; Delpech et al., 1977; Gilhuis et al., 2006; Mannoji et al., 1981a; Roggendorf et al.,

1996a; Salsman et al., 2011; Wright, 1910). Particularly in the molecularly defined SHH subgroup of medulloblastoma (Gibson et al., 2010; Jones et al., 2012; Pugh et al., 2012), we observed that tumor samples contained blood vessels (100%), macrophages (95%), and astrocytes (69%) (Figure 1.3). As interestingly, while tumor GNPs proliferate at a high rate *in vivo*, culturing them *in vitro* has been almost impossible. Taken together, these observations suggest that tumor GNPs may rely on critical support from niche cells, similar to normal GNPs during normal development.

To study tumor-niche interactions, we use a mouse genetic model termed Mosaic Analysis with Double Markers (MADM) that generates sparse mutant cells that are unequivocally labeled with fluorescent proteins (Zong et al., 2005). The generation of a small number of mutant cells not only closely mimics tumor initiation processes in humans, but also provides superb resolution for the visualization of cell behaviors throughout tumor regions. Recently, we generated a MADM-based medulloblastoma model with relatively consistent penetrance and latency by introducing oncogenic mutations found in human patients specifically into GNPs (Henner et al., 2013).

Since the tumor niche in human medulloblastoma samples consists of, at a minimum, blood vessels, microglia/macrophages, and astrocytes, our model, if successful, should reflect the cellular composition seen in human biopsies (Figure 2.1). More importantly, the specific GFP-labeling of tumor GNPs should

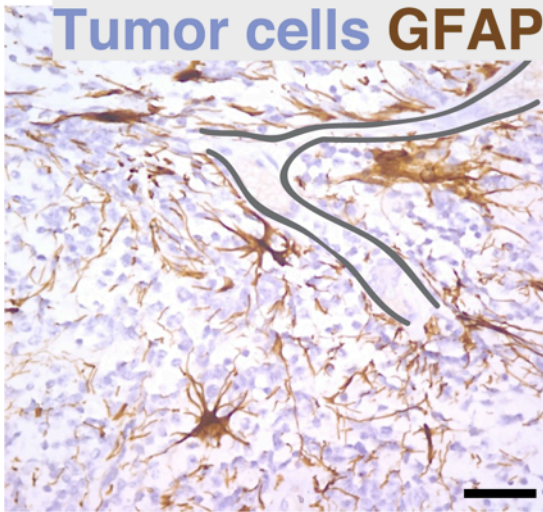
allow us to study intricate interactions between colorless niche cells and green tumor cells at a level of cellular resolution (Figure 2.1).

In this thesis project I used the MADM medulloblastoma model to examine niche establishment at distinct tumor stages by assessing interactions between GFP-positive mutant GNPs and colorless niche cells. While most niche cells were colorless, such as vascular endothelial cells and brain-specific microglia/macrophages, we were surprised to find that cells bearing astrocytic morphologies and markers were also GFP-positive throughout tumors. Since normal GNPs are unipotent and never give rise to astrocytes, this observation suggested that some tumor GNPs diverted from their normal lineage restriction and trans-differentiated into tumor “astrocyte-like” cells. This phenomenon was confirmed in human medulloblastoma since tumor cells and astrocytes were shown to share the same chromosomal aberrations. Also the proliferation of small lesions throughout the cerebellum was positively correlated with the presence of astrocytes. To assess the functional contribution of TuAstros *in vivo*, several genetic models were employed to ablate TuAstros specifically. However these models had several technical limitations that precluded definitive conclusions (Appendix 1). Finally, we used co-culture assays to demonstrate that TuAstros provide support to tumor GNPs by sustaining proliferation and inhibiting differentiation and apoptosis. In conclusion, taking advantage of the spatial resolution provided by MADM, we have identified a self-building tumor niche in medulloblastoma. Determining the molecular nature of trans-differentiation and

tumor-niche communication should provide highly effective therapeutic targets.

Figure 2.1 Visualizing niche cells in medulloblastoma.

Human Tumor Niche



MADM Tumor Niche

- High cellular resolution
- Distinct lineage tracing



Figure 2.1 Visualizing niche cells in medulloblastoma.

Human medulloblastoma tumors have many niche cells, including GFAP+ astrocytes and blood vessels (outlined, left panel). The MADM medulloblastoma model will generate GFP-positive tumor cells to clearly visualize their interactions with colorless niche cells (right panel).

*Human tumor image provided by Drs. Charles Eberhart and Fausto Rodriguez.

Results

2.1 The medulloblastoma tumor niche.

Inducing mutations in the proper cell of origin for medulloblastoma is critical to generate tumors which are populated with representative tumor niche cells. As described previously in Chapter 1, granule neuron progenitors (GNPs) serve as a cell of origin in medulloblastoma. To target MADM recombination to GNPs we employed the *Math1-Cre* recombinase transgene (Matei et al., 2005). Since GFP-labeling will be used to distinguish tumor from niche cells, recombination induced by *Math1-Cre* in cells other than GNPs could fundamentally compromise data interpretation. Therefore, we verified the faithfulness of *Math1-Cre*-mediated recombination in MADM without mutations (MADM-WT). All MADM-labeled cells in adult cerebella were found to reside in the inner granule layer and were NeuN-positive granule neurons (Figure 2.2A-C). Furthermore, potential niche cells were not labeled, including blood vessels, microglia, and astrocytes (Figure 2.2D-F).

Next, we characterized tumor development in MADM medulloblastoma (MADM-MB) mice, and found that tumors invariantly originated from green mutant GNPs and progressed along a relatively consistent time course. Tumors initiated focally (Figure 2.3A), despite the great number of GFP-labeled cells (granule neurons) in the rest of the cerebellum, suggesting a clonal origin of tumors in this model. Small tumors (~P60, early stage) tended to be found in remnant EGL regions between single folia (Figure 2.3B) and were readily

distinguishable from normal tissue by the presence of focal GFP signals and Ki67 staining (Figure 2.3E). Medium sized lesions (~P75, mid stage) were present in multiple folia and infiltrated into normal tissue (Figure 2.3C). Finally, late-stage malignant tumors that distorted normal cerebellar structure and lead to mortality were mostly found in mice older than 90-days of age (Figure 2.3D). With this MADM medulloblastoma model it is now possible to assess tumor niche cell interactions throughout tumors.

To investigate whether there were different tumor-niche populations in the MADM model, we first surveyed tumor regions to determine if there were distinct spatial patterns. We expected that the majority of early tumor masses would be superficial to normal tissue (Figure 2.3B,E), and as mutant GNPs expand from the surface of the cerebellum they would progressively infiltrate normal cerebellar tissue (Figure 2.3C). When the locations of the tumor were surveyed across the brain, small and mid-stage tumors occupied regions that were superficial to the cerebellum, as well those that had infiltrated into normal tissue (Figure 2.4A). It was possible to determine the boundary of normal tissue by visualizing the parallel fibers in the molecular layer (ML) from MADM-labeled granule neurons whose cell bodies resided in the inner granule layer (Figure 2.4A, right panel). Higher magnification of boxed regions in Figure 2.4A showed that GFP-positive tumors were indeed superficial to the cerebellum (Figure 2.4B) and also infiltrated into the ML and IGL of the cerebellum (Figure 2.4C). As tumors grew larger, it

was difficult to demarcate boundaries, as the tumor cells have invaded most of the normal cerebellar tissue and distorted normal tissue structure.

After establishing that there were regional differences within GFP-positive tumor tissue we wondered whether the composition of niche cell populations was also different between regions. First, we determined the presence of niche cells in the vicinity of GFP-positive tumor cells. Colorless niche cells (GFP-negative, DAPI-positive) are distributed throughout infiltrative (Figure 2.5A) and superficial (Figure 2.5B) regions of tumors. Next, based on the niche cell types in human tumors (Figure 1.3), we evaluated their presence with a panel of markers for blood vessels, brain-specific immune cells, and neuroglia.

Figure 2.2 Math1-Cre specifically targets granule neuron progenitors.

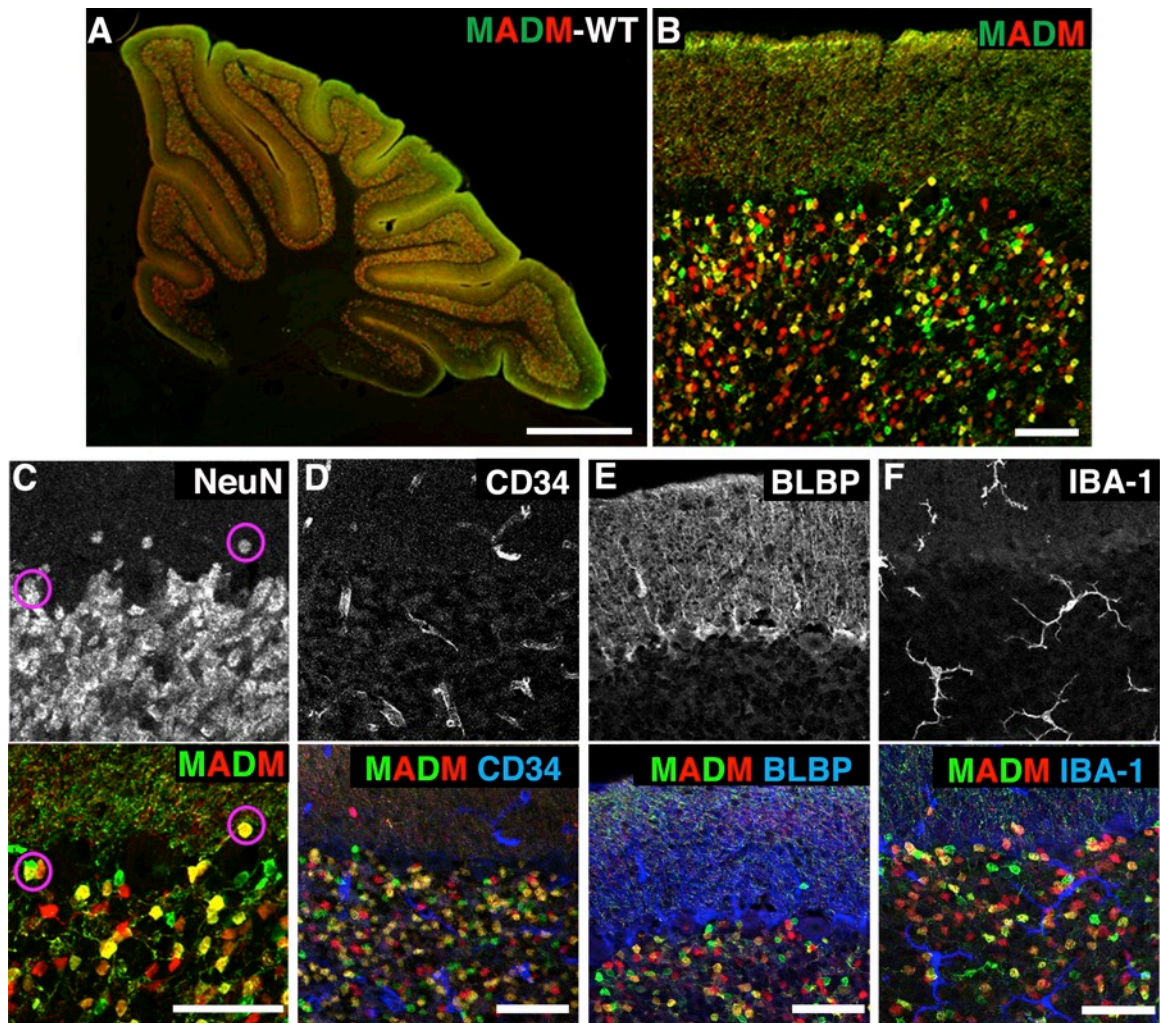


Figure 2.2 *Math1-Cre* specifically targets granule neuron progenitors.

(A-B) MADM with *Math1-Cre* without mutation labeled sparse cells (cells dot the entire IGL). A single folia is magnified in (B).

(C) *Math1-Cre* MADM-labeled cells are granule neurons (circled MADM-labeled cells are NeuN+ granule neurons).

(D-F) *Math1-Cre;MADM* did not label prospective niche cell types in normal cerebellar tissue, as there was no co-localization of MADM fluorescence, seen as small round neurons, with markers for CD34+ blood vessels (D), BLBP+ Bergmann glia and astrocytes (E), IBA-1+ microglia (F).

Scale bars: A= 500 μ m; B-F= 50 μ m.

Figure 2.3 MADM enables distinct visualization throughout tumor development.

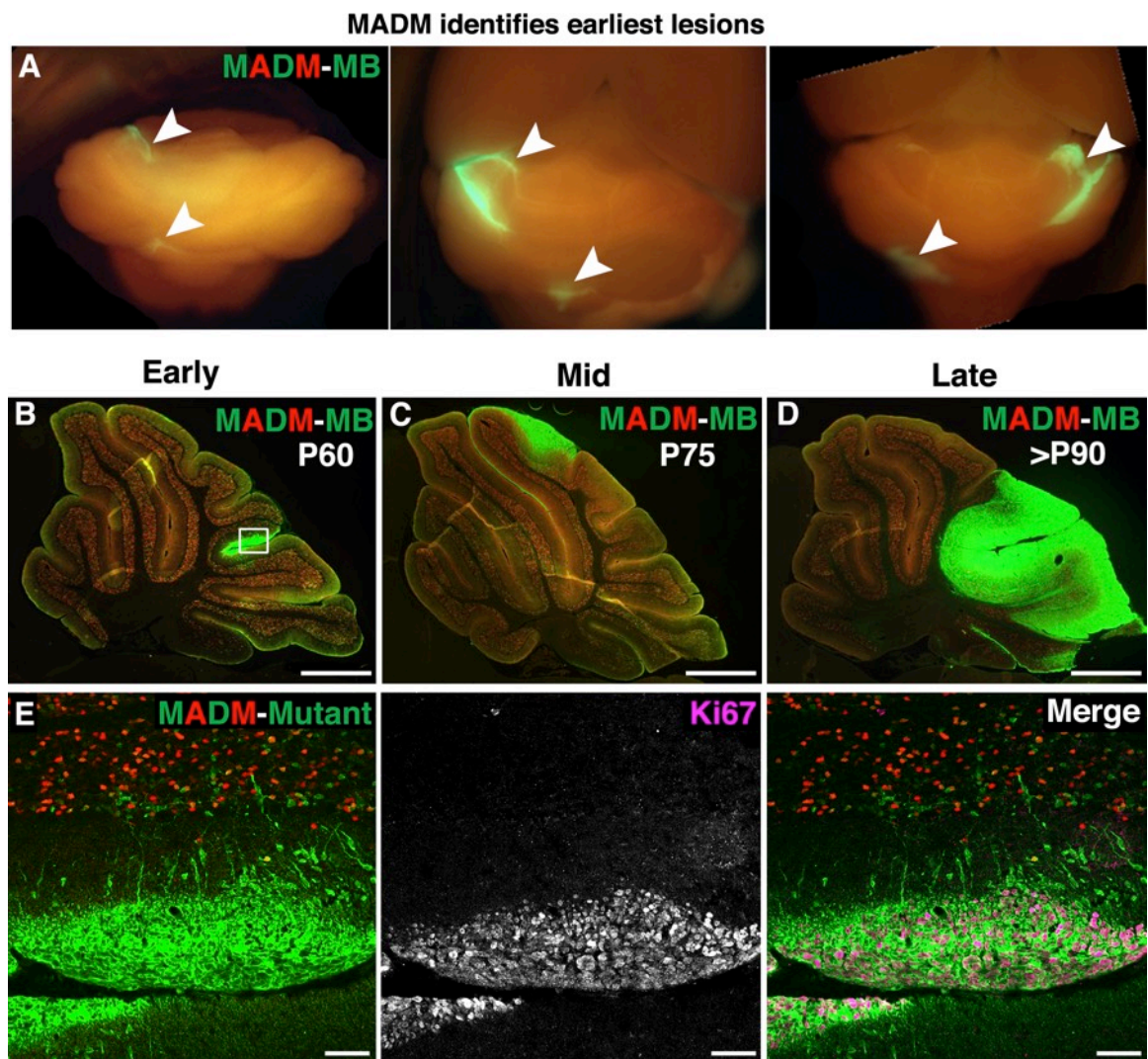


Figure 2.3 MADM enables distinct visualization throughout tumor development.

(A) MADM identified small lesions throughout the cerebellum. Focal GFP signals were readily identifiable in macroscopic views of cerebella at P50-60 (arrowheads).

(B-D) Tumors displayed three characteristic stages. Small tumors appeared as focal GFP signals on single folia that begin to infiltrate normal tissue at P60 (B, left). Medium tumors further infiltrated and continued to grow superficially over the cerebellum at P75 (C, middle). Large tumors infiltrated multiple folia and distorted normal cerebellar structure at >P90 (D, right).

(E) Small, focal accumulations of GFP-positive cells were proliferating (Ki67-positive, from boxed region in B).

Scale bars: B-D= 500 μ m; E= 50 μ m.

Figure 2.4 Two distinct physical regions in MADM medulloblastoma.

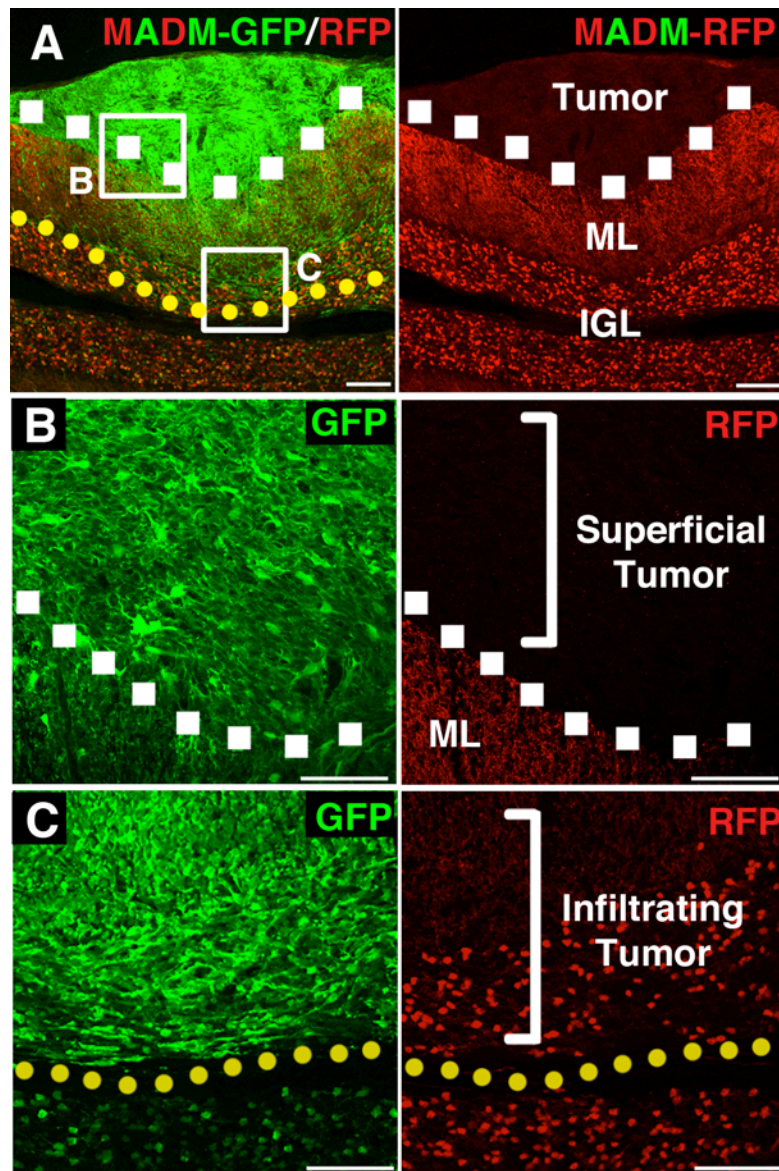


Figure 2.4 Two distinct physical regions in MADM medulloblastoma.

(A) MADM medulloblastoma were distinguished by GFP+ regions.

(B) Tumors reside on the surface of cerebella (superficial). Superficial tumor regions did not contain normal cerebellar cells (B, white dotted line demarcates normal tissue boundary). Red dots are RFP+ granule neuron parallel fibers in the adjacent molecular layer (ML).

(C) GFP+ tumor cells also invaded (infiltrating) normal cerebellar tissue from superficial regions. Infiltrating tumor cells bordered resident cerebellar cells (C, yellow dotted line is tumor-normal tissue boundary) with RFP+ parallel fibers of granule neurons in the ML and their respective cell bodies in the IGL).

[ML=molecular layer, IGL=inner granule layer]

Scale bars: A-C 100 μ m

Figure 2.5 Niche cells exist in both tumor regions.

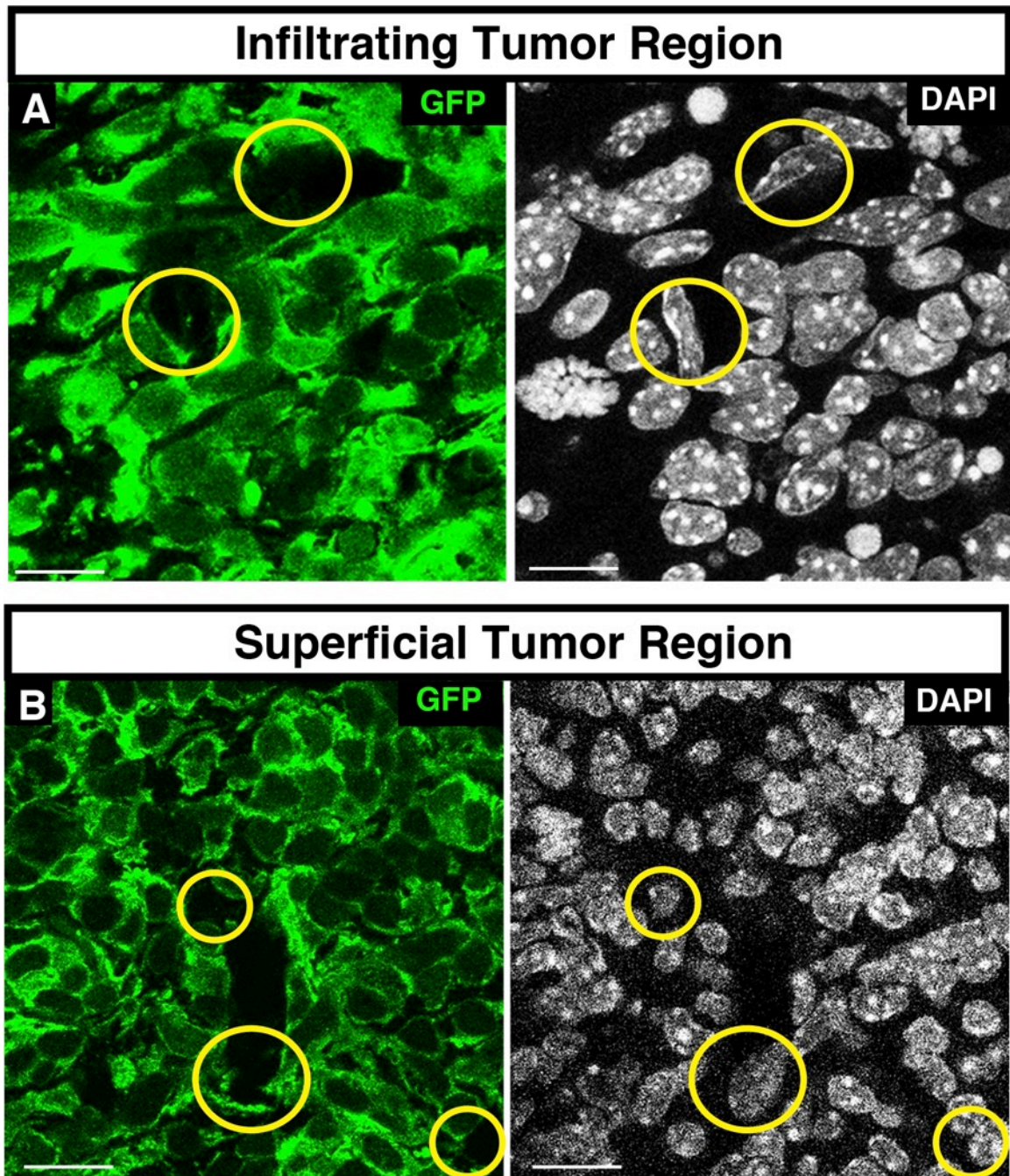


Figure 2.5 Niche cells exist in both tumor regions.

(A-B) Prospective tumor niche cells are colorless (circled GFP-,DAPI+) and closely associated with GFP+ tumor cells in infiltrative (A) and superficial (B) regions.

Scale bars: 10 μ m.

2.1.1 Blood vessels

One of the hallmarks of cancer progression is angiogenesis, the process of forming new blood vessels from existing vessels, which supply the growing tumor with essential nutrients and oxygen (Hanahan and Weinberg, 2011). Angiogenesis is often initiated by the tumor itself. For example, hypoxic tumor cells upregulate the transcription factor HIF1 α , which promotes VEGF secretion to drive angiogenesis (Plate et al., 1992; Shweiki et al., 1992). It is difficult to analyze the degree of angiogenesis in tumors because it is a very dynamic process that results in disordered vascularization, with vessels lacking clear orientations and variations in size throughout tumor regions. Therefore we assessed relative increases in blood vessel presence and changes in relative luminal sizes.

Vascularization (CD34-positive endothelial cells) was increased in GFP-positive tumor regions compared to adjacent normal tissue, evident by increased luminal space (Figure 2.6A). Superficial tumor areas were also highly vascularized, which suggests angiogenesis had taken place because tumor tissue formed beyond the normal tissue boundary and blood supply (Figure 2.6B). In large tumors, blood vessels were present throughout all regions and further increases in luminal diameters were observed (Figure 2.6C). Furthermore, there was a close association of GFP-positive tumor cells with blood vessels throughout tumor regions. However, the endothelial cells were colorless,

suggesting they were distinct from surrounding tumor cells (Figure 2.6A-C, right column).

Figure 2.6 Blood vessels in tumor regions.

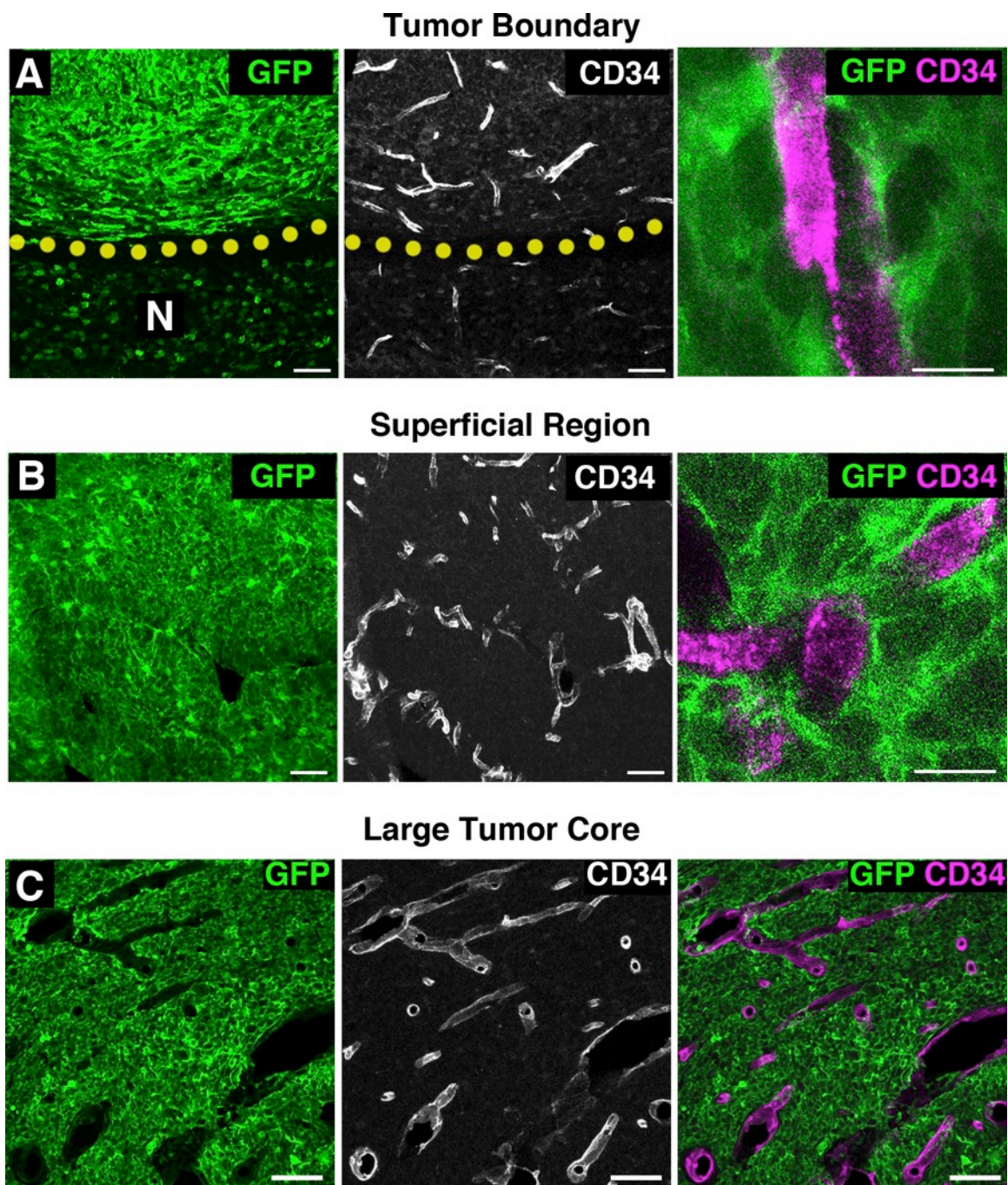


Figure 2.6 Blood vessels in tumor regions.

(A-C) Blood vessels (CD34+) were enriched with enlarged luminal space in GFP+ infiltrative region compared to adjacent normal tissue (A) and persisted in superficial (B) regions, as well as in large tumor cores (C). GFP+ tumor cells were in close association with vessels, yet distinct (A,B, right panels).

[N= normal tissue]

Scale bars: A-B left and middle panels 50 μ m, A-B right panel 10 μ m, C= 50 μ m.

2.1.2 Tumor-associated microglia/macrophages

When microglia become activated, due to stimulation by chemokines for example, they change physically and enter a protective state. Microglia become enlarged amoeboid-like cells distinct from non-activated microglia which have multiple fine processes (Figure 2.2F) (Hanisch and Kettenmann, 2007). Activated microglia are very similar to macrophages in terms of molecular profile and behavior, therefore activated microglia are often termed microglia/macrophage because a clear distinction between the cell types has not been fully elucidated (Hanisch and Kettenmann, 2007; Nimmerjahn et al., 2005).

Compared to normal tissue, tumor-associated microglia/macrophages (TAMs), which express ionized calcium-binding adapter molecule 1 (IBA-1), were enriched in the infiltrating tumor regions (Figure 2.7A), the superficial tumor core (Figure 2.7B), and in large tumors (Figure 2.7C). TAM nuclei and cell bodies were always distinct (GFP-negative) from surrounding GFP+ tumor cells. However, interestingly, amoeboid-shaped TAMs appeared to phagocytose tumor cells, seen as punctate GFP-positive foci in the cytoplasm (Figure 2.7A-B, right panels). Furthermore, TAMs that appeared to have phagocytosed tumor cells were observed in early tumor lesions (53% with GFP foci in cytoplasm), and in both mid- (79%) and late (78%) stage tumors. This observation suggests TAMs may play an active role in cell clearance to allow sustained tumor growth.

Figure 2.7 Tumor-associated macrophages in tumor regions.

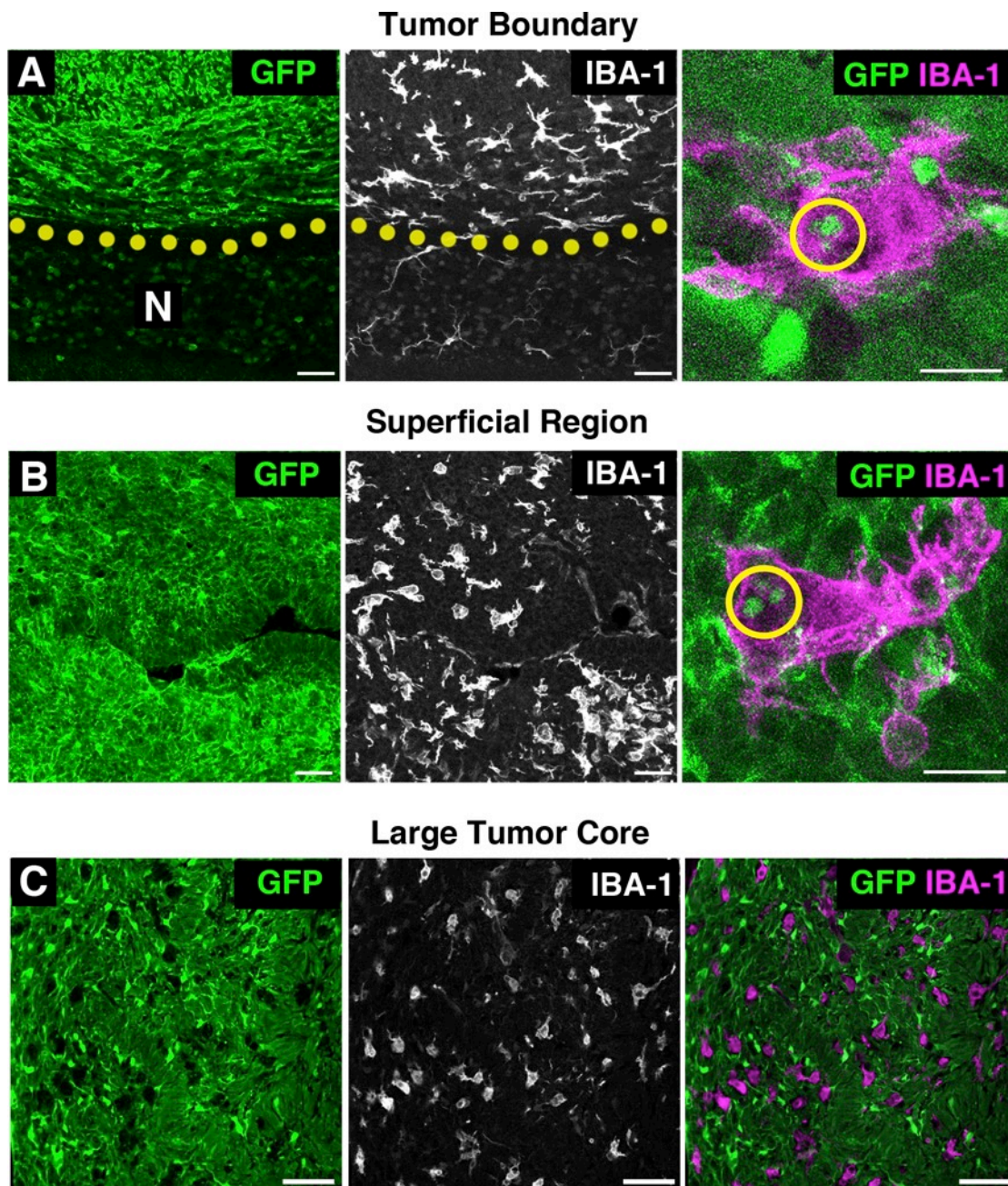


Figure 2.7 Tumor-associated macrophages in tumor regions.

(A-C) Tumor-associated microglia/macrophages (TAMs) (IBA-1+) were enriched in the infiltrative (A), superficial (B) regions, as well as large tumor cores (C). GFP+ tumor cells were phagocytosed by these cells (A-B, GFP+ punctate foci in cytoplasm, circled in right panel).

[N= normal tissue]

Scale bars: A-B left and middle panels 50 μ m, A-B right panel 10 μ m, C= 50 μ m.

2.1.3 Oligodendrocyte precursor cells

Next, we assessed the presence of neuroglia in the tumor niche. We determined whether oligodendrocyte precursor cells (OPCs) were present in tumors. OPCs are a highly dynamic cell population in the brain that respond to injury and growth cues (Hughes et al., 2013). To assess the presence of OPCs in the tumor we visualized the platelet-derived growth factor alpha receptor (PDGFR α) by immunofluorescence. Interestingly, PDGFR α -positive OPCs were greatly enriched in infiltrating and superficial tumor regions (Figure 2.8A,B), and also in large tumors (Figure 2.8C). OPCs were distinct (GFP-negative) from surrounding tumor cells throughout all regions and tumor stage (Figure 2.8A-C, right panels). A trophic tumor environment may recruit OPCs, adding further complexity to the tumor niche. OPCs represent a new population of cells in the tumor niche that may have a functional role not yet understood or considered in medulloblastoma.

Figure 2.8 Oligodendrocyte precursor cells in tumor regions.

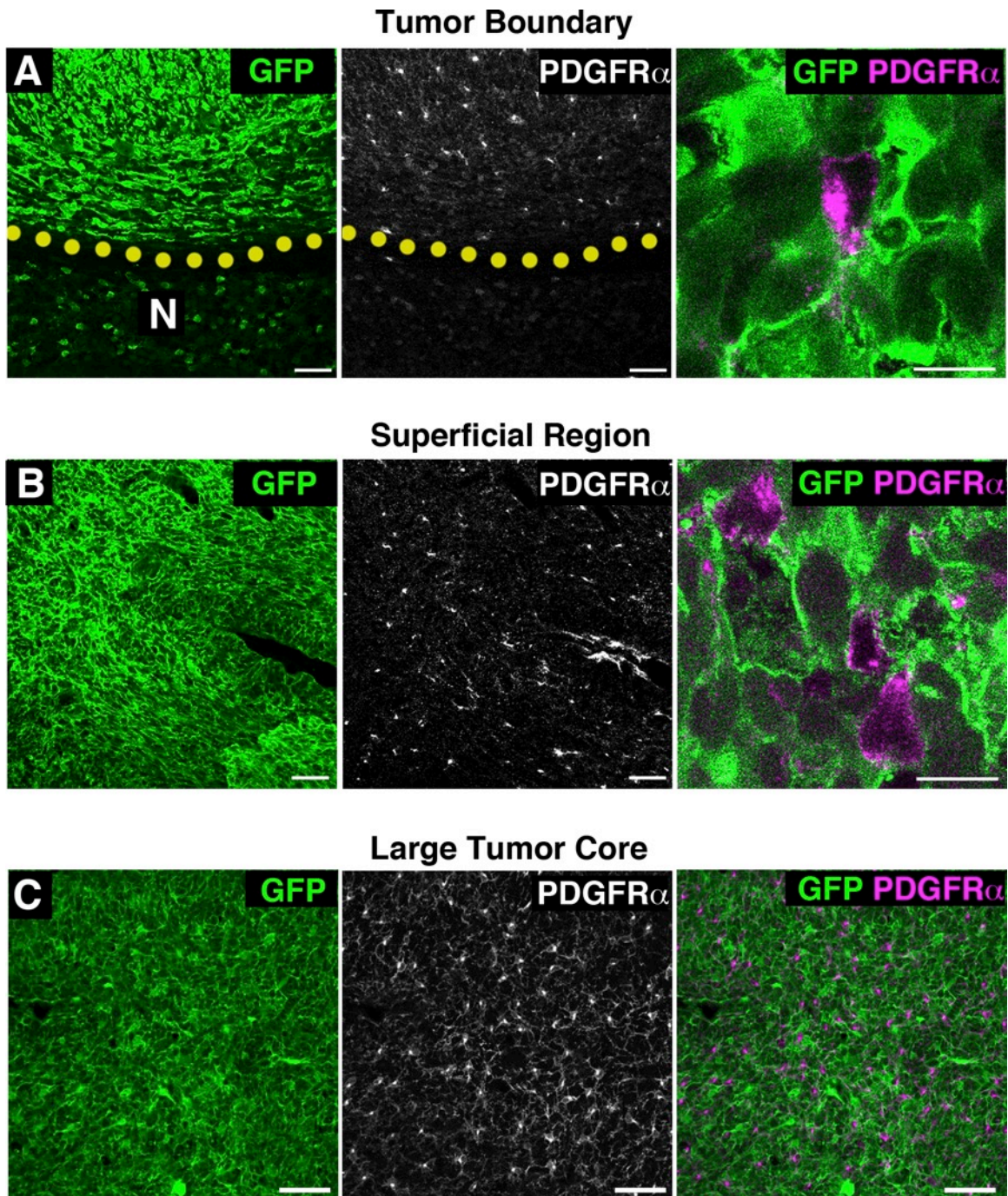


Figure 2.8 Oligodendrocyte precursor cells in tumor regions.

(A-C) Oligodendrocyte progenitor cells (PDGFR α +) were enriched throughout the infiltrative (A) and superficial (B) regions, as well as larger tumor cores (C). OPCs were distinct from GFP+ tumor cells (A-B, right panels).

[N= normal tissue]

Scale bars: A-B left and middle panels 50 μ m, A-B right panel 10 μ m, C= 50 μ m.

2.1.4 Astrocytes

Since astrocytes are present in human medulloblastoma tumor samples (Figure 1.3), we assessed the astrocyte population in our model with glial fibrillary acidic protein (GFAP) immunostaining. GFAP-positive cells were enriched in infiltrative and superficial regions, as well as in large tumors (Figure 2.9A-C, respectively). Surprisingly, some GFAP-positive cells in the infiltrating region were also GFP-positive (Figure 2.9A, right panel, arrowheads) and had a distinct astrocyte-like morphology, while GFAP-positive cells that were GFP-negative represented *in situ* Bergmann glia in the molecular layer. Furthermore, all GFAP-positive cells in the superficial region and in all large tumors were green as well (Figure 2.9B-C, respectively). The fact that all GFAP-positive cells were green suggests transdifferentiation of some tumor GNPs into GFAP-positive tumor “astrocyte-like” cells (herein referred to as, TuAstros). Also, we did not observe MADM labeling of astrocytes from previous Math1-Cre lineage analysis (Figure 2.2E) and all cerebellar astrocytes outside of the tumor were colorless (Figure 2.9D), therefore tumor GNPs must be the precursor for TuAstros.

Next we assessed the prevalence of TuAstros in all tumor stages (Figure 2.10A). We used an additional astrocyte marker that is present on the cell body and processes, brain lipid binding protein (BLBP), to visualize TuAstros rather than GFAP, which localizes mostly in processes. We quantified the ratio of double positive (BLBP and GFP-positive) TuAstros relative to total tumor cells (DAPI-labeled nuclei) (Figure 2.10B). The denominator for these studies was

total tumor cells rather than total GFP-positive cells for two reasons. First, identifying individual tumor GNPs based on GFP signal was nearly impossible given the dense cellularity of tumors and high proliferation rates that dilute the GFP signal. Second, more than 95% of all the cells in a tumor were GFP-labeled cells, therefore using DAPI-labeled nuclei as a surrogate had an acceptable 5% margin of error. In all tumor stages, TuAstros comprised approximately 1% of total tumor cells (Figure 2.10C) and their processes extend to contact the majority of tumor cells. This suggests that transdifferentiation may be a regulated process designed to maintain a population of TuAstros throughout tumor development. I will discuss this hypothesis further in Chapter 3.

Figure 2.9 Astrocytes are derived from GNPs in tumor regions.

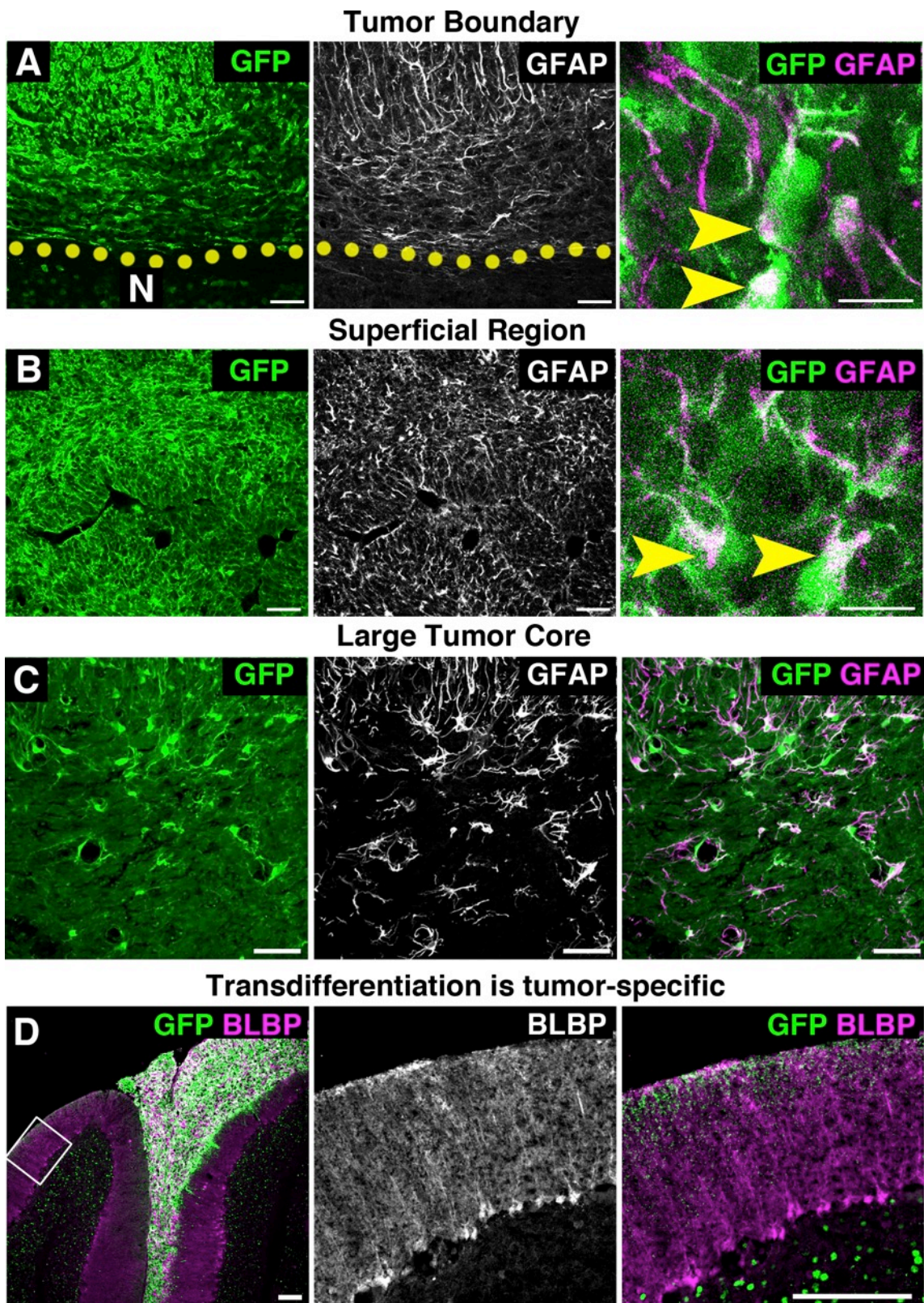


Figure 2.9 Astrocytes are derived from GNPs in tumor regions.

(A-C) Astrocytes (GFAP+) are present in the infiltrative (A) and superficial (B) regions, as well as large tumor cores (C). In infiltrating regions (A) certain GFAP+ cells were also GFP+ (arrowhead). All GFAP+ cells were GFP+ in superficial regions and large tumors (B-C). Colocalization suggests transdifferentiation of mutant GNPs (GFP+) into tumor astrocyte-like cells (GFP+/GFAP+).

(D) Transdifferentiation is tumor-specific. Astrocytes (BLBP+ Bergmann glia) outside of GFP+ tumor regions are not generated from GFP+ mutant cells (boxed region in left panel is magnified in middle and right panels).

[N= normal tissue]

Scale bars: A-B= left and middle panels 50 μ m, A-B= right panel 10 μ m, C= 50 μ m, D= 100 μ m.

Figure 2.10 Tumor astrocytes are consistently generated throughout tumor development.

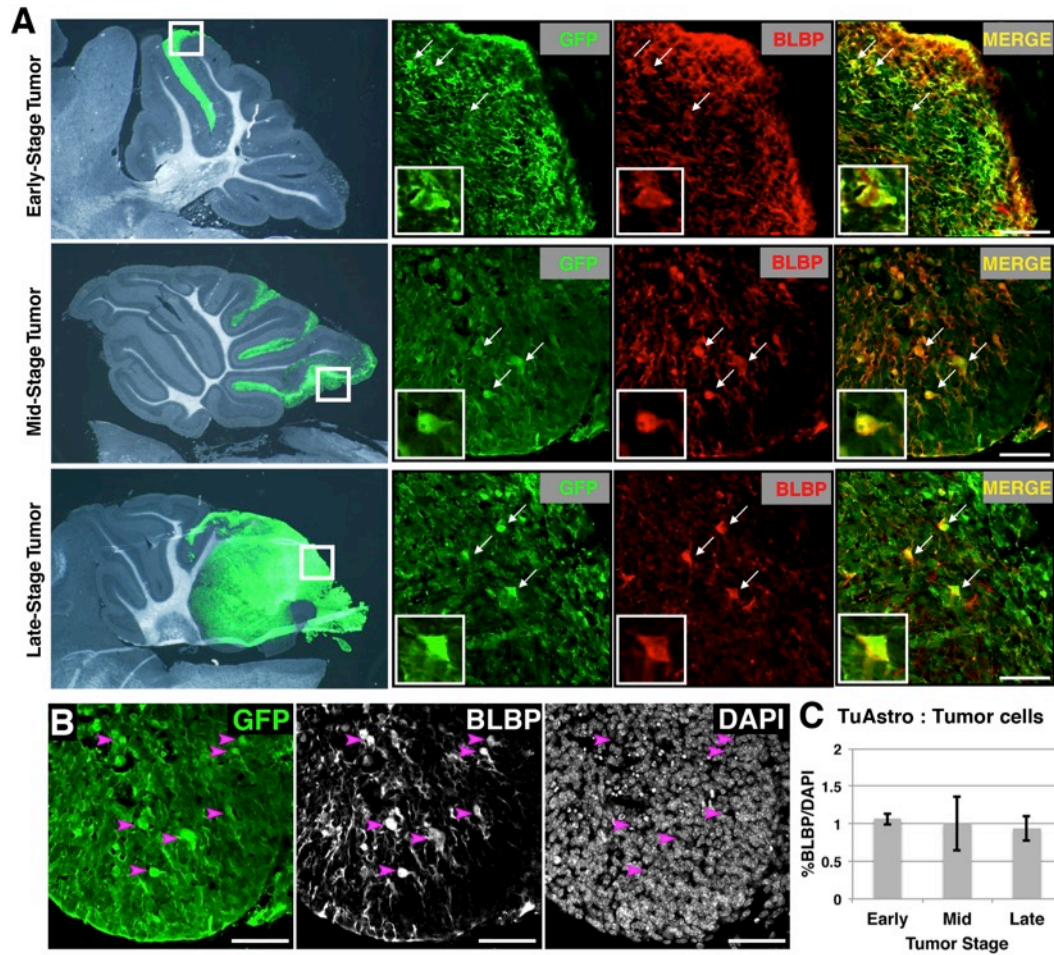


Figure 2.10 Tumor astrocytes are consistently generated throughout tumor development.

(A) Early, mid, and late stage tumors were immunostained with GFP to visualize tumor cells and BLBP to see astrocyte cell bodies.

(B-C) Tumor astrocytes (GFP+ and BLBP+) are generated at a similar ratio to all tumor cells (DAPI+) from early to late stage tumors (C, ~1% of total tumor cell population, $n=3$ per stage).

Scale bars: A-C= 50 μ m.

*Images and quantification provided by Kelsey Wahl.

2.2 Multiple phenotypes confirm astrocytic transdifferentiation in MADM as well as in human tumors.

2.2.1 Tumor astrocytes express mature astrocytic markers.

Next, we sought to assess the astrocytic nature of TuAstros in the MADM medulloblastoma model and in human tumors. To verify TuAstros were indeed astrocytes we assessed multiple phenotypic markers, morphologies, and functional attributes. First, all cells with the highest GFP fluorescent signal that exhibited astrocyte-like morphology were shown to express at a minimum GFAP and/or BLBP (Figure 2.11A). Next, we determined whether TuAstros also expressed the mature functional astrocyte protein ALDH1L1, an aldehyde dehydrogenase that has a role in the regulation of folate metabolism (Cahoy et al., 2008). We analyzed the expression of *Aldh1L1* in tumor astrocytes using a GFP transgene expressed under the control of the *Aldh1L1* promoter (*Aldh1L1-GFP*) (Gong et al., 2003; Zamanian et al., 2012). To distinguish *Aldh1L1*-expressing TuAstros from tumor GNPs, we incorporated the *Aldh1L1-GFP* transgene into the medulloblastoma model with red fluorescent protein (RFP) tracing GNP lineage. The majority of TuAstros that were RFP- and GFAP-positive also expressed *Aldh1L1-GFP* (~90% RFP/GFAP/*Aldh1L1-GFP*-positive, $n=3$) (Figure 2.11B). These data provide additional validation indicating that TuAstros are bona fide astrocytes.

Figure 2.11 Tumor astrocytes express multiple astrocyte markers.

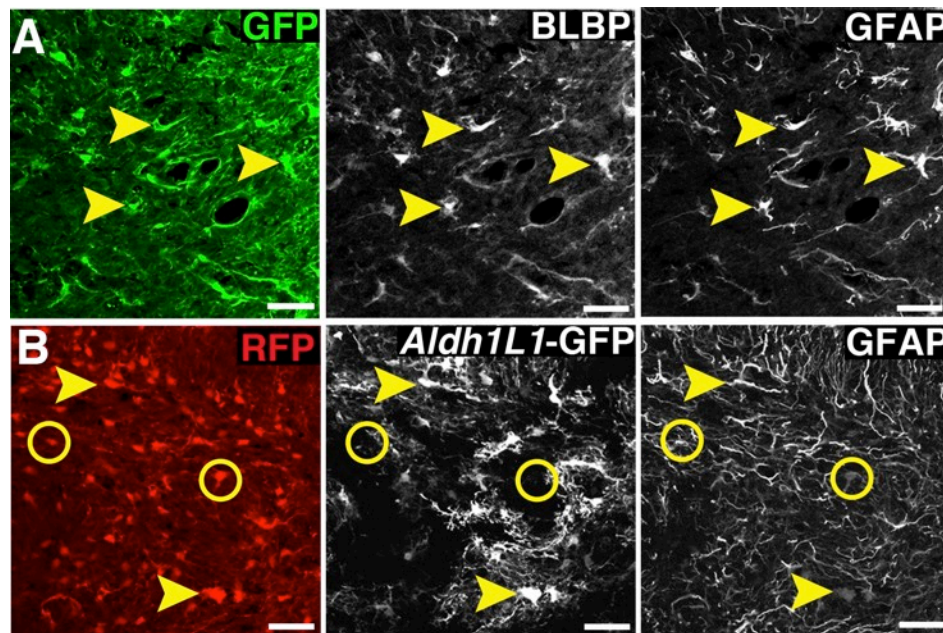


Figure 2.11 Tumor astrocytes express multiple astrocyte markers.

(A-B) Tumor astrocytes express prototypical markers (A, mutant cells with strong GFP+ signal express GFAP and BLBP) while ~90% have mature astrocytic *Aldh1L1* expression (B, arrowheads indicate GFAP/*Aldh1L1*-GFP+ and circles are GFAP+ only, $n=3$).

Scale bars: A-B = 50 μ m.

2.2.2 Tumor astrocytes display similar functional phenotypes of mature astrocytes.

We next sought to assess whether TuAstros displayed the characteristic morphology of canonical astrocytes. In the cerebellum Bergmann glia are defined by their distinctive radial fibers that project through the ML toward the surface of folia (fibers are GFAP-positive) (Figure 2.12A). Folia-like structures are also evident in tumors (Figure 2.12B, outlined). TuAstros in the folia-like structures exhibited a similar radial-like morphology, as visualized with GFAP/BLBP co-staining (Figure 2.12C). These observations further support the astrocytic classification of TuAstros.

One of the hallmarks of homeostatic astrocytes is their interaction with blood vessels for trophic support, blood-brain barrier maintenance, and blood flow regulation (Foo et al., 2011; Iadecola and Nedergaard, 2007; Sofroniew and Vinters, 2010; Takano et al., 2005). As tumors are highly vascularized, we investigated interactions of TuAstros with blood vessels (CD34-positive endothelial cells). Throughout tumor regions, TuAstros were seen to closely contact blood vessels (Figure 2.12D). We also observed TuAstros wrapping entire vessels (Figure 2.12D). The close interaction of TuAstros with blood vessels throughout the tumor highlights a possible functional relationship between TuAstros and blood vessels. Similarly, GFAP-positive astrocytes in human tumors were also seen to contact blood vessels (Figure 2.12E). Together,

these data show that TuAstros display phenotypic, morphological, and functional attributes similar to normal astrocytes.

Figure 2.12 Tumor astrocytes display similar functional phenotypes of canonical astrocytes.

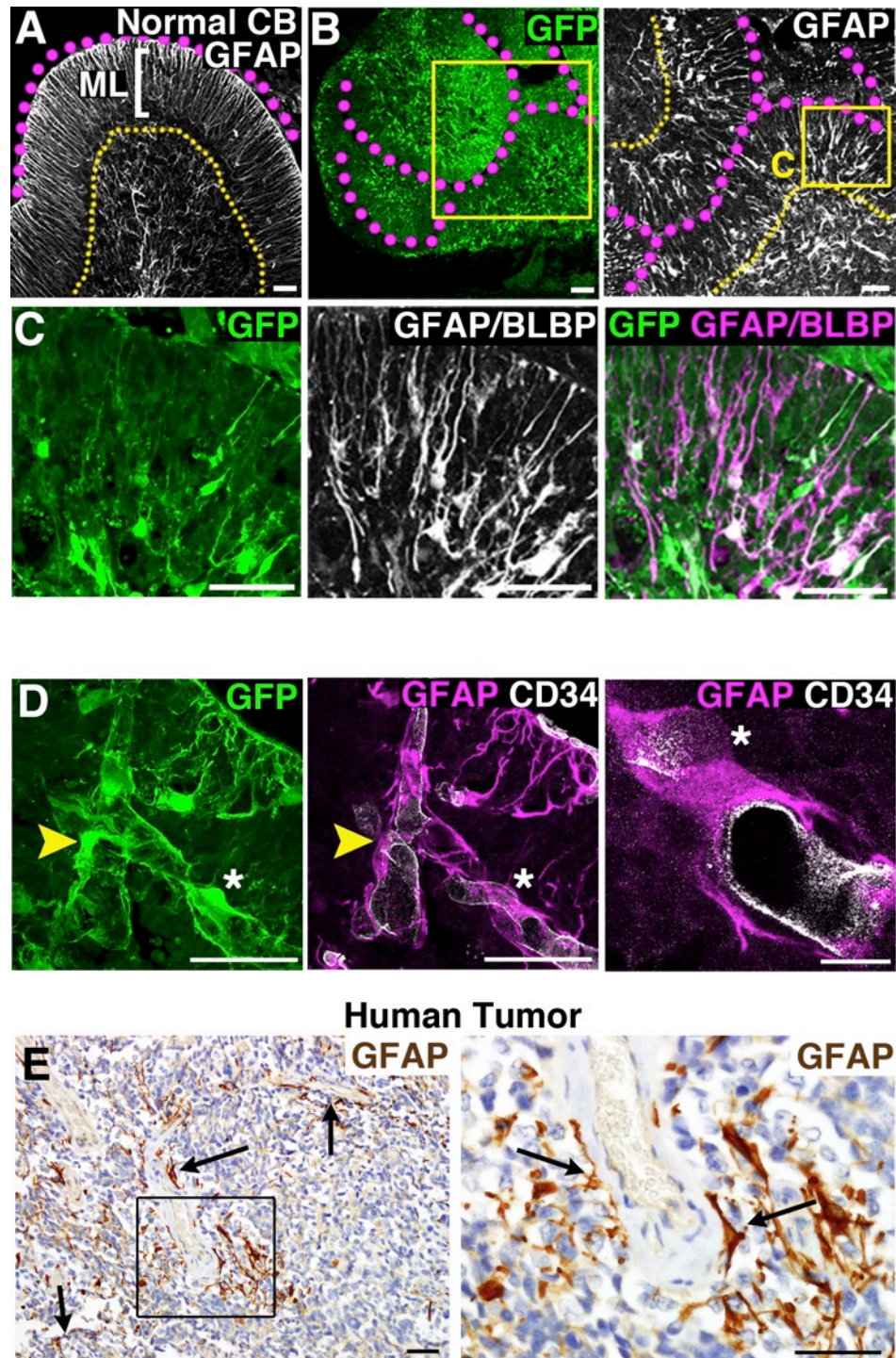


Figure 2.12 Tumor astrocytes display similar functional phenotypes of canonical astrocytes.

(A-C) In the normal cerebellum (A), Bergmann astroglia are GFAP+ and have distinct radial processes through the ML of all folia. Tumors can have folia-like structures (B, outlined in dotted magenta lines) where tumor-derived astrocytes have a very similar morphology to normal Bergmann astroglia (B, right panel with GFAP processes projecting in outward fashion of pseudo-folia). High magnification (C) confirms the radial morphology of tumor astrocytes (GFP/GFAP/BLBP).

(D) Tumor astrocytes closely interact with blood vessels (D, CD34+ endothelial cells are often wrapped by GFP/GFAP+ tumor astrocytes).

(E) Astrocytes in human tumors also associate with blood vessels (arrows in right panel, zoom in left panel).

Scale bars: A-C,E = 50 μ m, D right and middle panels = 50 μ m, D left panel = 10 μ m.

*Human tumor images provided by Dr. Fausto Rodriguez.

2.2.3 Transdifferentiation is evident in human medulloblastoma.

Next, we determined whether astrocytes were derived from tumor cells in human tumors. We assessed the lineage relationship between astrocytes and tumor cells by examining shared cytogenetic aberrations with chromosomal fluorescent *in situ* hybridization (FISH) combined with cell type-specific immunofluorescence (IF). In these studies, astrocytes and tumor cells that are lineage-related will share the same chromosomal aberrations, whereas if astrocytes infiltrate the tumor they should not have the aberrations (Figure 2.13A). Specifically, they will share the same chromosomal loss at *9q21.33* and *PTCH1* loci, which are common aberrations in SHH-subgroup of medulloblastoma (Ellison et al., 2006; Northcott et al., 2012). However, this analysis could be complicated in patients with a germline *PTCH1* mutation, as all cells would show chromosomal loss at the *PTCH1* locus. To control for this possibility, we analyzed CD34-positive endothelial cells in tumors, which should have two signals at the *PTCH1* locus in patients if they do not have a germline *PTCH1* mutation (Figure 2.13B). Both tumor GNPs and astrocytes exhibited loss of heterozygosity at the *PTCH1* and *9q21.33* region (Figure 2.13C). Quantification of hundreds of cells in six samples showed that more than 80% of tumor GNPs and astrocytes shared the same pattern of *9q21.33* and *PTCH1* loss (Table 2.1). The similar cytogenetic defects in tumor GNPs and astrocytes strongly suggest they share a lineage relationship.

Figure 2.13 Transdifferentiation is evident in human medulloblastoma.

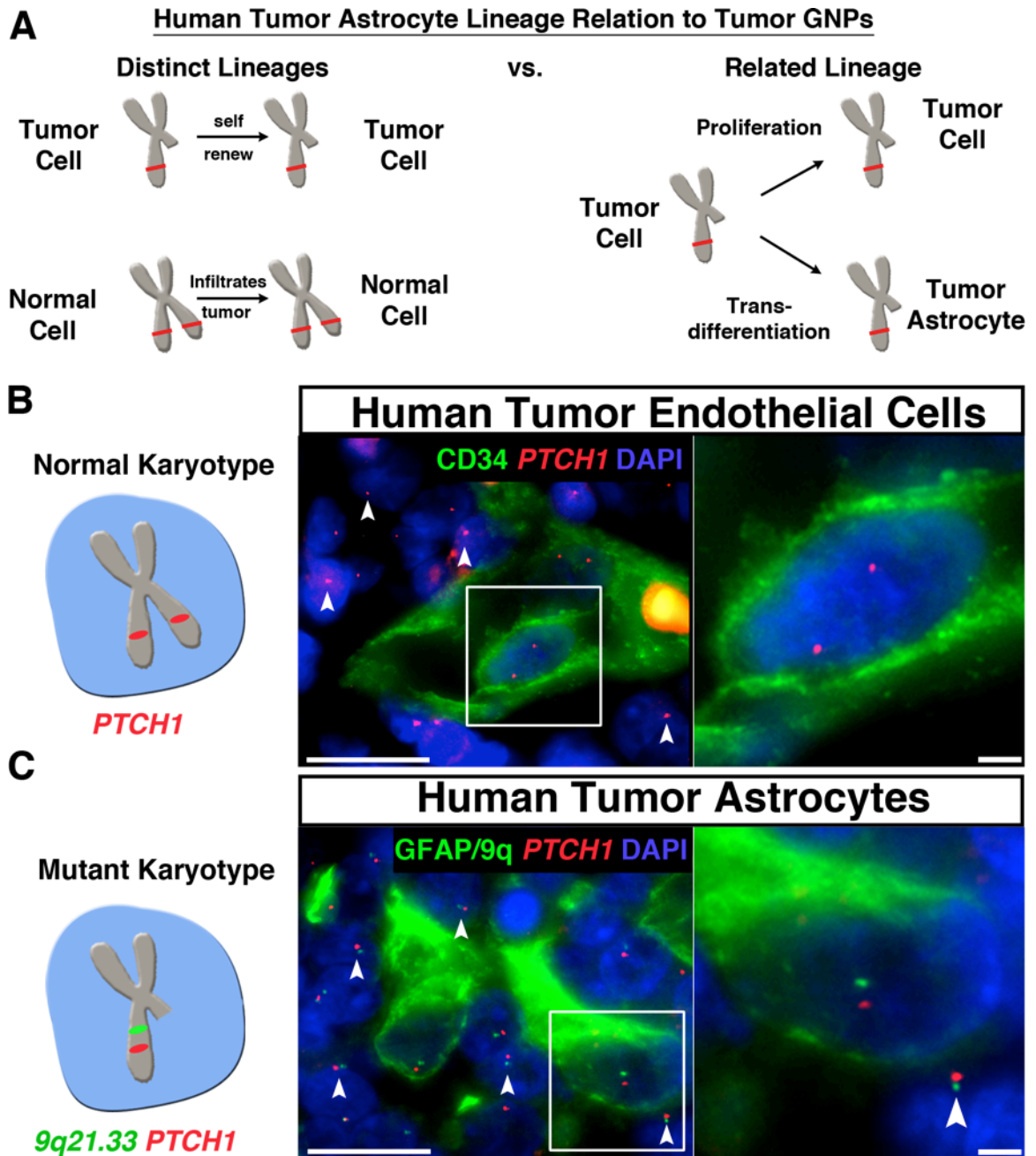


Figure 2.13 Transdifferentiation is evident in human medulloblastoma.

(A) Cytogenetic analysis with FISH can determine lineage relationships in human samples. Distinct cell lineages would be distinguished by different FISH patterns at loci known to be lost in tumor cells (one locus = one red band). If astrocytes are not derived from tumor cells, but instead infiltrate the tumor, they will have intact loci (two loci = two red bands). If astrocytes share the same FISH pattern with tumor cells it would suggest they are lineage related.

(B) An allele of *PTCH1* linked to the *9q21.33* region is frequently lost in tumor cells. Endothelial cells have a normal karyotype (CD34+ endothelial cells have both alleles of *PTCH1* = two red dots per nucleus compared to surrounding cells with one signal [arrowheads]). Boxed region in middle panel is further magnified in right panel.

(C) Astrocytes are related to surrounding tumor cells (nucleus of GFAP+ cells have single signal pattern similar to other tumor cells [arrowheads]). Boxed region in middle panel is further magnified in right panel.

Scale bars: (B,C) left panels = 25 μ m, right panels = 10 μ m.

*FISH and imaging were performed by Dr. Fausto Rodriguez.

Table 2.1 Quantification of FISH/IF signals between human tumor cells.

Cases	Tumor Cells (DAPI only) <i>-9q & -PTCH1 loss</i>	Tumor Astrocytes (GFAP+) <i>-9q & -PTCH1 loss</i>	Endothelial Cells (CD34+) <i>2xPTCH1</i>
1	53/58 (91%)	17/21 (81%)	9/23 (39%)
2	36/43 (84%)	16/18 (89%)	Faint Signals
3	50/57 (88%)	15/18 (83%)	2/5 (40%)
4	71/81 (88%)	31/35 (89%)	16/32 (50%)
5	51/56 (91%)	8/10 (80%)	Faint Signals
6	59/66 (89%)	26/32 (81%)	17/45 (38%)
TOTAL	320/361 (89%)	113/134 (84%)	*44/105 (42%)
**p-value	2.93E-07	5.60E-06	0.059

*Low % is due to a technical complication of sectioning. Many endothelial nuclei are not whole, because tissue sections are ~5um thick and sometimes shear nuclei in half.

**p-value was determined with Student's t-test between FISH-positive and negative cells in the population.

2.3 Fate-restricted GNPs can transdifferentiate after postnatal transformation.

One potential difference between human medulloblastoma and the MADM medulloblastoma model is that sequential mutations in humans may occur postnatally, whereas mutations are targeted embryonically in the MADM mice. To determine whether postnatal mutation can promote GNPs to form tumors and retain the ability to transdifferentiate in a similar manner to mutated embryonic GNPs, we used an inducible *Math1-CreER* to target *p53* loss postnatally. CreER is a fusion protein between Cre and a mutated ligand binding domain of the estrogen receptor, which upon binding of tamoxifen (TAM) translocates into the nucleus where Cre can perform loxP-mediated recombination (Feil et al., 1997). The use of *Math1-CreER* in MADM would result in too few mutant GNPs and would sacrifice consistent tumor penetrance and latency. Therefore we opted to use the *Math1-CreER* in a conditional knockout model (CKO) of medulloblastoma. In this conditional knockout model, tamoxifen administration induced loss of *p53* and concurrent permanent GNP lineage labeling with RFP in *Ptch+/-* mice (Figure 2.14A). Induction was performed at postnatal day 7-10 and mice were analyzed for tumor formation and transdifferentiation at postnatal day 90 (P90) (Figure 2.14B). We found 7 of 10 tamoxifen-injected mice formed tumors at P90. Among tumor-bearing mice, all had TuAstros that were RFP-positive and BLBP-positive (Figure 2.14C). These data indicate that transdifferentiation of mutant

GNPs into TuAstros is independent of whether GNPs are transformed embryonically or postnatally.

Figure 2.14 Fate-restricted GNP can transdifferentiate after postnatal transformation.

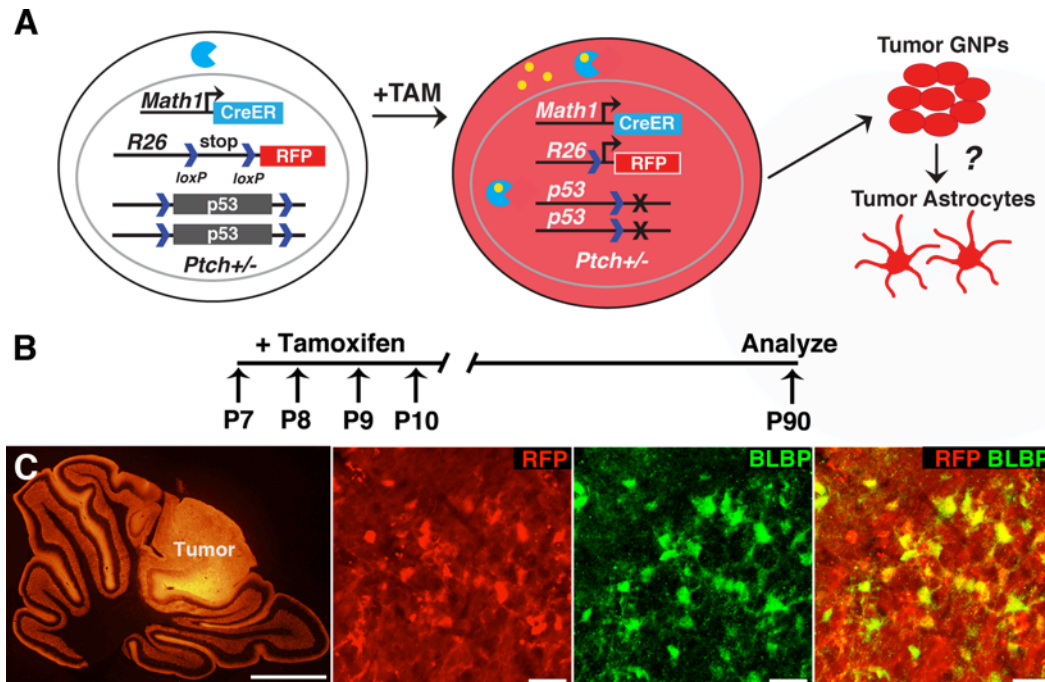


Figure 2.14 Fate-restricted GNP can transdifferentiate after postnatal transformation.

(A) An inducible conditional knockout model was used for postnatal transformation of GNP. Tamoxifen-inducible Math1-CreER excises a floxed stop sequence at the *Rosa26* locus to constitutively express RFP and creates null alleles of *p53* in *Ptch*^{+/-} mice. Lineage traced tumor GNP can now be analyzed for their transdifferentiation potential if tumors form.

(B-C) Tamoxifen induced transformation of GNP at P7-10 GNP (B) generated tumors with transdifferentiated tumor astrocytes (RFP/BLBP+) (C).

Scale bars: C= left panel 500 μ m, right panels 50 μ m.

*These experiments were performed by Dr. Maojin Yao.

2.4 Tumor GNPs retain the transdifferentiation potential in secondary tumors.

To further assess whether this transdifferentiation was a cell-autonomous feature of tumor GNPs we examined the ability of purified tumor GNPs to transdifferentiate in a secondary tumor orthograft. Tumors from CKO mice (similar to Figure 2.14A but with *Math1-Cre* instead of *Math1-CreER*) were dissected and enzymatically dissociated to yield a single cell suspension. Tumor GNPs were purified away from the other niche cells, including TuAstros, to minimize non-cell autonomous influences. A two-phase Percoll gradient was used to separate the tumor cells based on cell size (Hatten 1985). Following centrifugation the lower interface contained the small tumor GNPs (>99% pure), whereas the upper interface retained larger tumor cells, namely TuAstros (4-fold enrichment over whole tumor lysate) with minimal tumor GNP retention (Figure 2.15A). Separated tumor GNPs were then cultured in serum-free medium for 2 days *in vitro* (DIV) to expand the population and deplete any possible contaminating TuAstros (Figure 2.15A), as verified by quantitative real-time PCR for the astrocytic genes *Aldh1L1* and *Id3* (Figure 2.15B). Cultured tumor GNPs were then injected at low density (10,000 cells/brain) into the forebrain of non-obese diabetic/severe combined immunodeficiency (NOD-SCID) mice (Figure 2.15A) to assess tumor-forming ability and whether astrocyte transdifferentiation occurred. First, we verified that tumor GNP orthografts did not contain remnant TuAstros in early grafts at 10 days post-injection (dpi). Instead, GNP orthografts

were surrounded by native reactive astrocytes from the injection injury (Figure 2.15C). When analyzed 30 dpi large tumors were populated with TuAstros that were GFAP- and BLBP- positive (Figure 2.15D). Therefore, the ability of tumor GNPs to transdifferentiate into TuAstros appears to be an intrinsic feature that manifests as tumors grow and need further niche development. Further supporting evidence is shown later, when purified tumor GNPs differentiate into TuAstros in minimal growth conditions *in vitro*.

Figure 2.15 Tumor GNPs retain the transdifferentiation potential in secondary tumors.

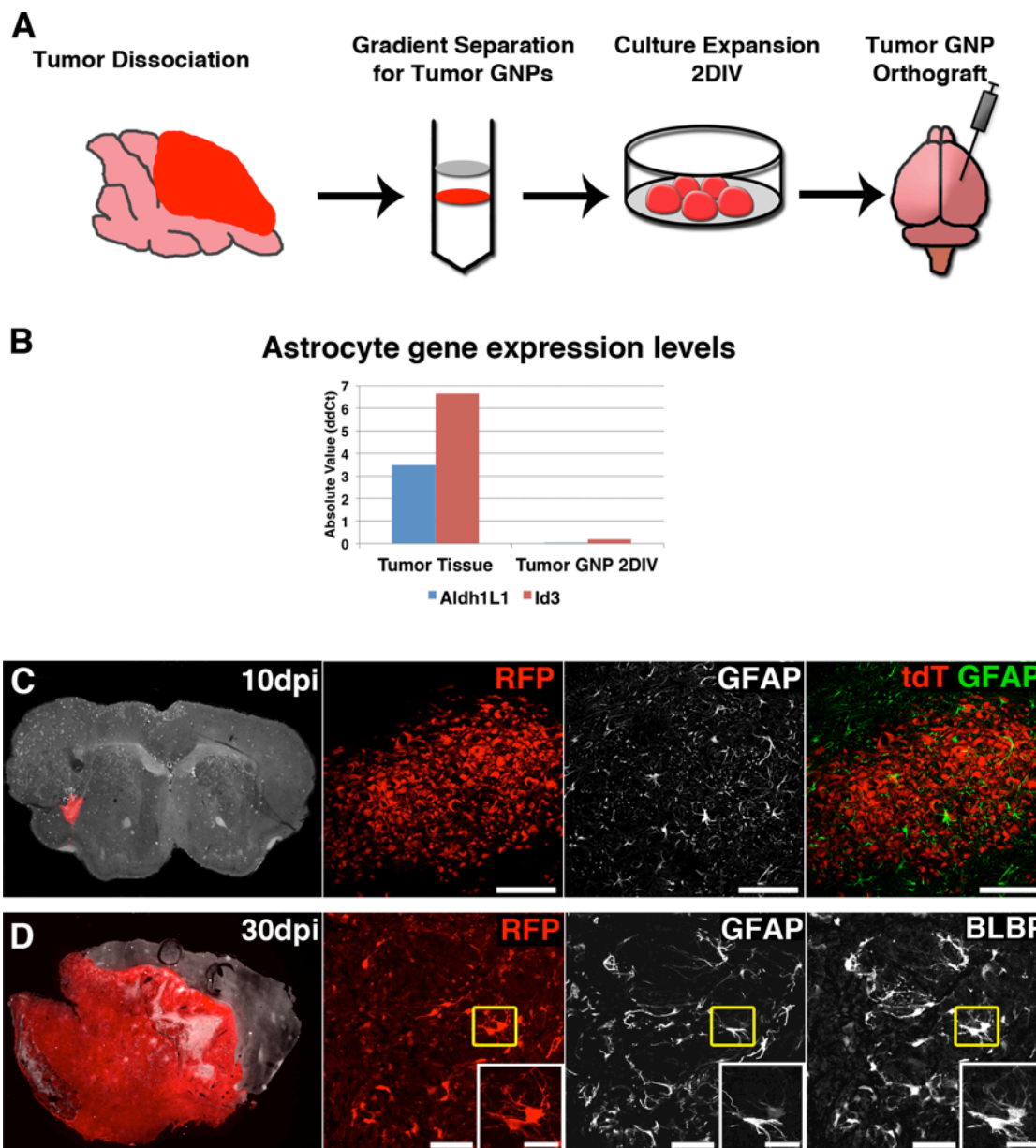


Figure 2.15 Tumor GNPs retain the transdifferentiation potential in secondary tumors.

(A) Purification of tumor GNPs through Percoll gradient size selection (tumor GNPs in lower fraction, some GNPs and glia in top fraction) enables pure population expansion *in vitro* followed by orthotopic injection to assess transdifferentiation ability in absence of initial tumor-generated astrocytes.

(B) Short term culture (2DIV) of tumor GNPs further purified the population as astrocytic gene expression (*Aldh1L1* and *Id3*) was greatly reduced compared to tumor tissue containing tumor astrocytes ($n=2$). Absolute values (arbitrary units) were normalized to *Gapdh* expression level in samples with the same amount of input cDNA.

(C) Early tumor GNP grafts (10dpi) did not display astrocyte transdifferentiation, but instead were surrounded by GFAP+ reactive astrocytes.

(D) Large secondary tumors (30dpi) were generated and tumor GNP transdifferentiation was evident by the presence of tumor astrocytes (RFP/GFAP/BLBP+).

[DIV = day *in vitro*, dpi = days post-injection]

Scale bars: C = 100 μ m, D = 200 μ m, inset 25 μ m.

2.5 Tumor astrocytes do not display cancer stem cell features.

During development and homeostasis of the central nervous system, neural stem cells generate neurons and glia and can express both GFAP and BLBP. (Alvarez-Buylla et al., 2001; Sofroniew and Vinters, 2010). Since TuAstros also express these markers, we hypothesized that they might have stem cell properties. To address this possibility we performed lineage tracing of TuAstros to assess whether any labeled tumor GNPs or other cell types were generated from TuAstros. We employed an inducible *Glast-CreER* (glutamate aspartate transporter, *Glast*) to permanently label the TuAstro lineage (RFP-positive) in colorless tumors arising spontaneously in *Ptch*^{+/-} mice (Figure 2.16). We predicted two possible observations following labeling and analysis at extended time points. If the TuAstros exhibited stem cell properties, they would generate both labeled GNPs and TuAstros over time. Alternatively, if the TuAstros did not have stem cell properties, labeling would be restricted to TuAstros over time (Figure 2.16).

First, we verified that TuAstros expressed *Glast-CreER* by pulsing with tamoxifen citrate gavage for two days and assessing the co-expression of RFP and BLBP (Figure 2.17A). TuAstros were RFP- and BLBP-positive, but tumor GNPs were not labeled (Figure 2.17B). This observation suggests *Glast-CreER* is faithful for TuAstros labeling. Following the labeling of TuAstros in primary tumors through a 4-day tamoxifen treatment, we assessed the identity of RFP-labeled cells ($n=2$ tumors) after 2 weeks (short term) of continued tumor growth.

We observed that all RFP-positive cells in tumors were also GFAP-positive and displayed the characteristic TuAstro morphology (Figure 2.18A), whereas all other tumor cells (DAPI-positive) were not labeled. We further extended the waiting period after initial labeling to rule out the possibility that TuAstros behave as cancer stem cells but exhibit long-term quiescence. However, waiting for 1-2 months following labeling was not possible in primary *Ptch*^{+/-} tumors, because the mice die from large tumors prior to analysis at these longer timepoints. Therefore, we performed the extended analysis in orthografted secondary tumors following injection of colorless cells from primary *Glast-CreER*; *Ptch*^{+/-} tumors that did not receive tamoxifen (50,000 cells injected into forebrain of NOD-SCID mice, as in Figure 2.15A). Secondary TuAstros were labeled by tamoxifen gavage at 14 and 21 dpi and then analyzed following a 1-2 month tumor growth period. Similar to primary tumors, all RFP-positive cells in tumors were also GFAP-positive, whereas the surrounding cells were colorless ($n=2$) (Figure 2.18B). Together, these experiments strongly suggest that TuAstros do not serve as stem cells in medulloblastoma.

Figure 2.16 Lineage tracing tumor astrocytes.

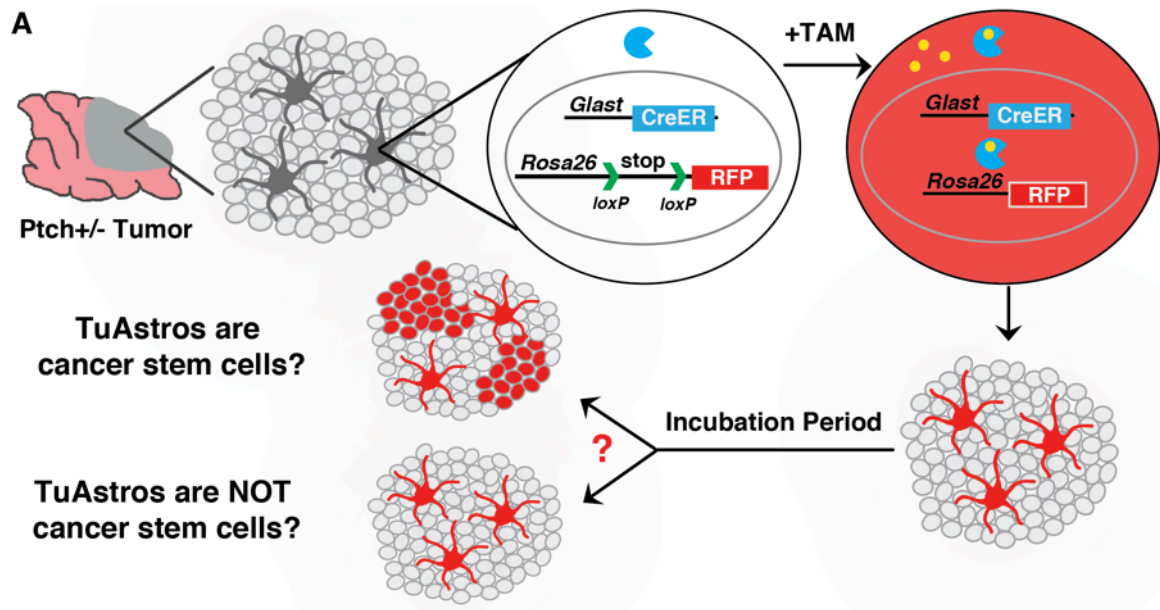


Figure 2.16 Lineage tracing tumor astrocytes.

(A) Astrocyte lineage tracing with inducible *Glast*-CreER in spontaneous *Ptch*^{+/-} mice (astrocytes were labeled with RFP following tamoxifen administration). Labeled tumor astrocytes could have two possible fates after extended tumor growth: 1) Tumor astrocytes function as stem cells that produce labeled tumor astrocytes and tumor GNPs, or 2) Tumor astrocytes do not function as stem cells and only tumor astrocytes become labeled.

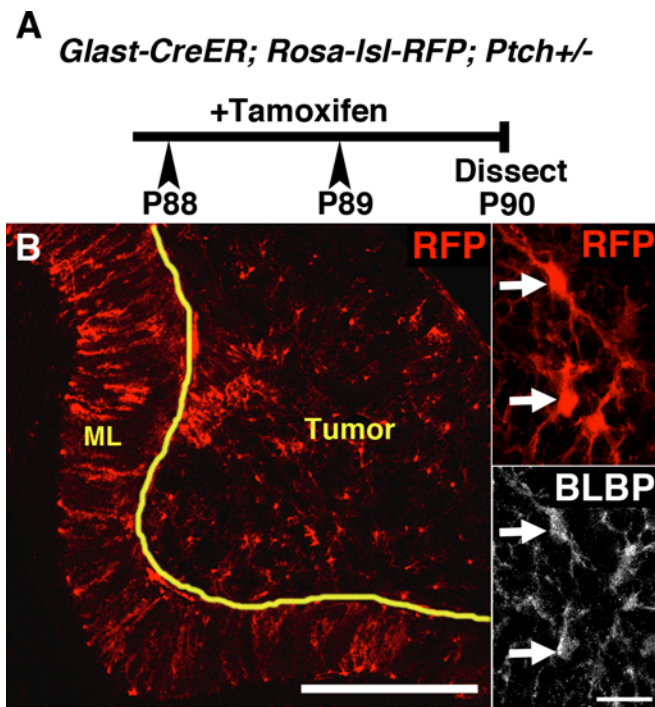
Figure 2.17 *Glast*-CreER labels tumor astrocytes.

Figure 2.17 *Glast*-CreER labels tumor astrocytes.

(A) Tumor astrocytes express *Glast*-CreER. Two days of tamoxifen administration prior to dissection labeled RFP+/BLBP+ tumor astrocytes, while adjacent Bergmann glia in ML served as a positive labeling control.

[*Glast*= Glutamate Aspartate Transporter, ML= Molecular layer]

Scale bars: B macro view = 50 μ m, Higher magnification panels = 20 μ m.

Figure 2.18 Tumor astrocytes do not generate tumor GNPs.

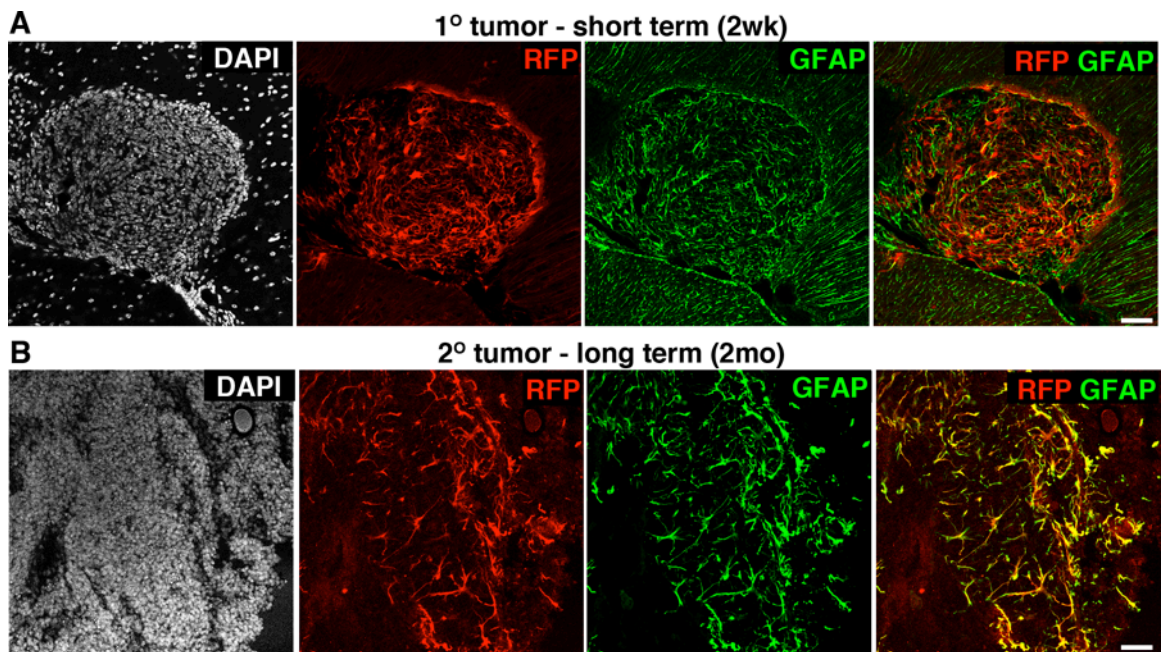


Figure 2.18 Tumor astrocytes do not generate tumor GNPs.

(A) Two weeks after labeling in primary tumors, only tumor astrocytes remain RFP+/GFAP+.

(B) Extended wait periods were performed in secondary orthograft tumors. Following tumor cell grafts, tumor astrocytes were labeled at 14dpi and analyzed 2 months later. All RFP+ cells were GFAP+ tumor astrocytes.

Scale bars: A-B = 50 μ m.

2.6 Astrocytes correlate with mutant GNP proliferation in early mutant cell expansions.

In *Ptch*^{+/-} mice distinct focal regions of GNP hyperproliferation throughout the surface of the cerebellum can potentially further transform leading to tumor formation (Oliver et al., 2005). These accumulations, termed pre-neoplastic lesions (PNLs), occur in ~70% of brains, however, the frequency of tumor formation is only 10-20% (Figure 2.19A). This discrepancy between the initial number of PNLs and the final penetrance of tumor formation could be explained by two possibilities. Either a subset of PNLs acquire additional mutations for further transformation, or there may be other factors, such as niche cells, which support GNPs to continue proliferating and subsequently allowing more time to accumulate oncogenic mutations. To investigate the possibility that niche cell interactions in PNLs could promote GNP growth we analyzed the PNL stage in MADM medulloblastoma mice.

Since our earlier observations revealed that tumor GNPs could transdifferentiate into TuAstros, we focused our analysis on whether astrocytes were present in PNLs and whether there was an associated growth phenotype. In the course of analyzing 10 brains, we identified PNLs by DAPI staining and assessed their proliferation status by Ki67 staining. When we assessed the presence of GFAP-positive astrocytes in PNLs, surprisingly we found that PNLs with proliferating cells were highly correlated with the presence of astrocytes (Figure 2.19B) compared to non-proliferating PNLs (Figure 2.19C). There were

also instances where multiple lesions that were proliferating in the same cerebellum had astrocytes (Figure 2.20A-C). Of proliferating lesions the presence of astrocytes within lesions could also vary (Figure 2.20D-E). There was a high correlation between PNLs that were proliferating (KI67) and the presence of GFAP-positive astrocytes, as 14 of 16 PNLs that were proliferating had astrocytes, whereas astrocytes were absent in 16 of 17 non-proliferating PNLs (Figure 2.19D). These results further suggest astrocytic support could be essential for the propagation of tumor GNPs to reach full malignancy.

Figure 2.19 Astrocytes correlate with mutant GNP proliferation in early mutant cell expansions.

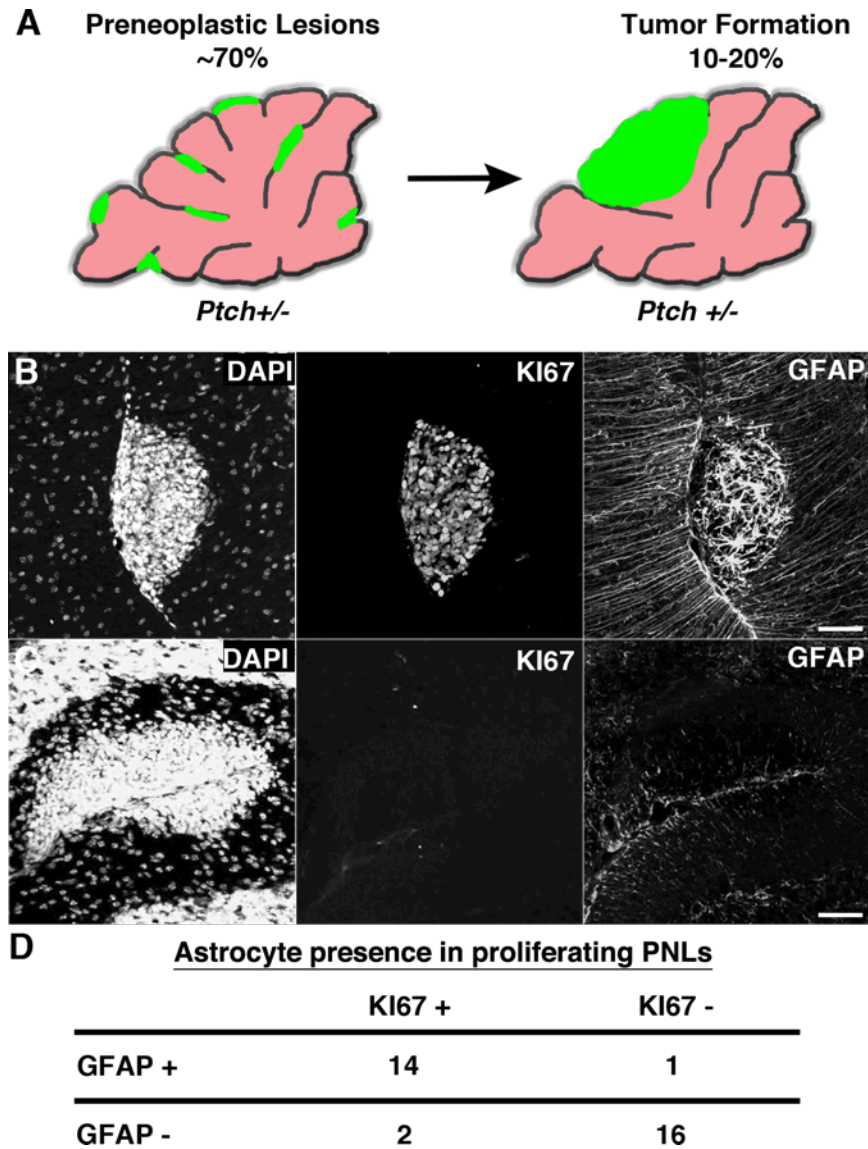


Figure 2.19 Astrocytes correlate with mutant GNP proliferation in early mutant cell expansions.

(A) Pre-neoplastic lesions (PNLs are small accumulations of GNPs on the surface of folia) occur at a 70% frequency in young cerebella of *Ptch*^{+/-} mice, but only 15-20% eventually form tumors (Oliver et al., 2005).

(B-C) Mutant GNPs (GFP⁺ from *Math1-Cre*; *MADM*) proliferate when GFAP⁺ astrocytes are present in PNLs (B), but are diminished when astrocytes are absent (C).

(D) Quantification of 33 different PNLs reveals a high correlation between PNLs with proliferating cells (Ki67⁺) and the presence of astrocytes (GFAP⁺).

[PNLs = pre-neoplastic lesions]

Scale bars: B-C = 50 μ m.

*Images and quantification provided by Maojin Yao.

Figure 2.20 Astrocyte presence varies in PNLs.

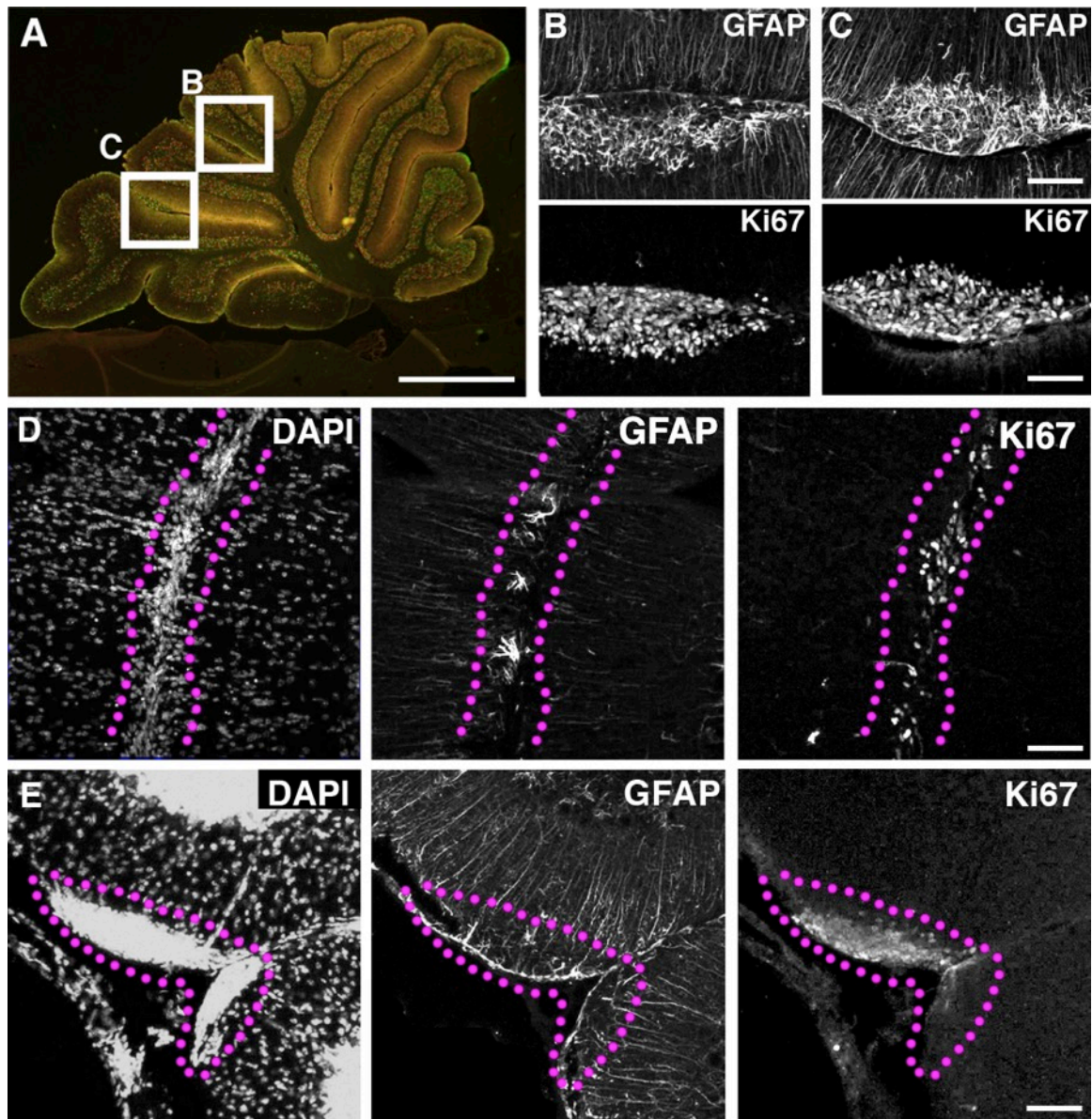


Figure 2.20 Astrocyte presence varies in PNLs.

(A-C) PNLs are defined by cell expansion at folia surface (A) and different PNLs in the same brain can proliferate in the presence of GFAP+ astrocytes (B,C).

(D) PNL (DAPI+) proliferation (right panel, Ki67+) can also occur while the presence of astrocytes is minimal (middle, GFAP+).

(E) Some PNLs with proliferating cells show no obvious presences of astrocytes.

Scale bars: A= 500 μ m, B-E= 50 μ m.

*Images provided by Maojin Yao.

2.7 Cultured astrocytes promote proliferation and suppress death and differentiation of tumor GNPs.

2.7.1 Normal astrocytes support wildtype GNP proliferation.

Genetic ablation of cerebellar astrocytes has highlighted the importance of their interaction with GNPs during development (Delaney et al., 1996b). Although migration deficits were suspected as the primary essential interaction, we wondered whether wild-type astrocytes support the growth of normal GNPs. We designed an *in vitro* co-culture assay to test this hypothesis. Wild-type astrocytes expressing *Aldh1L1-GFP* were isolated by means of fluorescence-activated cell sorting (FACS) from the cortices of perinatal mice, cultured to obtain a pure population, and then seeded onto coverslips for co-culture with purified wild-type RFP+ GNPs (Figure 2.30A). To assess proliferation, a short 3-hour EdU pulse was applied, which incorporates into synthesizing DNA of cells in S-phase of the cell cycle. In three separate experiments, GNPs co-cultured with astrocytes tended to double in proliferation rate compared to GNPs cultured alone (Figure 2.30B).

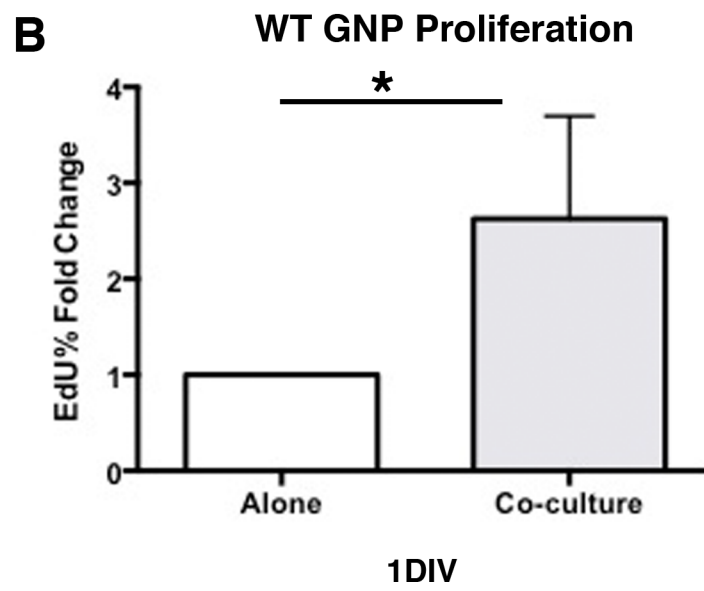
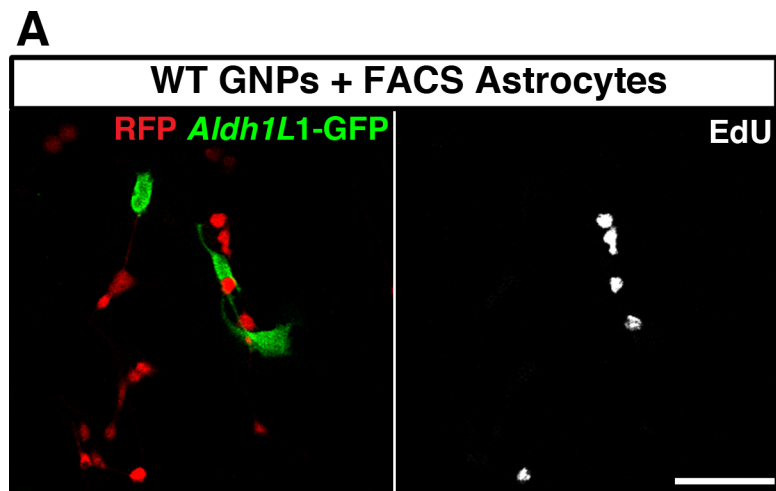
Figure 2.30 Normal astrocytes support wildtype GNP proliferation *in vitro*.

Figure 2.30 Normal astrocytes support wildtype GNP proliferation *in vitro*.

(A) Normal astrocytes were isolated from perinatal cortex of *Aldh1L1-GFP* mice and co-cultured with wildtype RFP+ GNPs. A short 3-hour EdU-pulse labeled cells that were actively proliferating. GNPs cultured alone were used as a control.

(B) Quantification of %EdU+ GNPs is represented as x-fold change in co-cultures normalized to GNPs cultured alone, set as 1 (Alone = 1, Co-culture = 2.62, $n=3$, $p= 0.027$).

Scale bars: A = 50 μ m.

*Performed by Dr. Ying Jiang.

2.7.2 Normal astrocytes support tumor GNP proliferation.

To further probe the nature of astrocytic support to tumor GNPs we performed co-culture experiments with wild-type astrocytes. We analyzed three possible fates of tumor GNPs, proliferation, cell death, and differentiation. First we sorted *Aldh1L1-GFP* astrocytes and co-cultured them with acutely purified RFP+ tumor GNPs. Astrocytes were seeded at 20,000/coverslip and tumor GNPs at 100,000, and cultured for 1, 3, and 6 days. We observed that tumor GNPs fully intercalated with astrocytes. In contrast, tumor GNPs cultured alone tended to aggregate (Figure 2.31A). This suggests that astrocytes provide favorable physical interactions for tumor GNPs.

To assess whether astrocytes influenced tumor GNP proliferation, a short 3-hour pulse of EdU was applied prior to fixation and quantified (Figure 2.31B shows representative EdU staining, arrowheads). Quantifications are represented as a percentage of the number of RFP+/EdU+ cell divided by the total number of RFP+ cells. Although the proliferation rate of tumor GNPs co-cultured with astrocytes was not significantly different at 1DIV compared to tumor GNPs alone (22% alone vs. 31% co-culture EdU+ tumor cells), a significant increase in proliferation of co-cultured tumor GNPs was evident at 3DIV (23% alone vs. 39% co-culture EdU+, * $p=0.025$, $n=3$) and 6DIV (34% alone vs. 53% co-culture EdU+, * $p=0.031$, $n=3$) (Figure 2.31C). These data indicate that normal astrocytes support tumor GNP proliferation.

The proliferative increase of tumor GNPs in co-cultures was inversely correlated with cell death over time compared to tumor GNPs alone (Figure 2.31D). Cell death was determined by punctate pyknotic nuclei in DAPI-stained samples (Figure 2.31B, circled). Cell death was significantly decreased in co-cultures compared to tumor GNPs alone at 3 DIV (47% alone vs. 23% co-culture, $*p=0.042$, $n=3$) and at 6 DIV (57% alone vs. 21% co-culture, $**p=0.0035$, $n=3$) (Figure 2.31D). The decrease from 3 to 6DIV in the co-culture suggests astrocytes may suppress cell death.

Finally, we assessed neuronal differentiation in co-cultures. It is uncommon for tumor GNPs to differentiate toward the astrocyte lineage in this culture condition as massive cell death occurs too quickly. To assess neuronal differentiation of tumor GNPs we immunostained for the neuronal marker Tuj1, a cytoskeletal protein in the processes of mature neurons (Figure 2.31B). We quantified the neuronal phenotype at 3 and 6 DIV, but not at an earlier timepoint, because 1DIV was not long enough for GNPs to mature into neurons. There was a significant difference in the neuronal differentiation of tumor GNPs when cultured alone compared to co-cultured at 6DIV (12% alone vs 1% co-culture, $*p=0.012$, $n=3$) (Figure 2.31E). Overall these data indicate that normal astrocytes support tumor GNP proliferation and suppress both cell death and differentiation.

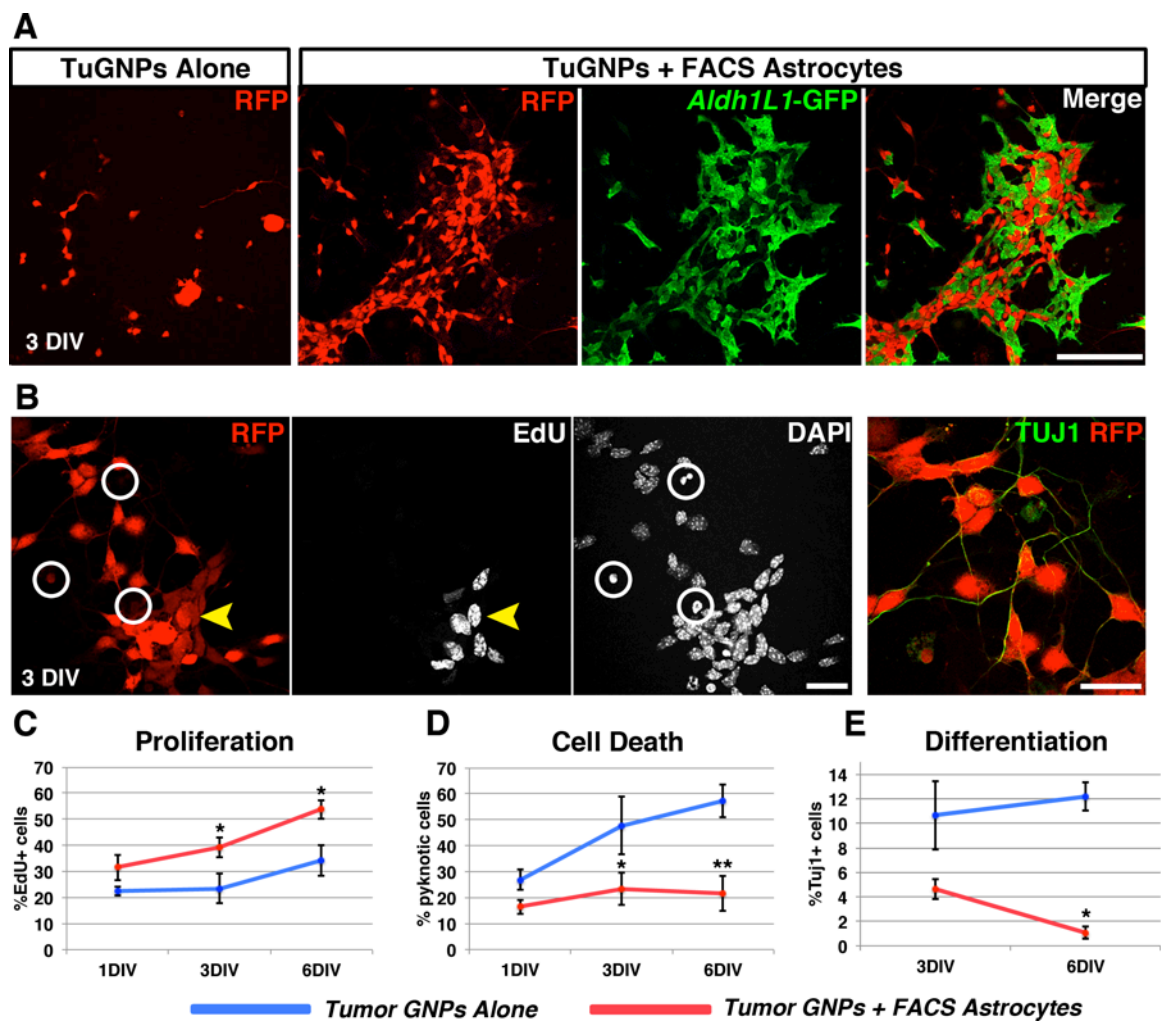
Figure 2.31 Normal astrocytes support tumor GNP proliferation *in vitro*.

Figure 2.31 Normal astrocytes support tumor GNP proliferation *in vitro*.

(A) RFP+ tumor GNPs were co-cultured with sorted *Aldh1L1-GFP* astrocytes or alone for 1,3, and 6 DIV (3DIV shown here).

(B) Representative images of RFP+ tumor GNPs cultured alone for proliferation (EdU+), cell death (pyknotic nuclei from DAPI stain), and neuronal differentiation (TUJ1 in processes).

(C) Proliferation determined by RFP+ EdU+ cells divided by total RFP+ cells. 1DIV alone 22% vs. co-culture 31%, *n.s.* $p=0.267$, 3DIV alone 23% vs. co-culture 39%, $*p=0.025$, 6DIV alone 34% vs. co-culture 53%, $*p=0.031$.

(D) Cell death determined by DAPI+ pyknotic nuclei divided by total RFP+ cells. Cell death was also assessed in astrocyte only cultures and represented <1% of DAPI+ cells, therefore the contribution of dead astrocytes would not significantly change cell death assessment in co-cultures using this method.

1DIV alone 26% vs. co-culture 18%, *n.s.* $p=0.202$, 3DIV alone 47% vs. co-culture 23%, $*p=0.042$, 6DIV alone 57% vs. co-culture 21%, $*p=0.003$.

(E) Neuronal differentiation determined by RFP+ TUJ1+ cells divided by total RFP+ cells. Mature phenotype needed for TUJ1 detection is >1DIV, therefore this timepoint was not analyzed.

3DIV alone 10% vs. co-culture 4%, *n.s.* $p=0.193$. 6DIV alone 12% vs. co-culture 1%, $*p=0.012$.

Scale bars: A= 100 μ m, B= 20 μ m.

2.7.3 Culture-derived tumor astrocytes (TuAstros) support tumor GNP viability.

To test whether TuAstros directly support tumor GNPs we designed a unique co-culture assay. Due to the small number of TuAstros in the tumor mass (~1% of total cells, Figure 2.10C), we tested multiple methods for the isolation and culture of TuAstros. First, we incorporated the *Aldh1L1-GFP* transgene into our RFP lineage-traced medulloblastoma model and attempted to use FACS to purify GFP-positive/RFP-positive TuAstros from whole tumor lysates. Unfortunately, no cells survived in culture, likely due to mechanical stresses throughout the lengthy sorting process that was necessary as a consequence of the low abundance of tumor astrocytes in whole tumor preparations. To reduce the duration of the sorting procedure we used a Percoll gradient to remove most of the tumor GNPs (bottom fraction) prior to sorting the top fraction that contained TuAstros (Figure 2.15A). However, cell viability was still too low to perform co-culture assays. To determine if low cell viability was due to tissue trituration or FACS, we simply cultured the upper fraction of the Percoll gradient separation, which retained TuAstros. The TuAstros survived poorly under these conditions, with only 0.1-0.4% of initial RFP-positive *Aldh1L1-GFP*-positive TuAstros surviving after 3 DIV (5-20 TuAstros remained per coverslip). Therefore, the culture conditions and the process of tumor tissue trituration greatly compromised cell viability, which is likely further decreased with FACS. This left us with the next best option, *in vitro* differentiation of tumor GNPs into TuAstros.

First, we cultured purified tumor GNPs in a medium containing heparin-binding epidermal growth factor (HB-EGF) to promote astrocyte survival (Foo et al., 2011) (Figure 2.32A). After at least 3DIV a small percentage of tumor GNPs differentiated into astrocyte-like cells (0.8-1.4% of initial seeded tumor GNPs = ~100 TuAstros per coverslip) (Figure 2.31B). The majority of the remaining tumor GNPs died in this medium. Second, we determined whether these culture-derived TuAstros resembled TuAstros in tumor tissue. We assessed the expression of GFAP in astrocytic cells that displayed a characteristic fan-like morphology (Figure 2.33A-B). We observed that the majority of cells (50-75%) throughout experiments were GFAP-positive (Figure 2.33C). Culture-derived TuAstros exhibited characteristic astrocyte morphology and expressed a marker of native tumor astrocytes. Therefore, we used these cells as surrogates for native TuAstros in subsequent co-culture assays.

Next, we performed a co-culture assay with tumor GNPs to determine if TuAstros support growth of tumor GNPs. For visual clarity we purified *Math1-GFP*-positive tumor GNPs to seed at low density (50,000 cells per coverslip) onto RFP+ TuAstros (Figure 2.32C, 2.34A). Following brief culture (2 h), we assessed the distribution of GNPs on tumor astrocytes. We found that GNPs were evenly distributed at this early time point and could divide (determined by EdU pulse for 2 h) regardless of their proximity to red TuAstros (Figure 2.34B). Given that there were so few TuAstros, after longer incubations of co-culture (3 DIV), we expected two possible outcomes (Figure 2.32D, 2.35A). If TuAstros do not provide local

support for tumor GNPs, then tumor GNPs would proliferate in aggregates irrespective of TuAstro proximity. On the other hand, if TuAstros provide local support to tumor GNPs, then tumor GNPs would localize to TuAstros and proliferate (Figure 2.35A). Our data support the second possibility: tumor GNPs adjacent to TuAstros survived and proliferated (Figure 2.35B), while those away from TuAstros exhibited a lower rate of survival and proliferation. We quantified the correlation between survival of tumor GNPs within 30 μ m to TuAstros, and found a strong correlation (78% <30 μ m of TuAstros vs. 22% >30 μ m from TuAstros, $n=3$, $*p=0.030$) (Figure 2.35C). Furthermore, more than half of tumor GNPs adjacent to TuAstros were proliferating, and those not associated with TuAstros had a significantly reduced proliferation rate (53% EdU+ <30 μ m to TuAstros vs. 27% >30 μ m from TuAstros, $n=3$, $*p=0.028$) (Figure 2.35D). These data support the hypothesis that TuAstros promote tumor GNP survival and proliferation.

In addition to fixed timepoint experiments, we also performed live imaging to visualize the dynamics of tumor GNP survival and proliferation in TuAstro co-cultures. With the same experimental setup as previously described (Figure 2.32A-C), we began brightfield live imaging following the addition of GFP-positive tumor GNPs onto RFP-positive TuAstros at 2 h intervals over the course of 48 h. An initial fluorescent image confirmed distribution of tumor GNPs randomly over TuAstros, with tumor GNPs settling both close to and far from TuAstros (Figure 2.36A, red box = >30 μ m beyond TuAstros, green box = <30 μ m to TuAstros). We

then identified RFP+ TuAstros, based on their characteristic astrocytic morphology and assessed GFP-positive tumor GNP migration and proliferation. We tracked tumor GNPs over time and made several observations. 1) GNPs that initially settled on top of TuAstros survived and proliferated (Figure 2.36C). 2) GNPs within a 30 μ m distance of TuAstros tended to migrate toward TuAstros and often aggregated with GNPs already on TuAstros (Figure 2.36E). 3) Of tumor GNPs that were farther than 30 μ m from TuAstros, some underwent at least a single division, but most eventually died (Figure 2.36B,E). We quantified the migration and proliferation of tumor GNPs that were either within, or beyond 30 μ m of a TuAstro at 0 h and 48 h time points (Figure 2.36E, diagrams). We found that the number of GNPs within 30 μ m of TuAstros more than doubled over 48 hours, but the GNP number beyond 30 μ m decreased by 50% due to cell death (Figure 2.36F). The survival and proliferation phenotype was specific to TuAstros, because co-culturing tumor GNPs with NIH-3T3 fibroblasts did not promote survival of tumor GNPs (Figure 2.36G). These real time data indicate that TuAstros support the growth of tumor GNPs by means of cell-to-cell contact.

Figure 2.32 Experimental design for tumor astrocyte and tumor GNP co-culture.

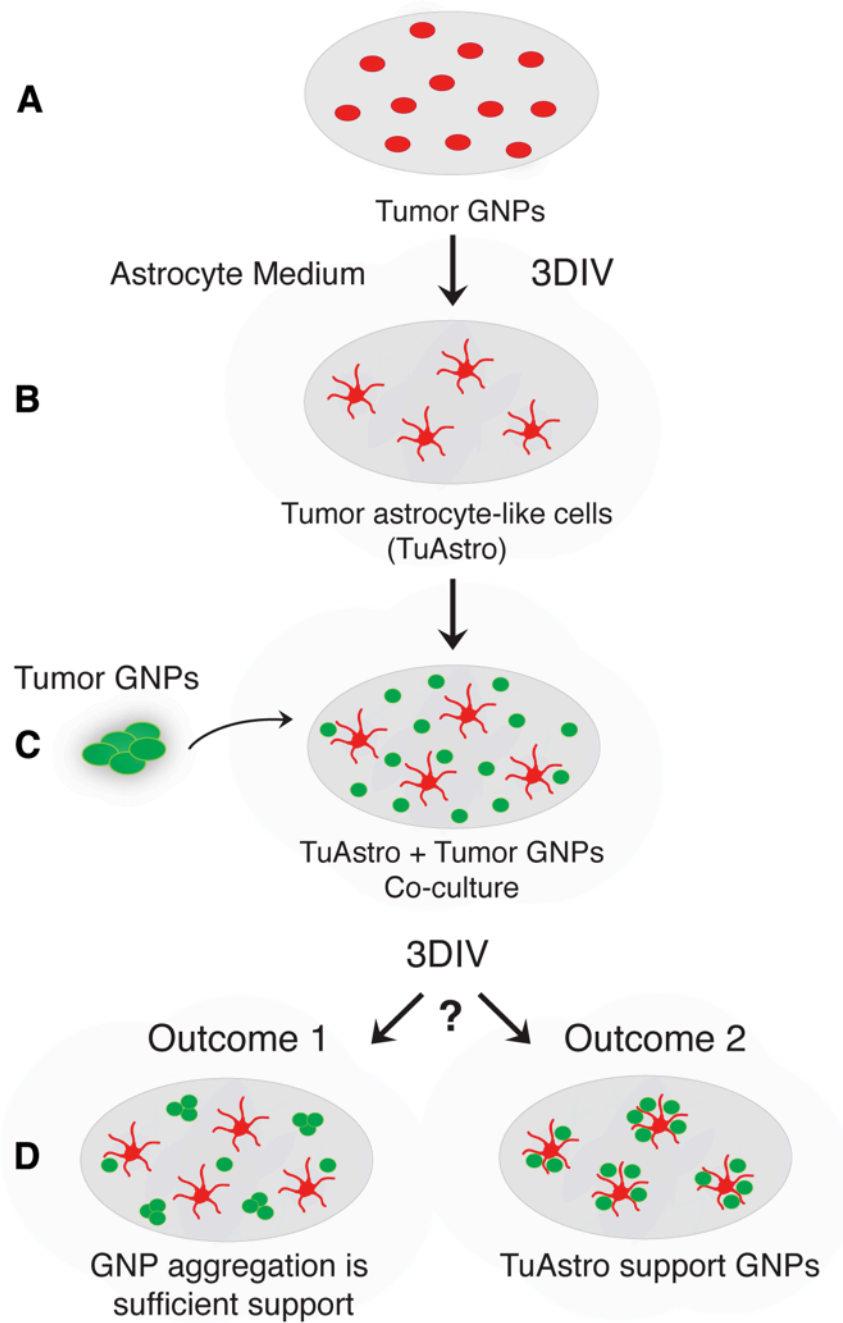


Figure 2.32 Experimental design for tumor astrocyte and tumor GNP co-culture.

(A) RFP+ tumor GNPs were acutely purified through a Percoll gradient and seeded at 500,000/coverslip in astrocyte growth medium for 3DIV. Most cells die and were removed by vigorous shaking and tapping of the plate.

(B) Following removal of dead and lightly attached cells, tumor “astrocyte-like” cells (TuAstros) remained attached (0.8-1.4% of initial tumor GNPs seeded).

(C) *Math1-GFP* tumor GNPs were purified and seeded onto TuAstros at 100,000 cells/coverslip for 3DIV.

(D) We predicted two possible outcomes following short-term culture. Outcome 1 predicts that tumor GNPs would aggregate and grow irrespective of proximity to TuAstros. Outcome 2 predicts that tumor GNPs would localize to TuAstros and proliferate, suggesting TuAstros provide growth factors or substrate support.

Figure 2.33 Culture-derived tumor astrocytes.

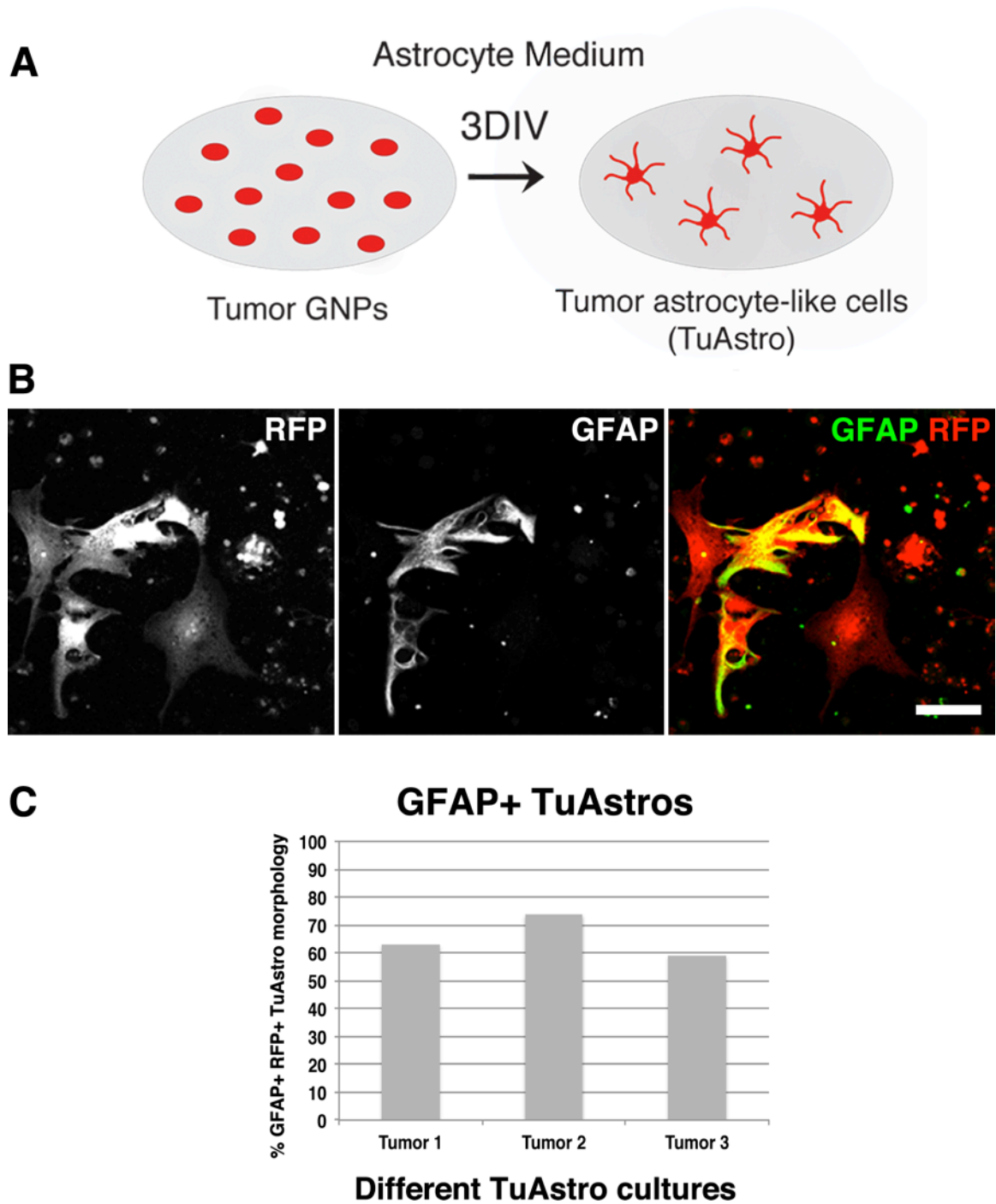


Figure 2.33 Culture-derived tumor astrocytes.

(A) Transdifferentiation of tumor GNPs into culture-derived TuAstros.

(B) Astrocytic nature of culture-derived TuAstros was assessed with GFAP immunostaining.

(C) Quantification of RFP+ GFAP+ TuAstros. Putative TuAstros were analyzed for GFAP expression based on fan-like astrocytic morphology in contrast to small, rounded tumor GNP morphology. In three separate experiments, the number of GFAP+ RFP+ cells was divided by the total RFP+ cells with TuAstro morphologies and ranged from 59-73% of the population.

Scale bars: B = 50 μ m.

Figure 2.34 Tumor GNPs were evenly distributed and proliferated when seeded on tumor astrocytes.

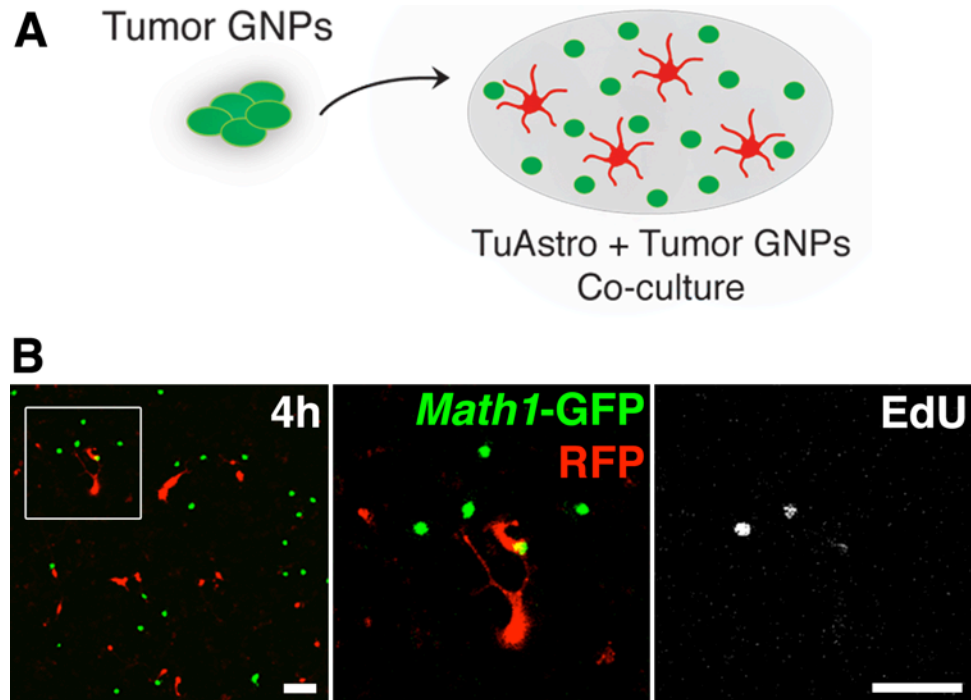


Figure 2.34 Tumor GNPs are evenly distributed and proliferating when seeded on tumor astrocytes.

(A) *Math1-GFP* tumor GNPs were purified and seeded at 50,000 cells per TuAstro coverslip.

(B) Initial seeding distribution and proliferative capacity of tumor GNPs. Tumor GNPs were evenly distributed across coverslip, located both on and away from TuAstros. A short 3-hour EdU pulse labeled proliferating cells, and EdU+ cells were dispersed throughout the coverslip.

Scale bars: A-B = 50 μ m.

Figure 2.35 Tumor astrocytes support tumor GNP proliferation and survival.

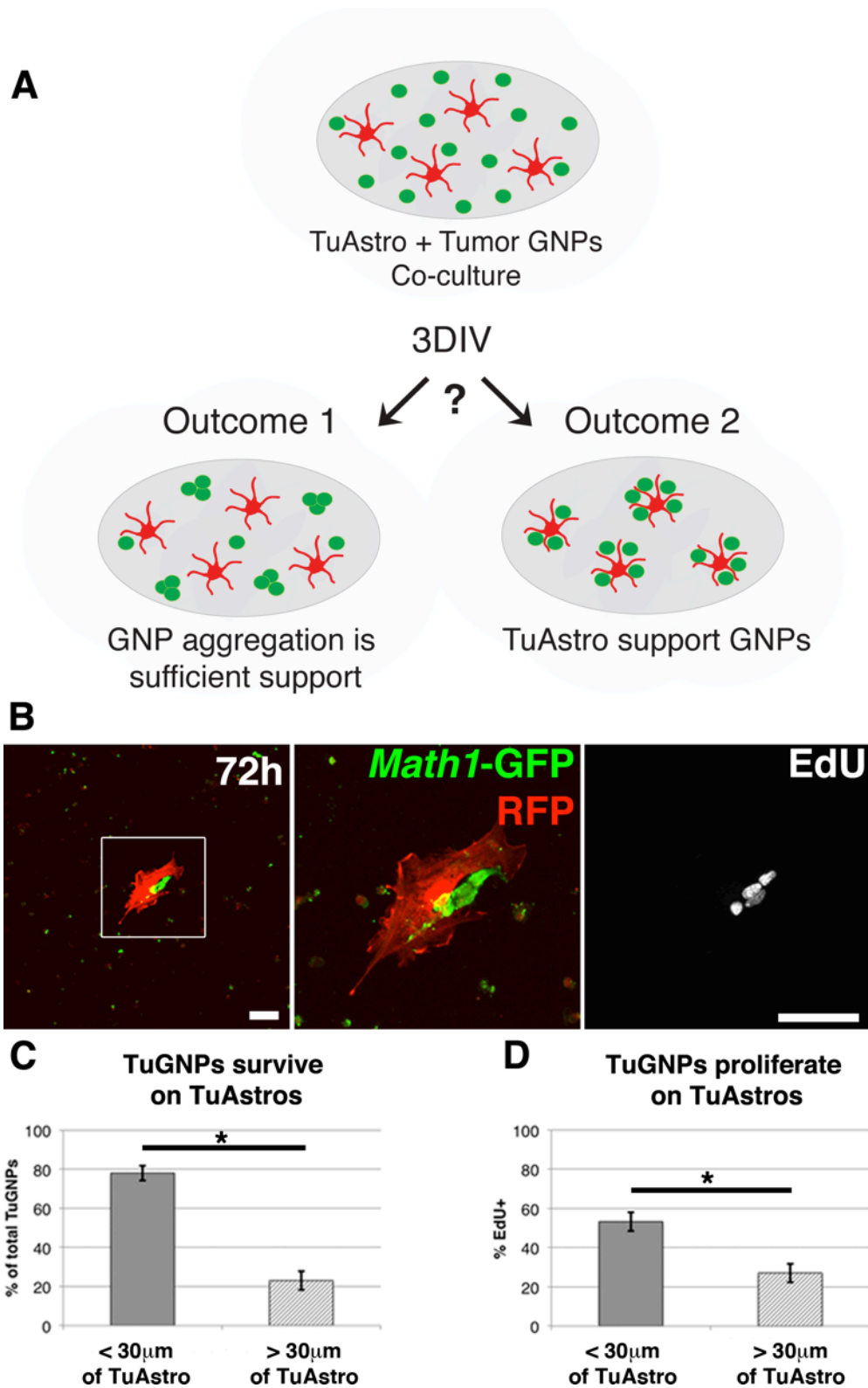


Figure 2.35 Tumor astrocytes support tumor GNP proliferation and survival.

(A) Following 3DIV, two outcomes were predicted for the TuAstro influence on tumor GNPs: 1) tumor GNP aggregation would be sufficient for growth support, or 2) tumor GNPs would localize and growth on TuAstros.

(B) After 3DIV, co-cultures were assessed for tumor GNP localization and proliferation. Tumor GNPs localized to TuAstros and were proliferating (EdU+).

(C) The tumor GNP population was analyzed for association with TuAstros. The majority of surviving tumor GNPs was located within 30 μ m of TuAstros (78% <30 μ m of TuAstros vs. 23% >30 μ m from TuAstros, * $p=0.030$, $n=3$).

(D) Proliferation of tumor GNPs was determined by the number of GFP+ EdU+ <30 μ m or >30 μ m of TuAstros divided by the total number of GFP+ cells (53% <30 μ m TuAstros vs. 27% >30 μ m TuAstros, * $p=0.028$).

Scale bars: B = 50 μ m.

Figure 2.36 Co-culture live imaging: Tumor GNPs migrate toward and proliferate on tumor astrocytes.

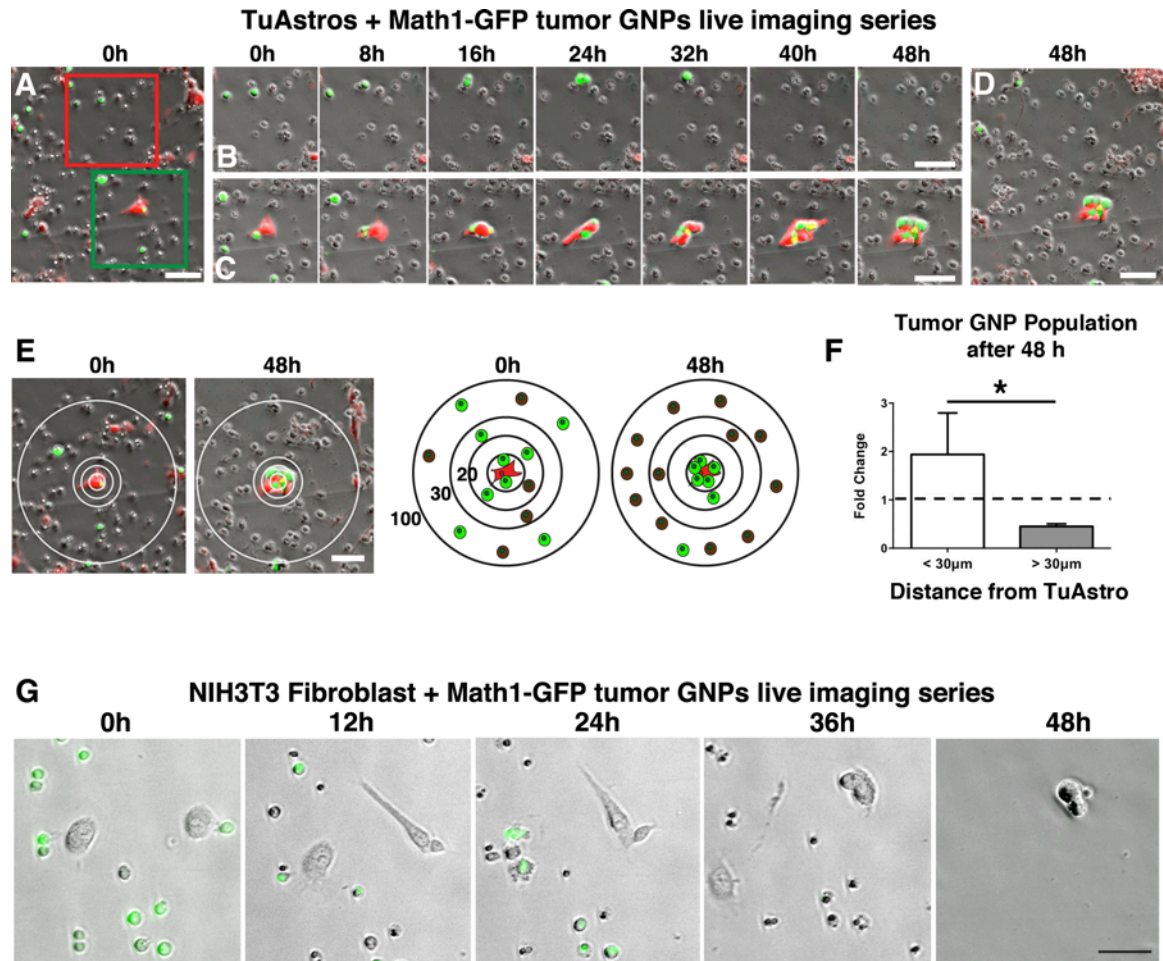


Figure 2.36 Co-culture live imaging: Tumor GNPs migrate toward and proliferate on tumor astrocytes.

(A) Initial brightfield and fluorescent composite image at time 0-hour. Note that some tumor GNPs were located at a distance TuAstros (red box, magnified in B) and others were close to or on TuAstros (green box, magnified in C). Live imaging was performed for 48-hours and shown at 8-hour intervals.

(B) Tumor GNPs located beyond 30 μ m of TuAstros were seen to aggregate (16-24h) and eventually die by 48h. Cells with a lack of iridescence suggest they are dead.

(C) Tumor GNPs migrate to (8-16h) and proliferate on (32-48h) TuAstros.

(D) After 48h, only tumor GNPs associated with TuAstros survive and proliferate (GFP+ cells on RFP+ TuAstros).

(E) Tumor GNPs within 100 μ m of a TuAstro at 0h were tracked for 48h to measure either migration toward TuAstro or cell death, depending on proximity to TuAstros. Tumor GNPs within 30 μ m of a TuAstro migrated and survived, while those beyond 30 μ m died (cartoon schematic of findings).

(F) Quantification of tumor GNP survival depending on distance from TuAstro.

The initial number of GNPs is set at 1 (dotted line) and an increase to 2 would represent a doubling of population size, i.e. the GNPs within 30 μ m, whereas a decrease in the population would be less than 1, i.e. the GNPs beyond 30 μ m of a TuAstro. (<30 μ m of TuAstro = 1.7 fold-increase vs. >30 μ m from TuAstro = 0.45 fold-decrease, * $p=0.011$, $n=>20$ counting fields).

(G) Tumor GNP survival and proliferation was specific to TuAstros, as tumor GNPs died over time when they were plated on NIH3T3 fibroblasts (loss of GFP+ cells from 0-48h).

Scale bars: A,D,E,G = 50 μ m, B,C = 20 μ m.

*Images and quantification provided by Dr. Jennifer Munson.

2.7.4 Testing whether astrocyte support is mediated through secreted factors or membrane-associated interactions.

While it's evident that astrocytes provide critical support for tumor GNPs, the mechanisms responsible for this support remains unknown. To narrow down the search, we investigated whether the mode of support is through secreted factor(s) or membrane-associated interactions.

To test if astrocytes support tumor GNPs through the secretion of growth factors, we performed a transwell co-culture assay (Figure 2.37A) and a conditioned media assay. For the transwell assay, sorted *Aldh1L1-GFP* normal astrocytes were seeded into the top of a transwell insert that only allows diffusion of proteins through a porous membrane. Tumor GNPs were seeded at 100,000 cells per coverslip beneath the insert. After 3DIV, transwells were removed in order to fix and stain the coverslips. However, the tumor GNPs were not attached to the coverslip and instead were seen floating in aggregates (Figure 2.37B). The aggregate number and size appeared similar between astrocyte transwells and empty transwell controls. A technical problem with the transwell assay was the observation that tumor GNPs formed aggregates in empty transwells as well, when they should have grown in a monolayer similar to tumor GNPs cultured alone in Figure 2.31A. This suggests that the transwell itself may change the fluid dynamics within the well prohibiting tumor GNP adherence and growth in a monolayer. To circumvent this problem we tested whether astrocyte-conditioned medium could support tumor GNP proliferation.

To determine if astrocyte-conditioned medium (ACM) contained labile growth factors we cultured tumor GNPs alone in the conditioned medium. The medium was changed daily for 3DIV in ACM and control wells. Again, we did not observe a difference in tumor GNP number when cultured in ACM or normal medium. These observations suggest that the mode of astrocyte support is not likely mediated through secreted growth factors, but perhaps through membrane-associated interactions. Live cell imaging of TuAstro co-cultures also suggested that astrocyte support is mediated by membrane-associated interactions as tumor GNP proliferation and survival depended on their contact with TuAstros.

To test if astrocyte support of tumor GNP proliferation was mediated by membrane-associated interactions, it was critical to generate astrocytes with intact membrane proteins but without the ability to secrete additional proteins. To achieve this, we tried to lightly fix astrocytes prior to co-culture with tumor GNPs. Normal astrocytes (*Aldh1L1-GFP*) were fixed with 1% paraformaldehyde for 15 minutes and then washed extensively to remove residual paraformaldehyde (Lim and Alvarez-Buylla, 1999). Tumor GNPs were seeded onto fixed astrocyte membranes and assessed for proliferation with a 3-hour EdU pulse prior to fixation at 2 DIV. There was no obvious localization of EdU-positive tumor GNPs (RFP+) onto remaining astrocytes and the distribution was similar to tumor GNPs cultured without fixed astrocytes (Figure 2.38A-B). One possible explanation for this observation is that fixation may have prevented the membrane proteins from interacting with tumor GNP surface proteins. Thus, it is still possible that bioactive

astrocyte membrane proteins could promote survival and proliferation of tumor GNPs, but we could not make definitive conclusions from this experiment. Again, because we used normal astrocytes in this and the transwell assays, normal astrocytes may not reflect the functional mechanisms of *in vivo* tumor astrocytes. Future studies should investigate the contribution of astrocytes toward tumor GNP growth and will be discussed in Chapter 3.

Figure 2.37 Astrocyte transwells were unable to test if astrocyte support mechanism was through secretion of growth factors.

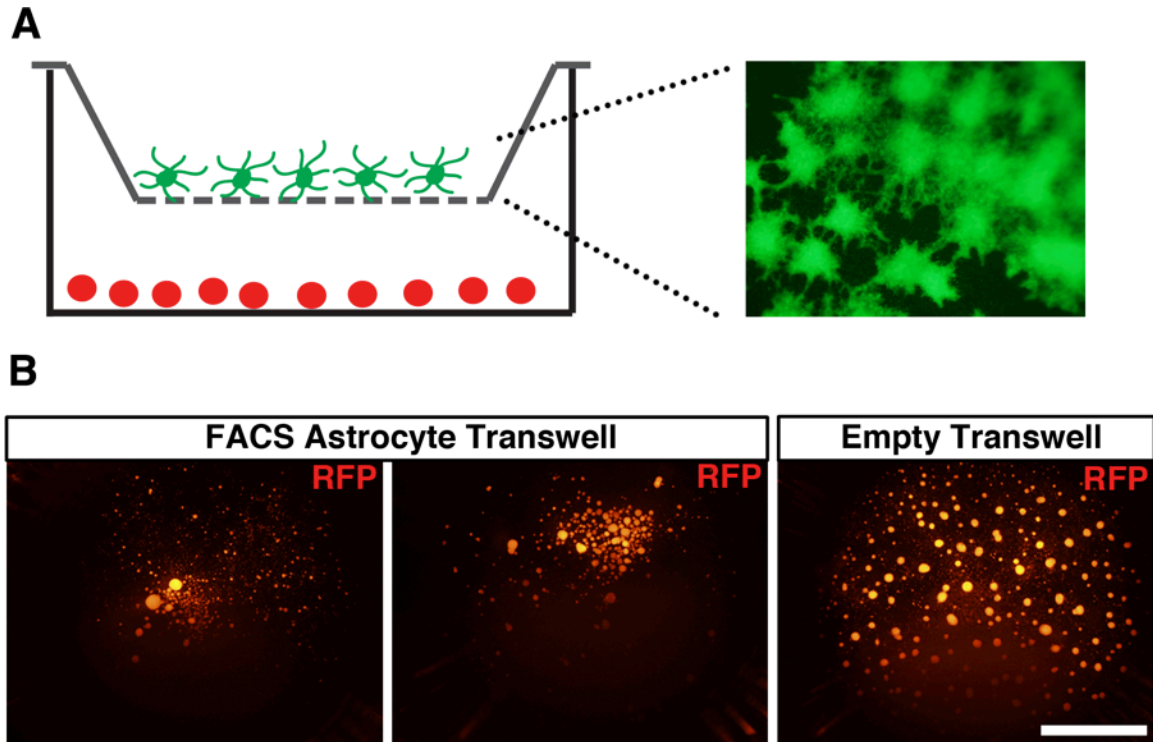


Figure 2.37 Astrocyte transwells were unable to test if astrocyte support mechanism was through secretion of growth factors.

(A) Normal astrocytes (*Aldh1L1-GFP*) were seeded onto the porous membrane insert over RFP+ tumor GNPs and cultured for 3DIV.

(B) Tumor GNPs formed floating aggregates in transwells. Viewing the entire well, there was no obvious difference in aggregate numbers or size between astrocyte transwells and control empty transwells.

Scale bar: 500 μ m.

Figure 2.38 Testing whether astrocyte support is mediated through membrane-associated interaction.

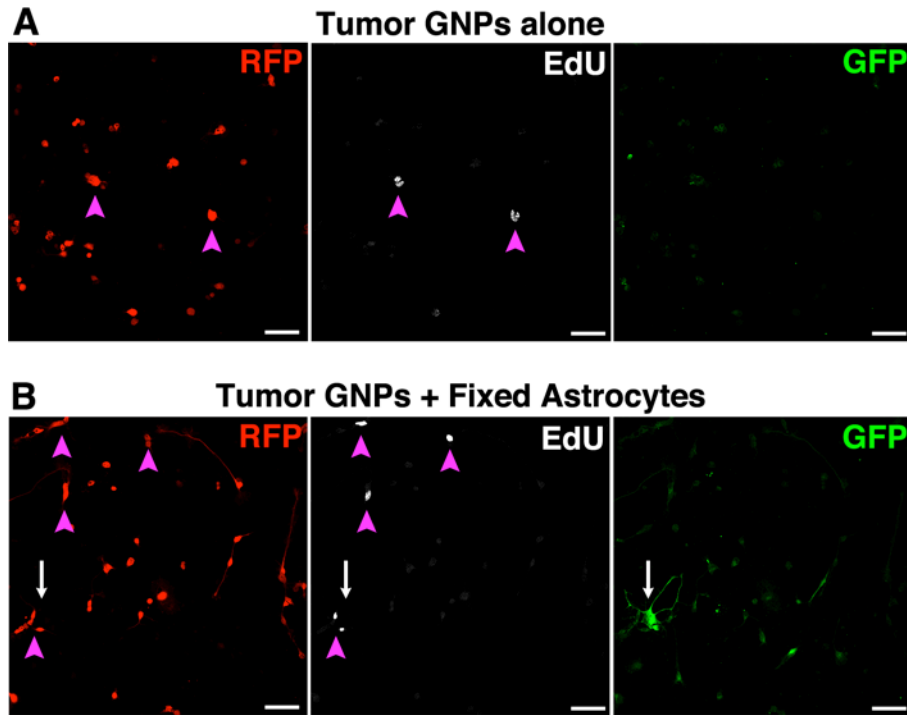


Figure 2.38 Testing whether astrocyte support is mediated through membrane-associated interaction.

(A) Tumor GNPs (RFP+) cultured alone for 3DIV with EdU-pulse to reveal actively proliferating cells.

(B) Tumor GNPs cultured on fixed astrocyte membranes do not show localization to astrocytes and proliferation is not dependent on proximity to astrocytes.

Scale bars: A-B = 50 μ m.

2.3 Discussion

Solid tumors are composed of many cell-types, where intimate interactions in the tumor niche can propagate malignancy. Here, we have discovered a diverse cellular niche in medulloblastoma that includes at least tumor cells, blood vessels, microglia/macrophages, and oligodendrocyte progenitor cells. Surprisingly, we also found that some lineage-restricted tumor GNPs consistently transdifferentiate into astrocyte-like cells throughout tumor development (Figure 2.39). The astrocytic nature of TuAstros is reinforced by morphological, phenotypic, and functional similarities to normal astrocytes. Also, TuAstros present in the earliest tumor stage were highly correlated with mutant cell proliferation. Finally, culture-derived TuAstros promoted the survival and proliferation of tumor GNPs *ex vivo*. These findings highlight an underappreciated role for tumor-derived niche cells as a self-building support network for tumorigenesis.

Figure 2.39 The MADM medulloblastoma tumor niche.

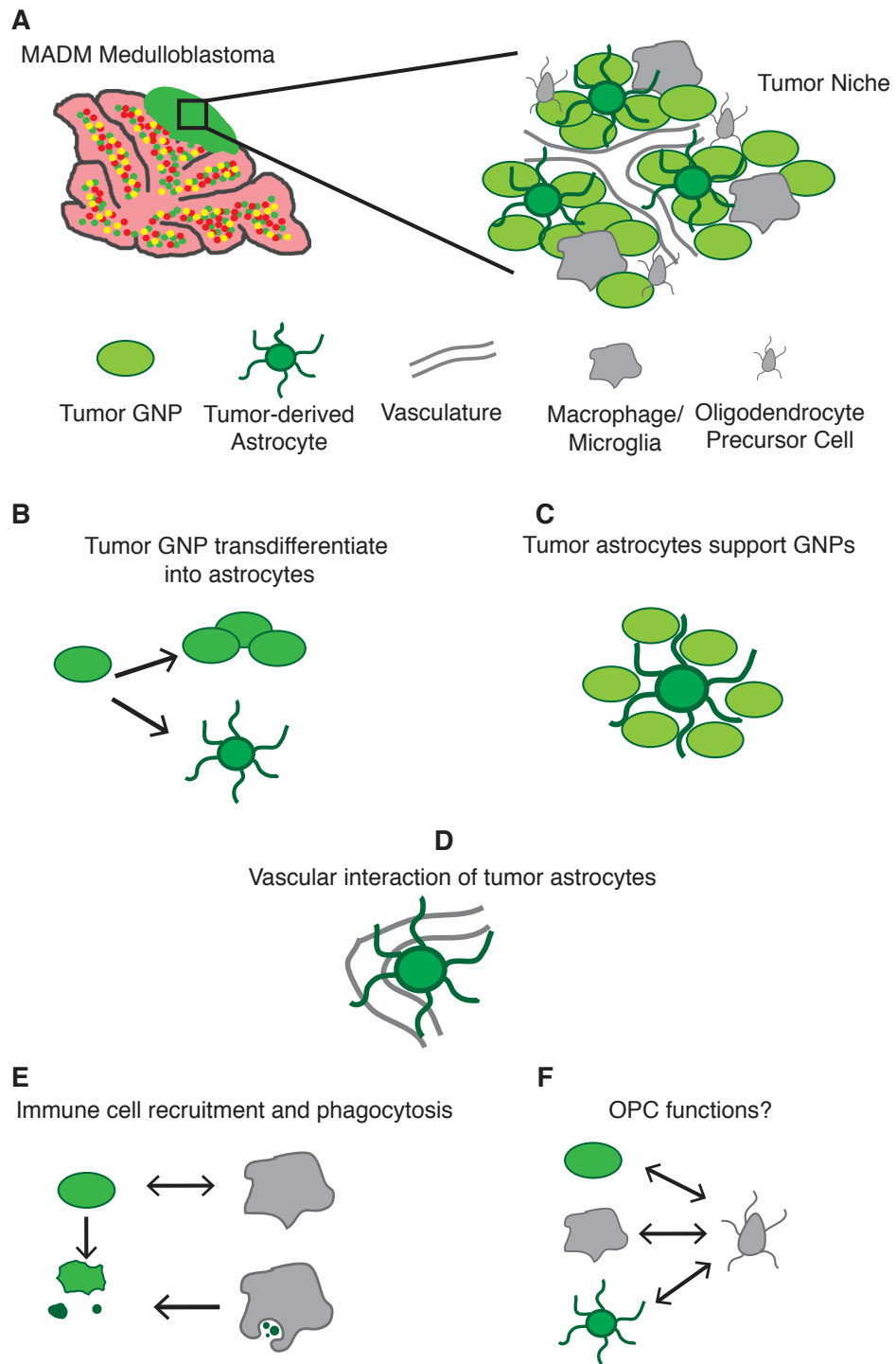


Figure 2.39 The MADM medulloblastoma tumor niche

- (A) The MADM model of medulloblastoma enabled characterization of tumor-niche cell types, with distinct GFP-labeling of the mutant GNP lineage.
- (B) Tumor GNPs were found to transdifferentiate into niche astrocytes within tumors.
- (C) Both in vivo and in vitro studies suggest that tumor-derived astrocytes support the survival and proliferation of tumor GNPs.
- (D) Tumor astrocytes were found in close contact with blood vessels throughout the tumor, which is similar to the behavior of astrocytes elsewhere in the brain.
- (E) Tumor-associated macrophages/microglia infiltrate into the tumor and were seen phagocytosing GFP⁺ tumor cells that were presumably dead.
- (F) OPCs were also observed throughout the tumor, yet their function in the tumor niche has not been studied.

2.D.1 MADM is a valuable tool to study tumor-niche interactions

While niche cells have been identified by pathological assessment in medulloblastoma, the establishment and function of the niche are not well understood. Mouse models that closely match the physiology of native tumors can provide important insights into these questions. To closely mimic the clonal origin of human cancer, an ideal model should allow medulloblastoma to develop from a small number of clearly labeled mutant cells. While commonly used conditional knockout models (CKO) with lineage tracing have been used to model medulloblastoma (Choi et al., 2012; Schüller et al., 2008; Yang et al., 2008), the MADM system offers several unique advantages. First, CKO models tend to generate large populations of mutant cells that greatly accelerate the transformation process, which could skew the formation of the tumor niche (Figure 1.5). In contrast, MADM generates many fewer mutant cells, from which focal neoplasia tends to form, closely mimicking the physiology of human tumor development. Second, sparse labeling of MADM provides superior resolution that allows one to locate very small lesions, including those that fail to progress further, as shown in Figure 2.19. Such spatial resolution allows the reconstruction of the entire process of niche establishment for deducing its function in tumor initiation, progression, and final transformation. Third, while findings from CKO models may have alternative explanations, MADM enables unequivocal interpretation of the data. For example, although transdifferentiation of tumor GNPs into astrocytes in CKO models could be achieved with Cre-mediated

lineage tracing of GNPs, the labeling of astrocytes could also be due to the promiscuity of the Cre promoter in the tumor mass. For example, aberrant activation of Cre could be caused by hypoxia and/or the presence of certain cytokines or growth factors from niche cells. In the MADM system, non-tumor derived astrocytes expressing *Math1-Cre* would appear yellow if they were not dividing, or as populations of green and red cells if they were dividing in the tumor mass (Zong et al., 2005). Since this was not observed in our model, as all TuAstros were strictly GFP-positive, we can firmly conclude that they were derived from tumor GNPs through a transdifferentiation mechanism.

2.D.2 Tumor GNP transdifferentiation generates true astrocytes.

Mutations in the cell of origin often perturb intracellular regulatory pathways that poise the cell for excessive proliferation and tumor formation. While the initial oncogenic event is necessary, progression toward a complex tumor often requires manipulation or creation of a supportive tumor niche. Here, initial perturbation of the SHH signaling pathway initiates mutant GNP hyperproliferation that eventually results in transdifferentiation to produce TuAstros from the earliest lesions throughout tumor development. Why do mutant GNPs do this? From a developmental perspective, GNPs in the EGL closely interact with astrocytic Bergmann glia to ensure proper maturation and possibly to support their proliferation, as we show in Figure 2.30. Therefore, when mutant GNPs accumulate on the cerebellar surface, where astrocytes are absent, the

supportive environmental context is missing and some mutant GNPs may transdifferentiate into astrocytes to fill the void. Here we have definitively characterized this transdifferentiation phenomenon throughout all tumor stages and further verified this event in human tumors.

Transdifferentiation has been shown to establish/contribute to the tumor niche in multiple cancers. Endothelial differentiation of cancer stem-like cells (CSCs) has been reported in leukemia, myeloma, neuroblastoma, and glioblastoma, as well as renal, ovarian, and breast cancers, (Alvero et al., 2009; Bussolati et al., 2008a; 2008b; Ricci-Vitiani et al., 2010; Rigolin, 2006; Shen et al., 2008; Soda et al., 2011; Streubel et al., 2004). Particularly in human glioma, it appears that CSC-to-endothelial transdifferentiation is a prominent event contributing to neovascularization and possibly chemoresistance (Soda et al., 2011). Here in medulloblastoma, we took a comprehensive approach to characterize the process of tumor GNP-to-astrocyte transdifferentiation, which was validated in human medulloblastoma. Yet further questions remain: 1) How does a subpopulation of GNPs acquire the ability to differentiate into astrocytes? 2) Does transdifferentiation occur through stochastic or programmed differentiation of tumor GNPs? 3) Is transdifferentiation extrinsically influenced or intrinsically determined?

How do certain tumor GNPs undergo astrocytic differentiation? There are two distinct mechanisms by which tumor GNP heterogeneity could manifest in astrocytic differentiation. First, retention of stem cell features in certain mutant

GNPs could persist through tumor development, as mutagenesis of GNPs begins during embryonic development. To test this hypothesis, we induced mutations in postnatal GNPs, when they are fully committed to become granule neurons, and still observed transdifferentiation in tumors. Therefore, it is unlikely that certain mutant GNPs retain embryonic stem cell features. However, it is a formal possibility that tumor GNPs could reacquire stem cell features upon additional genomic alterations. Second, it is possible that some tumor GNPs de-differentiate from a unipotent to multipotent state. Hence, if certain tumor GNPs are multipotent then we would expect differentiation into multiple cell lineages, including, but not limited to, neurons, astrocytes, and OPCs, with subsequent GFP lineage labeling from MADM. However, we only observed self-renewal and astrocytic differentiation, therefore de-differentiation is an unlikely mechanism and our observations favor direct transdifferentiation from tumor GNP to astrocytes.

Transdifferentiation can result from stochastic or pre-determined differentiation potentials in certain cells. During cerebellar development, GNP heterogeneity was been observed, where some GNPs showed transient GFAP promoter activity, yet astrocyte differentiation was not observed (Silbereis et al., 2010). Interestingly, it's possible this underlying glial phenotype manifested, through astrocytic differentiation, upon oncogenic transformation or morphogen saturation, as observed in *in vitro* studies (Okano-Uchida et al., 2004; Gao and Hatten, 1994). Is astrocytic differentiation of tumor GNPs stochastic or from

distinct GNPs? TuAstros were generated consistently throughout tumor development and across all regions of tumors, suggesting that a specific population of GNPs is maintained that can transdifferentiate. Further studies are needed to determine the distribution and extent of tumor GNP heterogeneity. An ideal approach would be intratumoral lineage tracing of GNPs with MADM, which I will elaborate on in Chapter 3.

Is transdifferentiation extrinsically influenced or intrinsically determined? Transdifferentiation can be induced through non-cell autonomous signaling from cancer cells to surrounding niche cells, such as the conversion of stromal fibroblasts into carcinoma-associated fibroblasts (Franco et al., 2010). For a number of reasons it is unlikely that extrinsic factors influence the direct transdifferentiation of tumor GNPs. First, orthografts of pure tumor GNPs formed secondary tumors in which certain tumor GNPs transdifferentiated into astrocytes. Second, when tumor GNPs were cultured alone, in the absence of exogenous factors, a subpopulation was seen to transdifferentiate. Therefore, the most probable hypothesis is that there are pre-determined intrinsic factors enabling transdifferentiation. To test this hypothesis, identifying a candidate gene expressed in a subset of tumor GNPs could afford loss- and gain- of function studies. However, the fact that transdifferentiation occurs at a low frequency (~1% of all tumor cells) means the tumor GNP subpopulation is also very small. Therefore, transcriptional analysis of the total tumor GNP population would likely result in signal dilution of this small subpopulation and prove difficult to isolate

candidates. One approach to circumvent this problem is the use of stochastic profiling from a pool of isolated GNP transcriptome data to identify unique candidates (Janes et al., 2010).

2.D.3 Astrocytes promote the growth and survival of tumor GNPs

While tumor GNP heterogeneity could explain a mode for transdifferentiation, the more important question is whether TuAstros functionally contribute to tumorigenesis. An appealing hypothesis is that TuAstros could serve as cancer stem cells. However, long-term lineage tracing of TuAstros demonstrated that only TuAstros were strongly labeled, suggesting they do not serve as stem cells in medulloblastoma (Figure 2.14,15). Therefore the more intriguing possibility is that TuAstros directly support tumor GNP growth dynamics. In normal cerebellar development, astrocytes are essential for proper histogenesis and ensuring granule neuron lineage development. Cerebellar astrocytes, namely Bergmann glia, have been shown to direct immature granule neuron migration inward through cell-cell interactions (Adams et al., 2002; Gao et al., 2009; Hatten and Liem, 1981). The necessity of these interactions was further supported when genetic ablation of Bergmann glia during cerebellar development resulted in a defect of inward migration of immature granule neurons (Delaney et al., 1996b). Furthermore, we found that cultured normal astrocytes could support the proliferation of the wildtype GNPs (Figure 2.30). Given the strong evidence that astrocytes were critical for normal GNP development, it is probable that

TuAstros support tumor GNPs. Indeed, tumor GNP proliferation and survival were enhanced in the presence of both culture-derived TuAstros and wildtype astrocytes *in vitro*. Similar cell culture studies have found that astrocytes also promote the self-renewal and survival of neural progenitors to sustain adult neurogenesis, yet definitive factors remain to be fully characterized (Lim and Alvarez-Buylla, 1999; Song et al., 2002). Further studies are warranted to identify candidate factors secreted from TuAstros that sustain tumor GNP dynamics in addition to other factors that could influence the niche development for targeted therapeutic research and development.

2.D.4 Concluding remarks and perspectives: a self-building tumor niche reveals increased complexity in tumor development

With a blueprint of the medulloblastoma niche and the discovery of an intriguing transdifferentiation phenomenon, we can begin to further probe into these complex niche interactions. The fact that the presence of astrocytes appears to be important for supporting the earliest mutant GNP expansion suggests this interaction is essential for tumor initiation and perhaps tumor maintenance. Furthermore, the close interaction of TuAstros with tumor vasculature also points to additional potential functions that regulate and perhaps maintain the integrity of nutrient dynamics in tumor development. Future mechanistic studies should reveal both the nature of tumor GNP transdifferentiation, which may identify unique targets to block this event, and

how TuAstros can contribute to niche development. Finally, investigating the mechanisms of TuAstros support toward tumor GNP growth and other niche cells could reveal molecular targets amenable to therapeutic intervention and ultimately to better treatment options in medulloblastoma.

Chapter 3 – Perspectives

In this thesis project, I have described a unique niche in medulloblastoma, where niche astrocytes are transdifferentiated from tumor GNPs. Furthermore, tumor-derived astrocytes provide critical support to promote tumor GNP growth. The observations made here invoke many intriguing questions. What mechanisms govern tumor GNP transdifferentiation into astrocytes? What is the role of transdifferentiation in tumor development? Do tumor astrocytes secrete growth factors and extracellular matrix components to promote tumor GNP proliferation? Do tumor astrocytes function to support other niche cells, such as blood vessels or microglia? Now, with a blueprint of tumor niche cell composition at distinct tumor stages, we can begin to address these questions. Ultimately, understanding the molecular mechanisms driving tumor GNP transdifferentiation and the functional contribution of tumor astrocytes will provide a framework for designing targeted therapies against tumor niche mechanisms to treat medulloblastoma more effectively.

3.1 Does tumor GNP heterogeneity enable transdifferentiation?

3.1.1 Is tumor GNP transdifferentiation stochastic or determined?

It is puzzling why only a small portion of tumor GNPs (~1%) transdifferentiate into TuAstros. This could be the result of either stochastic or pre-determined mechanisms. By definition, stochastic differentiation is a random process that does not necessarily follow a temporal or spatial pattern. The

following observation suggests that tumor GNP transdifferentiation may not be entirely due to stochastic differentiation. We observed that the number of tumor astrocytes is maintained at a constant ratio to tumor cells throughout the course of tumor development (Figure 2.9). This observation implies that there may be deterministic mechanisms driving transdifferentiation in a controlled manner since the ratio is constant over time. Ultimate proof of stochasticity is to show that all potential deterministic mechanisms are not sufficient to promote transdifferentiation. This is limited by our knowledge of potential mechanisms (Denny and Gaines, 2011). Deterministic mechanisms could be driven by one or many transcription factors that coordinate transdifferentiation in a subpopulation of tumor GNPs. Therefore, a more reasonable approach is to first determine if tumor GNPs are heterogeneous and whether it correlates with transdifferentiation patterns.

To address whether transdifferentiation is the result of a subpopulation of tumor GNPs with a pre-determined fate, MADM can be used to analyze the differentiation patterns of tumor GNP clones. In this experiment, MADM would not be used to induce tumor formation. Instead, its two-color labeling ability would be used to visualize sparse GNP clones. Colorless tumors would initiate spontaneously from *Ptch1*^{+/-} in mice that would also have the MADM cassettes, without linked mutations (Figure 3.1A). Sparse labeling of tumor GNPs could be achieved with a tamoxifen inducible *Math1-CreER*. When tumors appear between postnatal days 60-80, low levels of tamoxifen would be administered to

allow *Math1-CreER* to enter the nucleus and mediate MADM cassette recombination during cell division. Sparse labeling of dividing tumor GNPs would generate green and red sister clones (yellow and colorless cells not shown in diagram) (Figure 3.1A). Tumors would then be analyzed at sequential time points, following initial tamoxifen administration. Clonal analysis would consist of locating sister clones within close proximity to each other and assessing their astrocytic differentiation patterns (Figure 3.1B).

To assess whether distinct tumor GNP clones transdifferentiate, the differentiation patterns of sister clones described above could be analyzed. One possible result is that one clone would generate GNPs and transdifferentiate into astrocytes, while the other clone would only generate GNPs (Figure 3.1B, left panel). This observation would suggest that tumor GNP heterogeneity exists, as one clone transdifferentiated and the other did not. However, it is possible that the non-transdifferentiating clone could eventually transdifferentiate over time, outside of the time frame suggested. Therefore it would be necessary to perform a time course analysis and look at clone differentiation patterns in short-term (<1 week after induction) and long-term (1-2 weeks after induction) labeled tumors. If, in long-term labeled tumors, there are still clones that do not have astrocytic differentiation, this would suggest there is tumor GNP heterogeneity and deterministic mechanisms promote transdifferentiation in a subpopulation of tumor GNPs. However, if all clones have astrocytic differentiation in all of the

long-term labeled tumors, this would suggest tumor GNP transdifferentiation could result from stochastic mechanisms.

A second observation could be that both sister clones generate GNPs and astrocytes (Figure 3.1B, right panel). This would suggest that all GNPs have the potential to transdifferentiate over time. Furthermore, this result would indicate that the tumor GNP population is heterogeneous at any given time, as some self-renew, while others transdifferentiate. What factors influence the transdifferentiation mechanism? The mechanism could be influenced by both extrinsic (growth factors) and intrinsic (transcription factor fluctuations) factors. Below, I will discuss one intrinsic mechanism that could act as a possible molecular mechanism promoting transdifferentiation.

Figure 3.1 Clonal analysis of tumor GNP transdifferentiation potential.

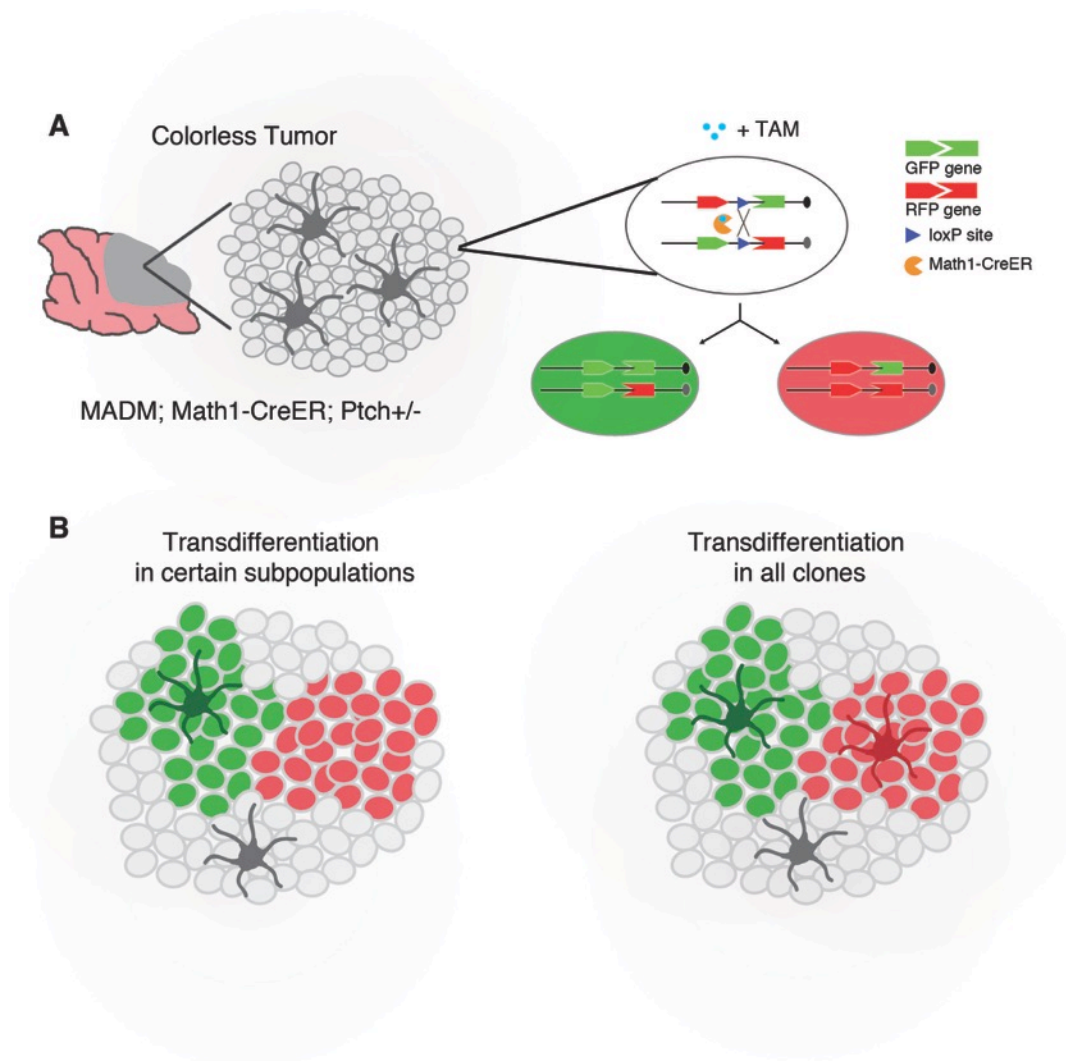


Figure 3.1 Clonal analysis of tumor GNP transdifferentiation potential.

(A) Sparse MADM labeling of tumor GNP clones. Colorless tumors develop in mice with *Ptch*^{+/-} (GNPs and astrocytes have no fluorescence). Tumor GNPs can be sparsely labeled with MADM from *Math1-CreER* mediated recombination following induction with tamoxifen. Upon cell division, green and red sister cells are generated (yellow and colorless cells are not shown). Transdifferentiation patterns of green and red tumor GNP clones can now be analyzed.

(B) There are two possible transdifferentiation patterns. Either only certain clones exhibit astrocytic transdifferentiation (left), or all clones can transdifferentiate (right).

3.1.2 Do dynamic transcription factor activities promote transdifferentiation?

To identify potential transcription factors in tumor GNPs that could promote transdifferentiation, we performed RNA sequencing on purified tumor GNPs. We compared expression levels of transcription factors between tumor GNPs and pre-transformed GNPs. Pre-transformed GNPs were isolated from perinatal cerebella, when GNPs have tumorigenic mutations (*p53*^{-/-} and *Ptch*^{+/-}), but are not yet oncogenic. Several transcription factors were increased in tumor GNPs compared to pre-transformed GNPs. As expected, because *Math1* expression defines the GNP lineage, there was a 4-fold increase in *Math1* in the tumor GNPs. Interestingly, two other bHLH transcription factors were also upregulated, *Olig2* was 2-fold higher and *Olig3* was 20-fold higher. It is well established that these three bHLH transcription factors are important regulators of neural and/or glial fate during development (Bertrand et al., 2002). For example, *Olig3* is involved in specifying neural progenitor fate toward different neuronal sub-types in the spinal cord (Liu et al., 2010; 2008; Storm et al., 2009). However a role for *Olig3* in glial fate determination has not yet been demonstrated, and thus it may not be an ideal candidate to test first since a role for *Olig2* in glial fate determination has been previously shown. For example, during postnatal forebrain development, a subset of astrocytes is generated from *Olig2*⁺ neural stem cells (NSCs). *Olig2* expression in NSCs is both necessary and sufficient for astrocytic differentiation (Marshall, 2005). Immature astrocytes have increased *Olig2* expression, while mature astrocytes no longer express

Olig2 (Marshall, 2005). From these studies, we assessed Olig2 expression patterns in tumor GNPs to determine if there was a correlation between Olig2 expression and tumor astrocyte differentiation.

By using immunofluorescence, we observed that Olig2 was expressed in a subset of tumor GNPs and tumor astrocytes. The majority of Olig2-positive tumor GNPs were in proliferative regions of tumors, particularly in superficial regions (Figure 3.2A). When tumor astrocytes (Figure 3.2B) were assessed for Olig2 expression, we found that tumor astrocytes in proliferative regions were also Olig2-positive (Figure 3.2C-D). The co-expression of Olig2 in both GNPs and astrocytes suggests that certain Olig2-expressing GNPs do in fact transdifferentiate into astrocytes. However other factors could also be responsible for mediating the transdifferentiation because the number of Olig2-positive astrocytes was far fewer than the number of Olig2-positive GNPs.

Does Olig2 expression in tumor GNPs broaden their differentiation potential to enable transdifferentiation? Is Olig2 important for tumor GNP self-renewal? The simplest way to address these questions would be to assess loss of Olig2 function in tumor GNPs. In order to remove Olig2 expression in our medulloblastoma model, addition of floxed Olig2 alleles would be necessary (Yue, 2006). In this model, from embryonic through postnatal stages, *Math1-Cre* will remove the floxed sequence and stop expression of Olig2 in all GNPs. A potential concern with this approach is that *Math1-Cre* removal of Olig2 in embryonic GNPs could disrupt development of the cell lineage and therefore

overall brain development. For example, lineage specification of NSCs into GNPs in the rhombic lip could rely on transient Olig2 expression (Machold et al., 2011; Schüller et al., 2008). This concern could be bypassed by removal of Olig2 in tumor GNPs of established tumors with an inducible *Math1-CreER*.

A number of results are possible upon removal of Olig2 in Math1-Cre expressing GNPs. One possible outcome is that the loss of Olig2 in GNPs prevents tumor GNP transdifferentiation into tumor astrocytes. This result would suggest that Olig2 is necessary for promoting transdifferentiation of GNPs. To test whether Olig2 is sufficient to promote transdifferentiation, Olig2 could be expressed in normal GNPs and assessed for their ability to transdifferentiate into astrocytes. A second possible outcome from Olig2 loss in tumor GNPs is that there could still be tumor astrocytes present. This observation would suggest Olig2 is not necessary for tumor GNP transdifferentiation and other transcription factors may be responsible for promoting transdifferentiation.

If Olig2 loss is found to prevent transdifferentiation, the impact of this on tumor progression would next be investigated. If tumor formation is halted when niche astrocytes are absent, it would suggest tumor astrocytes are necessary for tumor initiation. However, if tumors still formed without niche astrocytes, it would suggest tumor astrocytes are not necessary for tumor initiation or maintenance. Tumor formation in the absence of Olig2 would also imply that Olig2 is not involved in regulating tumor GNP proliferation. In contrast, if tumor initiation or progression were altered by loss of Olig2 in tumor GNPs, this would suggest

Olig2 is involved, at some level, in regulating tumor GNP proliferation. These experiments analyze the effect of Olig2 loss in the early stages of tumorigenesis and it would also be important to analyze the effect in established tumors. To assess the role of Olig2 for proliferation and transdifferentiation in tumor GNPs of established tumors, one could use the inducible *Math1-CreER* model discussed above. If loss of Olig2 affected proliferation or transdifferentiation of tumor GNPs, then further molecular studies to isolate and analyze Olig2-positive tumor GNPs could provide critical insights into tumorigenic mechanisms.

Molecular characterization of Olig2-positive tumor GNPs would involve using a secondary genetic reporter, single cell isolation, and bioinformatics to identify gene expression signatures that potentially regulate proliferation and transdifferentiation. To visualize Olig2 expression in tumors, the incorporation of an Olig2 reporter transgene, such as Olig2-RFP, in the MADM medulloblastoma model would be ideal. Transgene expression would enable distinction between Olig2-positive tumor GNPs (low GFP signal and RFP-positive), Olig2-negative tumor GNPs (low GFP signal and RFP-negative), Olig2-positive tumor astrocytes (high GFP signal and RFP-positive), and OPCs (only RFP-positive). Isolation of Olig2-expressing tumor GNPs could be achieved with FACS by gating for low GFP and RFP signals, and low GFP only would mark the control Olig2-negative population. Our previous studies have shown that astrocyte viability is greatly compromised during FACS, therefore tumor astrocytes would likely not be a source of contamination in the GNP fraction. If regional isolation of Olig2-positive

tumor GNPs is necessary, such as from superficial or infiltrative regions, then employing laser capture micro-dissection (LCM) of cells from tissue sections may be a better approach (Emmert-Buck et al., 1996).

To determine Olig2-target genes expressed in tumor GNPs, chromatin immunoprecipitation could be performed followed by sequencing (ChIP-seq) with Olig2-pulldown in isolated tumor GNPs. Analysis of sequencing data would involve pathway clustering to identify differences in expression levels between Olig2-positive and Olig2-negative tumor GNPs. Changes in cell cycle regulation pathways would be expected because we demonstrated that the majority of Olig2-positive tumor GNPs were actively dividing (Figure 3.2C-D). There could also be differences in cell differentiation pathways, either toward neuronal or astrocytic fates, which could reveal specific transcription and or epigenetic factors that could be manipulated. Loss-of-function and gain-of-function experiments to manipulate candidate factors in cultured tumor GNPs could identify key regulatory mechanisms governing proliferation and transdifferentiation. These results could provide insights that could be useful for developing a novel class of therapeutic targets that treat medulloblastoma by blocking transdifferentiation of tumor cells into niche cells.

Figure 3.2 Tumor GNPs and astrocytes express OLIG2.

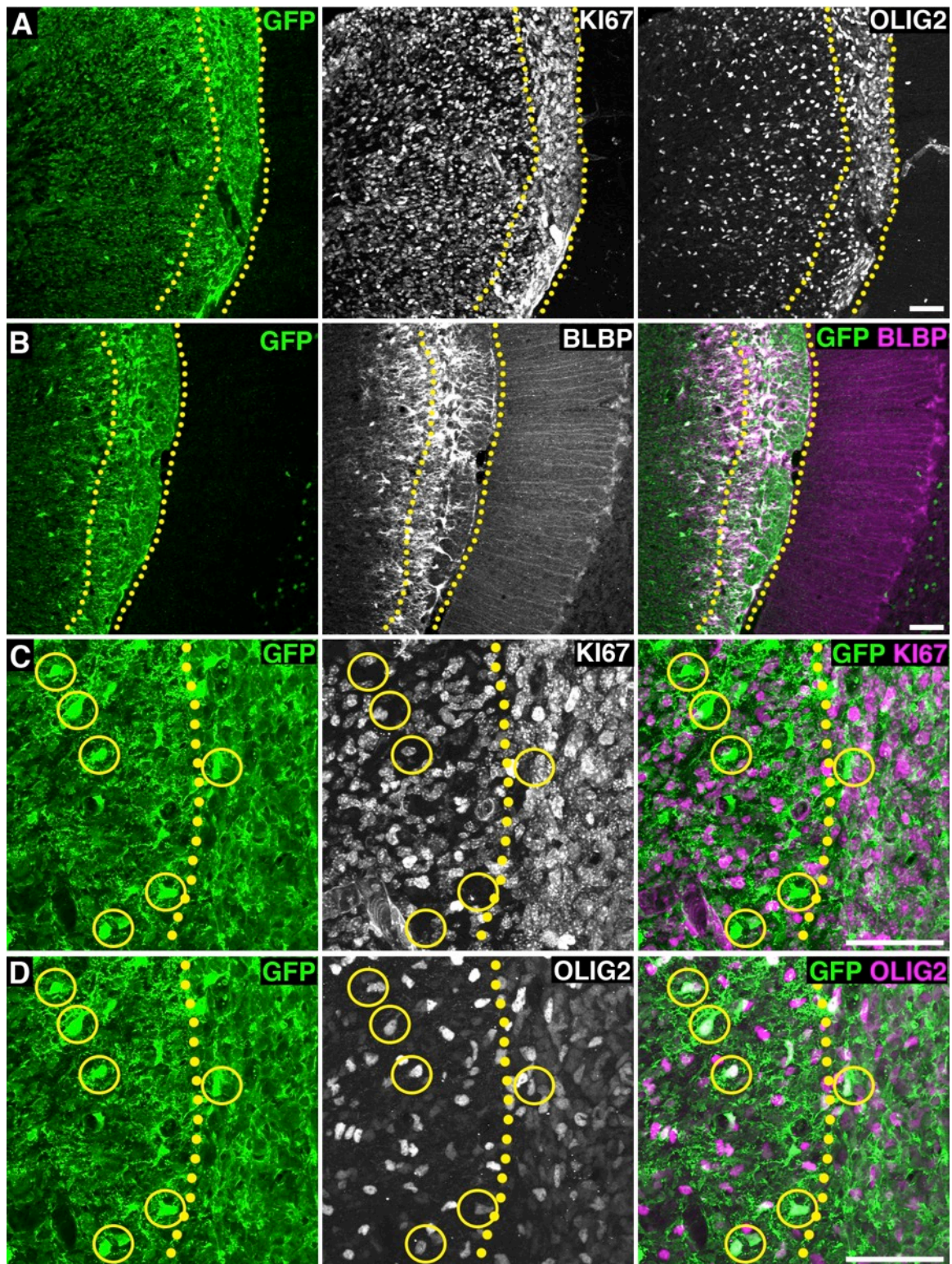


Figure 3.2 Tumor GNPs and astrocytes express OLIG2.

(A) Olig2 is expressed throughout tumor regions. GFP-positive tumor cells were proliferating (KI67-positive) in infiltrating and superficial tumor regions (superficial region outlined in yellow). Olig2 was expressed in both regions and appeared to label more cells in the superficial region that is highly proliferative.

(B) Tumor cells with increased GFP signal were BLBP-positive tumor astrocytes in both superficial and infiltrating regions.

(C) Tumor astrocytes (greater GFP signal strength, circled cells) were not dividing (KI67-negative).

(D) Tumor astrocytes (circled) were OLIG2-positive. A majority of tumor cells in superficial region (demarcated with yellow dotted line, superficial to right of line) were OLIG2-positive. GFP-negative OLIG2-positive cells were oligodendrocyte precursor cells in the tumor.

Scale bars: A-D= 50 μ m.

3.2 Investigate tumor astrocyte support mechanisms in tumor development.

3.2.1 Develop new genetic cell ablation transgenes to target tumor astrocytes.

In Appendix 1, data were presented using multiple models of genetic cell ablation designed to target tumor astrocytes. From those approaches, the conditional expression of an attenuated diphtheria toxin A-chain (DT-A^a) under control of the *Aldh1L1* promoter in tumor astrocytes offered several advantages (transgene: *Aldh1L1-loxP-GFP-stop-loxP-DT-A^a*, for full details regarding the mode of action, please refer to Appendix 1) (Tsai et al., 2012) (Figure A1.9). First, DT-A^a was specifically expressed only in tumor-derived astrocytes. This intersectional genetic approach relies on *Math1-Cre* to remove the floxed *Gfp* and transcriptional stop sequences only in GNPs. If the tumor GNP transdifferentiates into an astrocyte, which expresses *Aldh1L1*, then the DT-A^a would be expressed and kill the cell. Indeed the genetics of this system held true because *Math1-Cre* removed GFP expression in the tumor regions, whereas GFP was still expressed in astrocytes outside of the tumor. This indicates that the transgene was not epigenetically silenced. However, if DT-A^a was expressed in tumor astrocytes, it did not appear to be expressed at a sufficient level to kill the astrocytes, as BLBP-positive astrocytes still populated the tumor (Figure A1.9B). Based on these results, this approach could be modified using the same transgene design to target tumor astrocytes, except to replace the attenuated form of DT-A^a with the full strength DT-A. If tumor astrocytes are susceptible to full strength DT-A mediated cell death, then this approach will reveal their

function in tumorigenesis. This approach will ablate astrocytes in the early stages of tumor growth when tumor GNPs start to transdifferentiate, and the newly generated tumor astrocyte will undergo cell death.

Several outcomes are possible following tumor astrocyte ablation: 1) tumor growth is suppressed, 2) the rate of tumor growth is reduced, 3) tumor growth is unaffected, or 4) the tumor niche composition is changed. First, if the initial loss of tumor astrocytes suppresses further tumor growth, this would suggest that tumor astrocytes are necessary for tumor initiation. Second, if the loss of tumor astrocytes reduces, but does not completely suppress tumor growth, this would suggest they provide limited growth support to tumor GNPs. Further, tumor GNP proliferation could be supported by compensatory growth support from other niche cells. Third, if tumor astrocyte loss has no effect on tumor growth, this would suggest that tumor astrocytes are not necessary to promote tumor GNP proliferation. Here again, it does not mean that astrocytes don't provide support to tumor GNP proliferation, rather that the support from other tumor niche cells could compensate upon the loss of tumor astrocytes. In this case, one would need to target multiple niche cells for effective treatment. Finally, loss of tumor astrocytes could alter the composition of the tumor niche affecting tumor growth. In this case, tumor astrocytes could contribute to tumor progression through niche organization by secretion of important extracellular matrix proteins or cytokines that recruit other cell types into the tumor to establish a growth-promoting tumor niche. For example, normal astrocytes can express

angiogenic factors like VEGF, which induces angiogenesis (Chow et al., 2001; Stone et al., 1995). It is possible that tumor astrocytes could also mediate angiogenesis in the tumor since tumor astrocytes were found closely associated with blood vessels throughout tumor regions (Figure 2.12). Tumor astrocyte ablation could shed light on a potential functional relationship between these niche cells.

While this genetic ablation approach addresses the role of tumor astrocytes in tumor initiation, a more clinically relevant approach would be to ablate tumor astrocytes in established tumors, similar to the disease state when patients are diagnosed. An ideal approach to ablating tumor astrocytes in established tumors is to use an inducible binary genetic ablation system. Rather than assessing the role of tumor astrocytes in tumor initiation, this approach would determine the function of tumor astrocytes in tumor maintenance. This binary system is similar to the inducible *Gfap-tTA* driven expression of *tetO-DT-A^a* transgene described in Figure A1.6. Since the *Gfap-tTA* transgene was not specifically expressed in tumor astrocytes, it could prove beneficial to generate a new *Aldh1L1-tTA* transgene that is specific to astrocytes similar to the *Aldh1L1-GFP* transgene (Figure 2.11). However, *Aldh1L1-tTA* would not only target tumor astrocytes, but would also target astrocytes outside of the tumor and in other cells in the body that express *Aldh1L1*, such as the skin and liver. The creation of an ablation tetO transgene that relies on conditional Cre modification to be expressed would further specify its *Aldh1L1-tTA* activation in tumor astrocytes.

Similar to the *Aldh1L1-loxP-GFP-stop-loxP-DT-A* transgene above, the tetO transgene would also have a floxed transcription stop sequence prior to the DT-A coding sequence (*tetO-loxP-GFP-stop-loxP-DT-A*) (Figure 3.3A). In this manner, all tumor GNPs expressing *Math1-Cre* would excise the floxed stop sequence (*tetO-DT-A*). When tumor GNPs transdifferentiate into astrocytes, *Aldh1L1-tTA* would be expressed, which could then bind to tetO and promote the expression of DT-A. To prevent expression of DT-A until a tumor is formed, mice would be fed doxycycline, which sequesters tTA in the cytoplasm. Once tumors are established, doxycycline would be removed, allowing tTA to enter the nucleus of tumor astrocytes and promote expression of tetO-DT-A to kill the cell (Figure 3.3B). Again, the same outcomes are possible as previously discussed. If a phenotype results that changes the growth dynamics or niche cell composition of the tumor, it will be necessary to determine the molecular mechanisms that contribute to the functionality of tumor astrocytes.

Figure 3.3 A binary genetic ablation model to target tumor astrocytes.

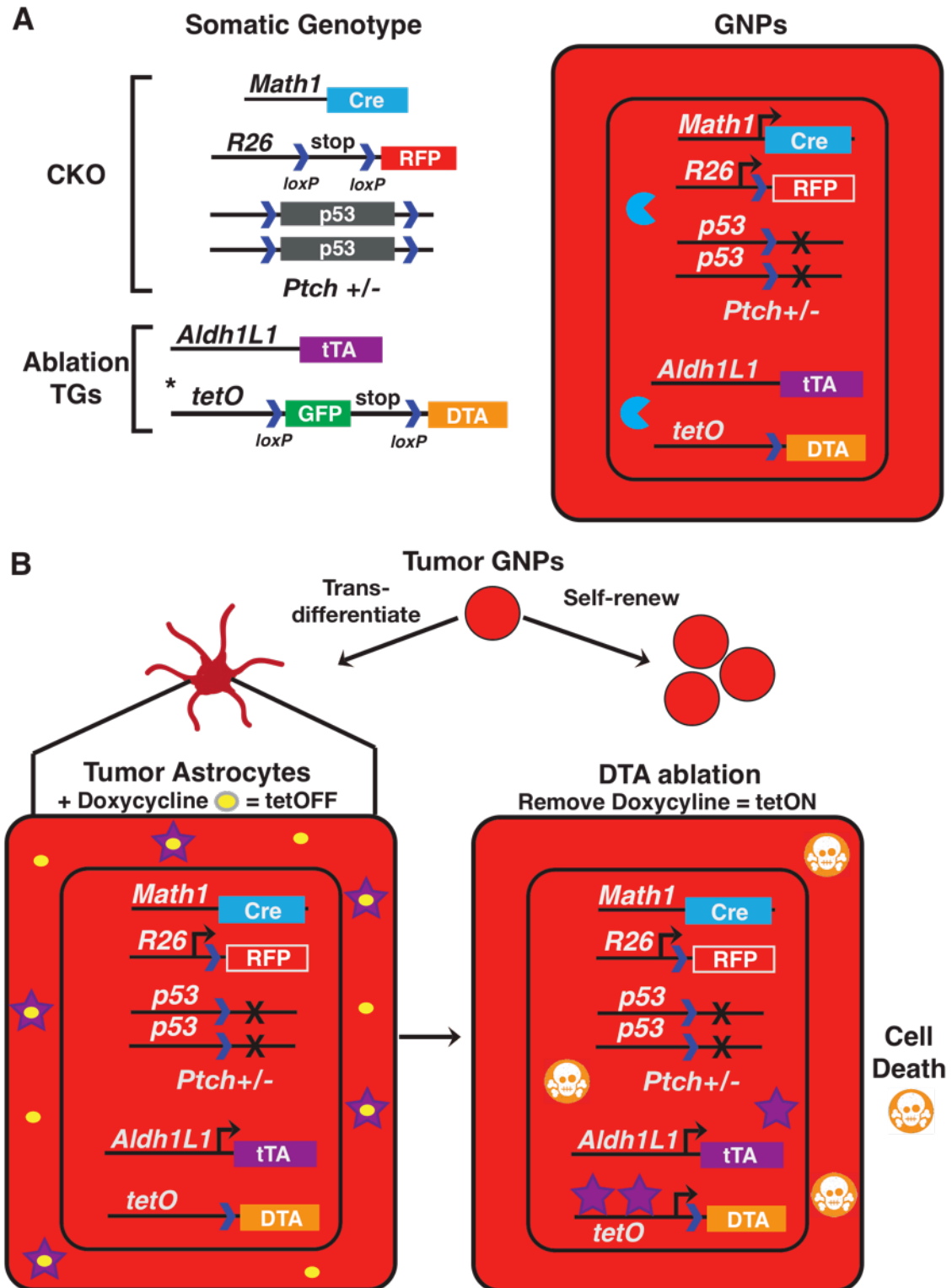


Figure 3.3 A binary genetic ablation model to target tumor astrocytes.

(A) A GNP lineage traced conditional knockout (CKO) model of medulloblastoma combined with astrocyte ablation transgenes (TGs). *Math1-Cre* specifically expresses in GNPs, resulting in excision of floxed sequences and constitutive RFP expression, null *p53* alleles, and an inducible tTA-tetO DT-A transgene in somatic *Ptch*^{+/-} mice. Both tumor GNPs and astrocytes are RFP⁺.

(B) Tumor GNPs can self-renew and transdifferentiate into tumor astrocytes. If a tumor GNP transdifferentiates into an astrocyte, the *Aldh1L1-tTA* transgene would be expressed. To inhibit the tTA protein from binding to tetO-DT-A, doxycycline would be fed to mice, which binds to tTA and sequesters it in the cytoplasm. When doxycycline is removed, tTA could enter the nucleus and bind to tetO-DT-A to promote DT-A expression. DT-A protein would inhibit protein synthesis and the cell dies.

3.2.2 Molecular characterization of tumor astrocytes.

Characterization of the tumor astrocyte transcriptome and proteome could reveal unique molecular mechanisms contributing to tumor growth. Unique transcription mechanisms in tumor astrocytes would be determined by comparing data sets between normal cerebellar and cortical astrocytes in tumor brains to identify genes either up- or down-regulated in tumor astrocytes. First, isolation of astrocyte populations would be performed with laser capture microdissection (LCM). This technique enables the collection of a relatively pure population of cells directly from a thin tissue section. To visualize tumor astrocytes with native fluorescent markers, incorporation of the *Aldh1L1-GFP* into a GNP RFP-lineage tracing model of medulloblastoma (Figure 2.11) would generate yellow tumor astrocytes for LCM isolation. RNA sequencing could then be performed to assess active gene transcription levels. Analysis would focus on growth factors, ECM, and cell surface molecules contributing to pathways that are active in tumor GNPs. Tumor GNPs would need to at least express the receptor for the tumor astrocyte ligand in order to further investigate whether the downstream signaling pathways are active.

There are a number of methods to test whether candidate molecules secreted by tumor astrocytes promote tumor GNP proliferation and survival. An *in vitro* approach would use neutralizing antibodies against the molecule in the TuAstro co-culture assay (Figure 2.32). Blocking the bioavailability of these molecules could result in reduced proliferation and survival rates of tumor GNPs.

An *in vivo* genetic approach could be taken that would induce loss of the molecule under investigation in astrocytes present in tumors from *Ptch*^{+/-} mice. Targeted removal of floxed alleles encoding the molecule in question, which often include the exon with the transcription start site (ATG), in tumor astrocytes could be achieved with the inducible *Glast-CreER* (Figure 2.17). When tumors are present, tamoxifen administration would induce Cre-mediated excision of the floxed alleles and the molecule would no longer be expressed in tumor astrocytes. This approach would also remove expression of the molecule in *Glast*-expressing astrocytes outside of the tumor. However based on the growth factor selection criteria, only factors that are upregulated in tumor astrocytes compared to normal astrocytes would be tested and therefore should not affect normal astrocyte physiology.

While these approaches seek to determine transcriptional dynamics in tumor astrocytes that impart a functional role, it is possible that transcription levels may not entirely reflect protein levels. Post-translational modifications of proteins could impart different protein expression levels and/or affect the activity of proteins. For example, post-translational modifications of p53 have been extensively studied (Bode and Dong, 2004). Under genotoxic stress conditions, wildtype p53 amino acid residues can be phosphorylated and acetylated, which stabilizes the protein and enables it to promote transcription of genes involved in cell cycle arrest and DNA repair (Appella and Anderson, 2001). In cancers, mutant p53 proteins often exhibit extensive inhibitory phosphorylation and

acetylation at domains responsible for promoting cell cycle arrest or apoptosis, and under these conditions, the mutant p53 acts as an oncogene rather than a tumor suppressor (Bode and Dong, 2004). Therefore analyzing the proteome of tumor astrocytes could provide another level of insight into their molecular contribution toward tumor GNP proliferation and survival.

Mass spectrometry of isolated cancer cells has revealed unique protein expression profiles in many cancers, including lung, endometrial, ovarian, colon, prostate, and pancreatic cancers (Cazares et al., 2002; DeSouza et al., 2005; Friedman et al., 2004; Jones et al., 2002; Sitek et al., 2009; Zhukov et al., 2003). During pancreatic cancer development, Sitek et al. identified differentially expressed proteins between distinct stages of pancreatic intraepithelial neoplasia, that further progress to become pancreatic ductal adenocarcinoma, which have the potential use as biomarkers for determining the disease state (Shekouh et al., 2003; Sitek et al., 2009). A similar approach could be applied to determine the distinct protein profile of tumor astrocytes compared to normal astrocytes. This technique determines differential protein expression between experimental groups of LCM isolated cells by identifying differential protein blots using 2-dimensional gel electrophoresis, which separates proteins based on their molecular size and charge. Individual protein spots that are different between groups are isolated and cleaved into short peptide sequences and the molecular composition is determined by mass spectrometry. This process is termed peptide fingerprinting. Sequences are then matched to a database of all known peptide

sequences to reveal the protein identities. Potential candidate molecules could be manipulated *in vivo* and *in vitro* to determine their function, similar to the experiments described above. From a comprehensive proteome profile of tumor astrocytes, other candidates may be revealed that could be important for establishing and maintaining the tumor niche. These candidates could either be critical mediators of angiogenesis, or they may act to recruit other niche cells, such as microglia, by secretion of cytokines. Finally, there is the potential to develop targeted therapies against tumor astrocyte molecular mechanisms revealed by these transcriptome and proteomic studies.

3.3 Therapeutic implications

3.3.1 Designing anti-transdifferentiation therapies to target tumor astrocytes

The studies proposed here have the potential to identify transcription factors that promote the transdifferentiation of tumor GNP into tumor astrocytes. Furthermore, loss-of-function studies would determine the necessity of these transcription factors for transdifferentiation. One possible therapeutic approach to block transdifferentiation, given that tumor astrocytes are found to support tumor growth, would be to develop anti-transdifferentiation therapies. While genetic loss of function studies are not possible in human patients, efforts to improve gene therapy techniques are emerging to manipulate gene expression in cancer cells. Recently, studies have reported promising outcomes from targeting transcription factor expression levels in human cancer cells with small interfering RNAs

(siRNA) (Yeh et al., 2013). In principle, the use of siRNAs to promote degradation of mRNA, which effectively reduces respective protein levels, is an attractive therapy to manipulate oncogenic pathways in cancer cells. However, a technical hurdle has been the delivery of siRNAs to cancer cells *in vivo*. Recent studies reported improvements in siRNA delivery to cancer cells *in vivo* with the use of modified nanoparticles and graphene oxides, which resulted in reduced tumor cell proliferation (Su et al., 2012; Yin et al., 2013). In terms of the future potential to application of these therapies in medulloblastoma, our data would suggest that an effective approach would be to target factors that promote transdifferentiation using delivery vehicles that can penetrate the blood-brain barrier, which is notorious for impeding drug delivery to the parenchyma.

In this thesis, I have presented data that reveals multiple tumor niche cells in medulloblastoma and that tumors actually generate a particular niche cell, tumor-derived astrocytes. Future studies should investigate the functional contributions of all tumor niche cells to better understand their role in the tumorigenic process. Insight into these functional mechanisms will undoubtedly generate novel platforms to develop and test targeted therapies to improve the treatment of medulloblastoma.

Chapter 4 Methods and Materials

4.1 Mouse Lines

All animal procedures were based on animal care guidelines approved by the Institutional Animal Care and Use Committee at the University of Virginia. The following mouse lines were used to generate MADM experimental and control mice: MADM-ML pair TG11ML, GT11ML (Henner et al., 2013) JAX#022977, 022976, Math1-Cre (Matei et al., 2005) JAX#011104, p53KO (Jacks et al., 1994) JAX#002101, and Ptch+/- (Goodrich et al., 1997) JAX#003081. For the conditional knockout model these additional lines were used: Math1-CreERT2 (Machold and Fishell, 2005) JAX#007684, GLAST-CreER JAX#012586, p53flox (Marino et al., 2000) JAX#008462, Rosa-floxed stop- tdTomato JAX#007908, Math1-GFP (Lumpkin et al., 2003), Aldh1l1-GFP MMRRC#011015-UCD, GFAP-TK (Bush et al., 1999) JAX#017523, GFAP-tTA (Wang et al., 2004) JAX#005964, tetO-DT-A (Lee et al., 1998) JAX#008168, tetO-H2B:GFP (Tumbar et al., 2004) JAX#005104, Aldh1L1-lsl-DT-A (Tsai et al., 2012).

4.2 Tamoxifen Administration

For perinatal mice, tamoxifen (Sigma T5648) was dissolved in 100% ethanol at 200mg/mL in 37°C water bath, then further diluted in corn oil to 20mg/mL. Solution was injected s.c. at the nape. For adult mice, tamoxifen citrate tablets (20mg/tablet; Mylan) were ground and dissolved at 20mg/mL and delivered via oral gavage(150mg/kg ; final concentration).

4.3 5-bromo-2'-deoxyuridine (BrdU) Administration

BrdU (Sigma Aldrich #B5002) was prepared in 0.9% saline solution and was injected intra-peritoneally into adult mice at a final concentration of 50mg/Kg body weight. To determine actively proliferating cells, BrdU was administered 4 hours prior to dissection.

4.4 Ganciclovir Administration

Ganciclovir (APP Pharmaceuticals #402441) was reconstituted with 0.9% saline to a final concentration of 50mg/mL. Ganciclovir was injected intra-peritoneally in perinatal and adult mice at a concentration of 12.5mg/Kg and 100mg/Kg, respectively. Mice were treated with ganciclovir once daily for 1-5 days. For cell culture studies, ganciclovir was applied at 1 μ M final concentration.

4.5 Tissue Preparation

Following anesthesia, mice were transcardially perfused with cold pre-perfusion buffer (PBS, 1% Procaine, 0.01% Heparin) followed by cold 4% paraformaldehyde (PFA) according to standard procedure. Brains were removed and postfixed in 4% PFA overnight, then cryoprotected in 30% sucrose overnight, all at 4 $^{\circ}$ C. Tissue was embedded in optimal cutting temperature medium for cryosectioning and stored at -80 $^{\circ}$ C. Tissue blocks were sectioned at 20 μ m on a cryostat, allowed to dry at room temperature for ~1hr before storing at -80C or proceeding to immunostaining.

4.6 Tissue Immunofluorescence

Fluorescent labeling from MADM cassette recombination produces cells expressing GFP or tdTomato, which occupy the green (~488nm) and red (~543nm) spectra, therefore other antibodies used on MADM brains were primarily detected in the far-red (~635nm) and ultraviolet (~405nm) spectra. For conditional knockout models and secondary orthografts, tdTomato occupied the red (~543nm) spectra.

Detailed staining procedures:

Tissue section slides were re-hydrated and washed in PBS 3 times for 5 minutes. Slides were then incubated in permeabilizing/blocking buffer (0.3% Triton-X 100 in PBS [PBT] plus 5% normal donkey serum) for 30 min at room temperature. Slides were then incubated with appropriate combination of primary antibodies (Table S1) in PBT+0.5% bovine serum albumin overnight at 4C. Sections were washed three times in PBT (10 minutes each) followed by incubation with appropriate fluorophore-conjugated secondary antibody (Table S1) overnight at 4C or at room temperature (RT) for 4 hours. Sections were then washed three times in PBT (10min each) and one time in PBS.

*To visualize nuclei, slides were incubated in DAPI solution (1ug/mL in PBS) for 10 minutes then washed once with PBS before coverslip mounted with anti-fade mounting medium.

*If four primary antibodies were used and secondary antibodies to all four fluorescent channels were assigned (488,555,647,405), DAPI step is excluded. For extensive procedural details refer to (Liu et al., 2011).

4.7 Cell Culture Immunofluorescence

Coverslips of cells for immunofluorescence were fixed with 4% PFA for 20 minutes at RT and washed with PBS. Cells were permeabilized with 0.1%PBT for 10 minutes before addition of blocking solution (10% NDS in 0.1%PBT) for 20 minutes at RT. Appropriate primary antibodies (Table S1) were incubated on slides in antibody solution (PBS + 0.5% BSA) for 1hr at RT then washed twice in PBS and once in 0.1% PBT (5 minutes each). Appropriate secondary antibodies were incubated on slides in 0.1%PBT for 30 minutes at RT. Slips were then washed twice in PBS and once in 0.1% PBT (5 minutes each). To visualize nuclei, slips were incubated in DAPI solution (1ug/mL in PBS) for 3 minutes then washed once with PBS before mounting on glass slides with anti-fade mounting medium.

4.7.1 EdU labeling and Click-iT Detection

To assess *in vitro* cell proliferation, 5-ethynyl-2'-deoxyuridine (EdU) (Invitrogen-A10044) was added to wells (10uM final concentration) three hours prior to fixation. Following fixation and permeabilization as described above, Click-iT reaction was performed prior to incubation with block and primary antibody.

Briefly, for a single reaction at 250uL per coverslip the following are combined in this order: Deionized water (175uL), 1M Tris-HCL pH8.5 (25uL), 1M CuSO₄ (0.25uL), Alexa Fluor 647 Azide (Invitrogen-A10277), mix, then just prior to application add 0.5M sodium L-ascorbate (50uL) and mix. Apply 250uL of reaction solution to permeabilized cell coverslip and incubate for 30 minutes at RT protected from light. Wash twice with PBS (5 minutes each) and proceed with primary antibody incubation as described above while protecting from light.

4.8 Imaging

Fluorescent images were acquired on a Zeiss LSM 710 at the Advanced Microscopy Facility at the University of Virginia. For live imaging, an initial fluorescent image was taken at start of experiment followed by consecutive brightfield images taken every 2 hours for a 48 hour period and a final fluorescent image taken at the end. These experiments were performed on EVOS FL Auto Cell Imaging System (Life Technologies) equipped with environmental control platform. Both confocal and live images were processed with ImageJ and Adobe Photoshop.

4.9 Quantification & Statistics

4.9.1 Tumor astrocyte quantification throughout tumor development

Tissue sections from at least 3 mice at 3 distinct stages (early, mid, late) of tumor development were immunostained for MADM fluorescent proteins, BLBP to

visualize astroglia cell bodies and DAPI for all nuclei. Three images were taken per tumor at 200X magnification across all tumor regions. Due to ambiguity in determining individual tumor GNPs, given the dense cellularity of these tumors, DAPI was used as a proxy for total tumor cell number. Some niche cells will also be included in this number but their presence is so low compared to GFP+ tumor cells, inclusion of these cells in total tumor cell number won't effect interpretation. The number of tumor astrocytes per field of view was determined by counting the number of GFP/BLBP+ cells. The percentage of tumor astrocytes in the tumor was calculated by dividing the # of GFP/BLBP+ cells by the # of total DAPI+ cells in the same field of view and multiplied by 100.

4.9.2 In vitro quantification of proliferation, cell death, and differentiation in co-culture assay

After coverslips were immunostained for EdU (proliferation), DAPI (pyknotic nuclei for cell death), or Tuj1 (neuronal differentiation) 6 images (200X) were taken across two coverslips per group. Tumor cells were counted as tdT+ and verified with DAPI when cells were aggregated. Cell phenotype markers were counted and divided by the total number of tumor cells, then multiplied by 100 to represent % of population. Significance of quantification was determined using a paired Student's T-test with SEM.

4.10 Purification of Tumor GNPs and FACS purification of Aldh1L1-GFP

Astrocytes

Perinatal mice up to P5 were directly decapitated. >P5 tumor mice were anesthetized with ketamine/xylazine (80-100mg/kg and 10-20mg/kg, respectively) followed by cervical dislocation and decapitation.

4.10.1 Tissue Dissociation for tumor GNP purification and Aldh1L1-GFP cortex

This procedure is adapted from (Foo, 2013; Foo et al., 2011).

Briefly, tumor tissue was microdissected away from normal tissue under a fluorescent microscope to visualize GFP or tdTomato tumor regions. For Aldh1L1-GFP cells, P1-7 cortical caps dissected off and cut into ~2mm pieces. Tissue pieces were digested in oxygen-equilibrated enzyme stock solution (final conc. 1XEBSS [Sigma E7510], 0.46% D-glucose, 26mM NaHCO₃, 0.5mM EDT-A, deionized water) plus 150U papain (Worthington LS003126) and DNaseI (250mg/mL final conc; Sigma DN25) at 37C in 5%CO₂ for 45 minutes, swirling every 15 minutes. Digestion solution with tissue pieces was transferred to a 50mL conical tube and liquid aspirated leaving tissue pieces. Enzyme neutralization was achieved by adding 3ml of Low Ovo inhibitor solution (final conc. 1XEBSS, 0.46% D-glucose, 26mM NaHCO₃, 0.15% BSA, 0.15% ovomucoid [Worthington LS003086], 250mg/mL DNaseI), swirling then aspirating liquid, leaving tissue pieces. Begin trituration of tissue pieces by adding 5mL of Low Ovo solution and using a 10mL serological pipette slowly triturate tissue up

and down approximately 5-10 times depending on amount of tissue. After remaining tissue pieces settle, collect supernatant into a new 50mL conical (these are all tumor cells). Repeat trituration with 5mL Low Ovo and collect supernatant until only few tissue pieces are remaining (myelin-dense tissues). Underlay Low Ovo cell suspension with 10mL High Ovo solution (final conc. 1XEBSS, 0.46% D-glucose, 26mM NaHCO₃, 0.3% BSA, 0.3% ovomucoid [Worthington LS003086], 250mg/mL DNaseI). Spin down cells at 1000rpm (180rcf) for 7 minutes. Aspirate liquid and resuspend cell pellet in 8mL panning buffer (final conc. 0.2%BSA, 1.2% D-glucose, DPBS-CMF [Invitrogen 14190-250]). To achieve single cell suspension, strain cell suspension from 70uM cell strainer (Fisher 22-363-548).

4.10.2 Percoll gradient subfractionization for GNP purification

Adapted from (Baptista et al., 1994; Hatten, 1985):

Transfer cell suspension to a 15mL polystyrene conical tube. Underlay cell suspension with 35% Percoll solution (For 10mL: 4mL sterile deionized water, 2.5mL 4X CMF-PBS-EDT-A [NaCl 32g/L, KCl 1.2g/L, D-Glucose 8g/L, NaH₂PO₄.H₂O 2g/L, KH₂PO₄ 1g/L, NaHCO₃ 8ml/L of 2% stock, EDT-A 10ml/L of 1M EDT-A, pH8.0, deionized water, pH to 7.4 with NaOH, filter sterilize], 3.5mL Percoll [Sigma P4937], Phenol red indicator to a light pink, 2N HCl 10-20uL until solution is pink-orange) using a Pasteur glass pipette full of percoll solution. Underlay cell suspension/35% Percoll solution with 60% Percoll solution (For

10mL: 1.5mL sterile deionized water, 2.5mL 4X CMF-PBS-EDTA, 6.0mL Percoll, Phenol red indicator to a light pink, 2N HCl 15-30uL until solution is pink-orange, then add 30uL 0.4% Trypan Blue) again with Pasteur glass pipette full of percoll solution. Spin gradient suspension at 2700rpm (1300rcf) for 20 minutes at RT. Two bands of cells are present, one at the cell suspension/35% percoll interface and a second at 35%/65% percoll interface. Cells at the 35/65 interface are GNPs and are collected in new 15mL conical tube, and washed with panning buffer filled to top then pelleted and resuspended in desired medium and volume.

4.11 *In vitro* transdifferentiation of tumor GNPs into tumor astrocytes and co-culture

Purified tumor GNPs (RFP+ from CKO model) are seeded at high density (500,000) onto PDL-coated glass coverslips in astrocyte media: 50% Neurobasal (Invitrogen #21103-049), 50% DMEM (Invitrogen #11995-065), 2% B27 supplement minus insulin (Invitrogen #0050129SA), 1% Penicillin/Strepomycin (Invitrogen #15140122), 1mM Sodium pyruvate (Invitrogen #11360-070), 292ug/ml Glutamax (Invitrogen #35050061), 1x SATO (Foo, 2013), 5ug/mL N-Acetyl-cysteine (Sigma #A8199), 500ng/ml insulin (Sigma #I6634), 5ng/ml human recombinant heparin-binding epidermal growth factor, HB-EGF (Sigma #E4643). After 3DIV coverslip plate is vigorously shaken and a few horizontal taps to dislodge dead cells and any GNP aggregates (most cells will die), then media is

replaced. Tumor astrocytes are very few (>500 per coverslip) and recognized by larger flat fan-like morphologies compared to smaller round GNPs.

For co-culture, tumor GNPs were purified from CKO mice with Math1-GFP instead of Rosa-fsf-tdTomato. GFP+ tumor GNPs are seeded at low density (50,000) onto coverslips with RFP+ tumor astrocytes, or without astrocytes, and cultured for 2DIV in tumor GNP media: Neurobasal medium, 2% B27 supplement minus insulin, 1% Penicillin/Streptomycin, 0.45% D-glucose (45% stock in DPBS; Fisher #D16-1), 500ng/ml insulin and 5ng/ml HB-EGF for astrocyte survival.

4.12 Fluorescence Activated Cell Sorting (FACS) of Aldh1L1-GFP astrocyte and culture conditions

Strained cells from dissociation were sorted based on their GFP expression at the University of Virginia Flow Cytometry Core Facility on a BD FACSVantage SE TurboSort DIVA and BD Influx cell sorter according to standard gating for single cells and selection of all GFP+ cells. Sorted cells were spun down, resuspended and seeded into poly-D-lysine coated T25cm² flask in growth medium base (tumor GNP media) with 50ng/mL HB-EGF. To reduce growth and promote maturation when cells are seeded on coverslips for co-culture with tumor GNPs, HB-EGF was reduced to 5ng/mL.

4.13 Fluorescent In Situ Hybridization (FISH) of chromosome loci with immunofluorescence*

TMA Paraffin sections were mounted on silanized slides, baked for 5 minutes at 90°C, and then de-paraffinized in Xylene. Slides are briefly dehydrated in 100% ETOH followed by 35 minutes in hot 1mM EDT-A. Sections were rinsed in dH₂O and incubated with GFAP or CD34 primary antibodies (Abcam) diluted in CAS Block (Invitrogen Corporation). Slides were washed in 1XPBS and then incubated with FITC conjugated fluorescent secondary antibody (Abcam) diluted in CAS Block. There is an additional wash in 1XPBS followed by fixation in 4% paraformaldehyde (USB Corporation) for 20 minutes. Slides are dehydrated in an ethanol series and air-dried. 20 μ l of PTCH1/CEP9 (with GFAP) or PTCH1 only (with CD34) probe working solution (Empire genomics) is applied to the hybridization area, a 24x50mm coverslip is placed over the top, and the edges of the coverslip are sealed with a continuous bead of rubber cement. The slide and probe are co-denatured at 95°C for 4 minutes and hybridized 24 hours or more at 37°C in a humidified chamber. Slides are then washed in 2XSSC/0.1%NP40 at 70 degrees C for 1 minute and DAPI counterstain (Vector Laboratories) is applied as well as a glass coverslip. Visualization of the dual FISH/immunofluorescence signals is accomplished by use of a fluorescent microscope with standard filters.

*Provided by Dr. Fausto Rodriguez.

4.14 Tumor Cell Orthograft

All appropriate aseptic techniques including PPE and sterilization were followed in accordance with the UVa Rodent Survival Surgery Module with prior approval from IACUC. Purified tumor cells were obtained from primary tumor mice and 10,000 cells were injected into the striatum of NOD-SCID mice. Briefly, following anesthesia mice were mounted in stereotaxic apparatus, scalp incision made at midline and a hole drilled through skull at -1.0mm Bregma, 2mm lateral, and 2.5mm deep. A Hamilton syringe with 5,000 cells/uL was inserted and 2uL were slowly dispensed. Syringe was removed and scalp was sutured. Mice recovered and were given analgesics.

4.15 Quantitative real-time polymerase chain reaction (qPCR)

Total RNA was extracted with TRI Reagent (Sigma Aldrich) followed by phenol/chloroform extraction and ethanol precipitation (Gay et al., 2013). RNA was treated with DNase I to removed residual genomic DNA (Up to 10ug RNA were resuspended in 1X DNase I Reaction Buffer (NEB #B0303S-10X) to final volume of 100uL. Add 2 units of DNase I (NEB #M0303L), mix and incubate at 37 °C for 10 minutes. Add 1 uL of 0.5M EDT-A, mix and heat inactivate at 75 °C for 10 minutes.). cDNA was synthesized RNA with iScript Reverse Transcription Supermix for RT-qPCR (Bio-Rad #170-8841). qPCR was performed using an ABI 7900HT Real-Time PCR System for 40 cycles by denaturing at 95 °C for 15 seconds, annealing at 58°C for 30 seconds, and extending at 72 °C for 30

seconds, ending with a default dissociation curve program. Sample amplification was performed with KAPA SYBR FAST qPCR kit (Kapa Biosystems #KK4617) with 10ng per reaction of cDNA. Relative levels of cDNA were calculated based on expression of housekeeping control gene Glyceraldehyde-3-Phosphate Dehydrogenase (*Gapdh*) to normalize expression levels between samples. Cycle threshold (CT) values were measured within the geometric amplification phase and averaged for duplicate reactions. CT values over 35 were not considered. Arbitrary values for gene expression in samples were normalized by subtracting the average of the internal control gene *Gapdh*.

Primers used include:

Aldh1L1 (F; 5'-GCCTTCCAACCTTCTGTTGC-3', R; 5'-CGCCACCGAGGGAACTTAAA-3'),

Id3 (F; 5'-GCAGCGTGTCATAGACTACATC-3', R; 5'-GTCCTTGGAGATCACAAGTTCC-3'),

Gapdh (F; 5'-CGTCCCGTAGACAAAATGGT-3', R; 5'-GAA TTTGCCGTGAGTGGAGT-3')

4.16 Antibodies for Immunofluorescence

Primary Antibody	Vendor	Catalog #	Dilution/ Application
Rabbit anti-BLBP	Millipore	ABN14	1:250/Tissue IF
Rat anti-BrdU	Accurate Chemical	OBT0030	1:500/Tissue IF
Rat anti-CD34	Santa Cruz Biotechnology	Sc-18917	1:250/Tissue IF
Goat anti-cmyc	Novus Biologicals	NB600-338	1:200/Tissue IF
Goat anti-dsRed	Santa Cruz Biotechnology	Sc-33353	1:200/Cells IF
Rabbit anti-GFAP	Dako	Z033429-2	1:500/Tissue IF, 1:700/Cells IF
Mouse anti-GFAP	Millipore	MAB360	1:500/Tissue IF
Chicken anti-GFP	Aves Labs	GFP-1020	1:500/Tissue IF, 1:700/Cells IF
Rabbit anti-Iba1	Dako	019-19741	1:500/Tissue IF
Mouse anti-Tuj1	Sigma Aldrich	T5076	1:700/Cells IF
Goat anti-PDGFR α	R&D Systems	AF1062	1:200/ Tissue IF
Secondary Antibodies	Vendor	Catalog #	Dilution/Applicati on
Donkey anti-chicken Alexa Fluor 488	Jackson ImmunoResearch	703-545-155	1:250/Tissue IF, 1:500/Cells IF
Donkey anti-mouse Alexa Fluor 488	Invitrogen	A21202	1:250/Tissue IF, 1:500/Cells IF
Donkey anti-rabbit Alexa Fluor 488	Jackson ImmunoResearch	711-545-152	1:250/Tissue IF, 1:500/Cells IF
Donkey anti-goat Alexa Fluor 555	Invitrogen	A21432	1:250/Tissue IF, 1:500/Cells IF
Donkey anti-rabbit Alexa Fluor 555	Invitrogen	A31572	1:250/Tissue IF, 1:500/Cells IF
Donkey anti-mouse Alexa Fluor 647	Jackson ImmunoResearch	715-605-150	1:250/Tissue IF, 1:500/Cells IF
Donkey anti-rabbit Alexa Fluor 647	Jackson ImmunoResearch	711-605-152	1:250/Tissue IF, 1:500/Cells IF
Donkey anti-rat Alexa Fluor 647	Jackson ImmunoResearch	712-605-153	1:250/Tissue IF, 1:500/Cells IF
Donkey anti-rabbit	Jackson	711-475-152	1:250/Tissue IF

DyLight 405	Immunoresearch		
-------------	----------------	--	--

Appendix 1 Genetic ablation models to determine functional contribution of tumor astrocytes to tumor niche dynamics.

A1.1 Genetic techniques for cell ablation.

To test if TuAstros have a functional role in tumor development, we employed several genetic cell ablation models to address this hypothesis. These methods have been widely used to investigate the functional relationship of cell-cell interactions during development and disease. Transgenes encoding thymidine kinase and diphtheria toxin are commonly used for ablation. Thymidine kinase (TK) encoded by herpes simplex virus 1 (Borrelli et al., 1988; McKnight, 1980) induces apoptosis by phosphorylating the pro-drug ganciclovir (GCV), which is incorporated into DNA in place of guanine during DNA replication in proliferating cells (Figure A1.1A) (Elion et al., 1977; Furman et al., 1979). Phosphorylated GCV (pGCV) is initially incorporated into duplicating DNA, but does not affect the first round of cell cycle progression. Only when the cell enters S-phase for a second time after GCV exposure will apoptosis occur, because the pGCV in the template DNA inhibits the nucleotidyltransferase activity of DNA polymerase (Rubsam et al., 1998). TK-mediated cell ablation is performed by placing the TK coding sequence under the control of a cell-type specific promoter (Borrelli et al., 1988; Heyman et al., 1989; Lewandoski, 2014). For example, TK ablation of cells expressing glial fibrillary acidic protein (*Gfap-tk*) ablated enteric glia upon GCV treatment. Loss of enteric glia resulted in a inflammatory bowel

disease phenotype, suggesting the role of enteric glia to prevent the disease phenotype (Bush et al., 1998). In another study using *Gfap-tk*, ablation of GFAP-expressing Bergmann glia in the cerebellum during perinatal stages resulted in improper cerebellar histogenesis by inhibiting the migration of neuronal precursors (Delaney et al., 1996a). It is important to note that bystander killing of neighboring non-TK expressing cells can occur through pGCV transfer from GCV-treated TK+ cells via gap junctions (Mesnil et al., 1996). While bystander killing may be advantageous when the desired outcome is simply death of a whole cell population, such as in tumors, the bystander effect could confound clear distinctions between the role of TK+ and TK-negative cells in developmental ablation studies (Mesnil and Yamasaki, 2000).

A transgene encoding diphtheria toxin is another commonly used technique for cell ablation (Figure A1.1B). Diphtheria toxin is derived from the bacterium *Corynebacterium diphtheriae*. Diphtheria toxin has two chains, the A chain and B chain, linked by disulfide bonds (Collier, 1975). The intact toxin (DT-A and B chains together) enters the cell after binding to a heparin-binding epidermal growth factor (HBEGF) precursor on the cell surface, termed the diphtheria toxin receptor (DTR), which is conferred by the DT-B domain (Mitamura et al., 1997; Naglich et al., 1992). The toxin bound receptor is endocytosed and lysosomal proteolysis breaks the disulfide bonds between the A and B chain, which releases the effector A-chain (DT-A) into the cytosol. DT-A induces cell death by inhibiting protein synthesis through ADP-ribosylation of

elongation factor 2 (Collier, 1975). It is so potent that a single DT-A molecule is sufficient to kill a cell (Yamaizumi et al., 1978). Interestingly, diphtheria toxin has little effect in mice compared to primates, as the DTR in mice has a 10^5 lower affinity for the toxin due a difference in three amino acids in the EGF-like domain (Mitamura et al., 1997). To achieve cell ablation with this toxin, two strategies are generally employed. The first method places the coding sequence of the DT-A chain under the control of a cell-type specific promoter. In this way only DT-A-expressing cells are killed (Figure A1.1B) (Breitman et al., 1987; Palmiter et al., 1987). However, due to the potency of DT-A and low level transgene leakage in non-targeting cells, this often leads to off-target killing of unintended cells and even leads to death of transgenic mice. To circumvent this problem, a less potent attenuated form of DT-A (DT-A^a) is more commonly used in the field (Lewandoski, 2014; Maxwell et al., 1987). This ablation strategy has been used to study cell lineage and cell-cell interactions in the retina, lens, pituitary, and adipose tissue (Behringer et al., 1988; Breitman et al., 1990; Lem et al., 1991; Lowell et al., 1993). For example, ablation of brown adipose tissue with DT-A^a led to obesity in mice and demonstrated the importance of brown adipose tissue to maintain metabolic homeostasis and prevent obesity (Lowell et al., 1993). An alternative strategy to the DT/DTR system is to place human or simian DTR (*hbegf* gene) under the control of a cell type specific promoter (Figure A1.1C) (Buch et al., 2005; Saito et al., 2001). This strategy provides additional advantages. 1) DTR is

not toxic, and thus, will not kill the transgenic mouse. 2) Since DT is injected to induce cell ablation, researchers can control the timing of ablation.

For cell-type specific ablation, Cre-mediated conditional expression of DT-A^a or DTR is an optimal approach. Conditional expression of DT-A^a or DTR relies on Cre-mediated removal of loxP sites flanking (floxed) a “transcription stop” sequence prior to the toxin or receptor coding sequence (Figure A1.1D-E). Then, DT-A^a or DTR can either be constitutively expressed or expressed when activation of the cell-type promoter occurs. For DTR expression experiments, injection of DT-A^a would need to occur to induce cell death (Figure A1.1E). This approach allows both temporal and spatial control of cell ablation (Lewandoski, 2014).

There are two main differences regarding the mode of action between TK and DT-A. First, DT-A directly inactivates translational machinery to kill cells immediately, whereas TK must phosphorylate GCV. Subsequently, phosphorylated GCV needs to incorporate into DNA and requires a second cell division before ablation occurs. Second, DT-A can kill cells irrespective of cell cycle changes, while TK kills cells undergoing division and through bystander killing. Therefore, choosing to use DT-A or TK largely depends on experimental needs, whether specificity and timing is key, or if broad ablation is desired.

Considering the distinct pros and cons of these cell ablation strategies, I used both DT-A^a and TK in the medulloblastoma model to assess the effect of ablating tumor astrocytes. Despite extensive pilot testing, technical limitations in

each model precluded us from drawing definitive conclusions. In the following subsections I will explain my experiments and relevant caveats. In chapter 3, I will discuss new genetic ablation models that could ablate tumor astrocytes.

Figure A1.1 Genetic cell ablation models.

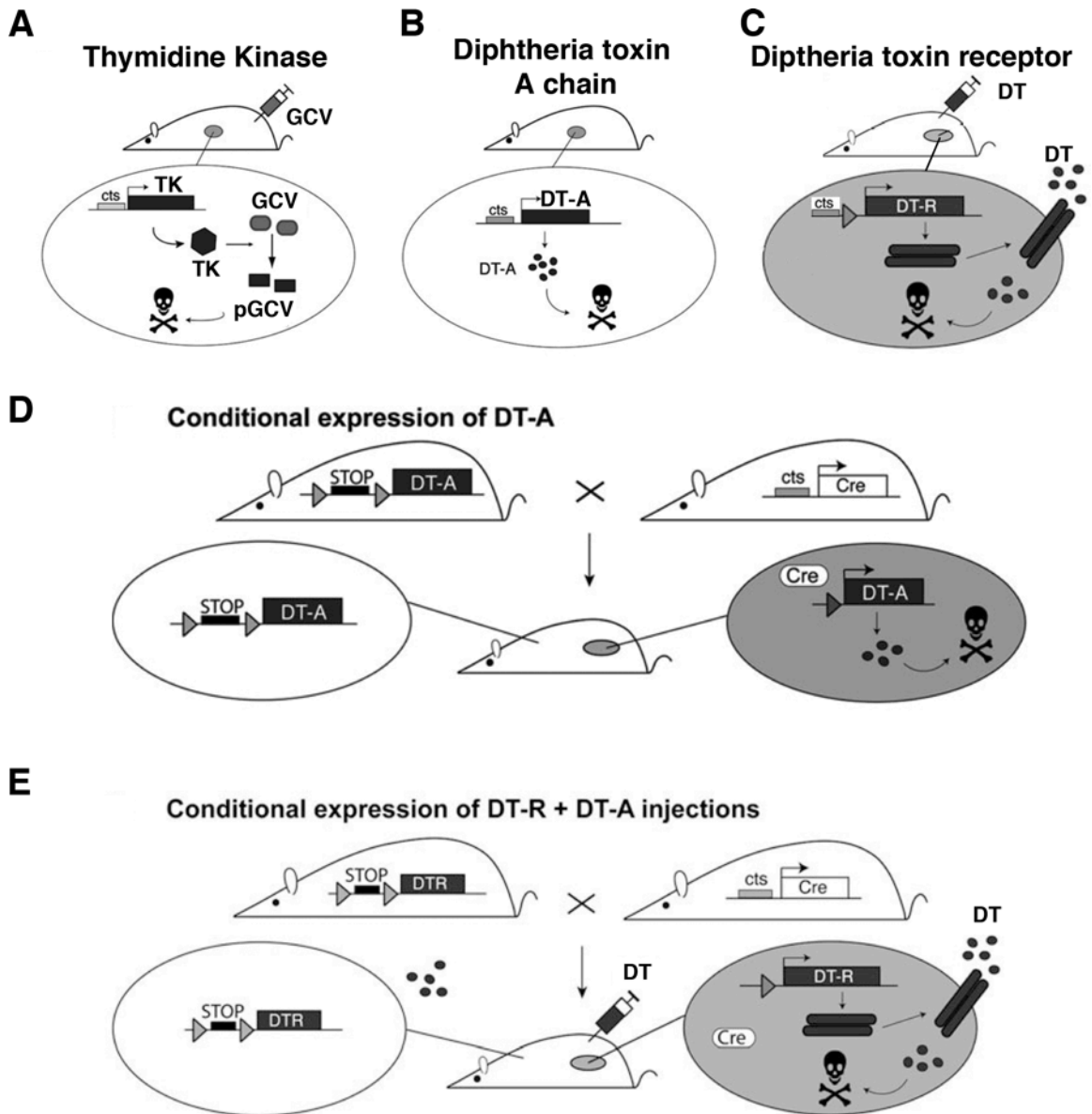


Figure A1.1 Genetic cell ablation models.

(A) Transgenic mice expressing the pro-drug metabolizing enzyme, thymidine kinase (TK) under control of a tissue-specific promoter. Upon injection of the pro-drug, ganciclovir (GCV), TK phosphorylates GCV, which incorporates into duplicating DNA and eventually leads to apoptosis.

(B) Transgenic mice carrying the diphtheria toxin A chain (DT-A) encoding gene under the control of a tissue-specific promoter. The cytotoxic effect of DT-A is restricted to cells expressing the transgene.

(C) Transgenic mice carrying the human diphtheria toxin receptor (DTR) encoding gene under the control of a tissue-specific promoter. DTR is expressed on the cell surface, where it can bind injected diphtheria toxin (DT) causing endocytosis following by proteolysis to generate the effector DT-A fragment that inhibits protein synthesis and causes cell death.

(D) Conditional expression of DT-A with loxP-Cre recombination. A floxed transcriptional stop sequence is removed by Cre recombinase and DT-A is expressed under control of cell-type specific Cre expression.

(E) Conditional expression of DTR with loxP-Cre recombination. A floxed transcriptional stop sequence is removed by Cre recombinase and DTR is expressed under control of cell-type specific Cre expression. Cell ablation is achieved by injection of diphtheria toxin and is processed as described in C.

[cts= cell-type specific promoter, TK= thymidine kinase, GCV= ganciclovir, pGCV= phosphorylated GCV, DT-A= diphtheria toxin A chain, DT= intact

diphtheria toxin A+B chains, DT-R= diphtheria toxin receptor]

*Adapted from (Lewandoski, 2014).

A1.2 Thymidine kinase-mediated astrocyte ablation.

To target tumor astrocytes for ablation, we employed the *Gfap-tk* transgene. As described earlier, GFAP-positive cells will express TK and phosphorylate GCV to induce apoptosis (Figure A1.2A). Previous studies have used *Gfap-tk* to ablate astrocytes in the forebrain and cerebellum (Bush et al., 1999; Delaney et al., 1996a). First, we verified *Gfap-tk* expression in cerebellar astrocytes. The TK protein was detected in white matter astrocytes and in Bergmann glia, while no obvious expression was detected in the EGL where GNPs, visualized with *Math1-GFP*, reside in the perinatal cerebellum (Figure A1.2B). Second, to ablate perinatal cerebellar astrocytes, according to a previous study (Delaney et al., 1996b), GCV was injected at postnatal day 5 (P5) in littermates with or without *Gfap-tk* and analyzed at P14 (Figure A1.2C). In wildtype mice treated with GCV, the cerebellum developed normally, as GNPs proliferated, differentiated, and migrated into the IGL to expand the cerebellum (Figure A1.2D). In contrast, mice harboring *Gfap-tk* that were treated with GCV had severe defects in cerebellar development. The cerebella in treated transgenic mice were almost half the size of controls, likely the result of impeded migration of immature granule neurons along Bergmann glial fibers to the IGL because cells appeared to accumulate in the EGL (Figure A1.2E). These observations suggest that cerebellar astrocytes could be ablated with *Gfap-tk*. Next, we designed experiments to ablate tumor astrocytes.

First, the *Gfap-tk* transgene was bred into a CKO model of medulloblastoma. To clearly distinguish between GNPs and tumor astrocytes, this CKO model utilized the GNP status marker *Math1-GFP*, rather than permanent GNP lineage labeling. Therefore, tumor GNPs are green and tumor astrocytes are colorless. Next, we confirmed expression of *Gfap-tk* in tumor astrocytes (Figure A1.3A). *Gfap-tk* had strong expression, as visualized with TK immunostaining, in GFAP-positive tumor astrocytes and was not detected in *Math1-GFP*-positive tumor GNPs (Figure A1.3A). One consideration is that *Gfap-tk* could express at low levels in tumor GNPs and be detectable with protein immunostaining, which would generate a false positive result if GCV-treated tumors have a positive ablation result, such as tumor regression. To address this possibility *Gfap-tk*-negative and *Gfap-tk*-positive tumor GNPs were purified and cultured in the presence of the GCV for 2 days (Figure A1.3B). To assess proliferation a short 3-hour EdU pulse was used prior the endpoint. Considering that both EdU and GCV would be incorporated into duplicating DNA in S-phase, all cells that are EdU+ should have also incorporated GCV. However, since GCV was present for 2 days, there was a greater chance that cells would have incorporated pGCV and undergone apoptosis. There was not a clear difference in the number of EdU-positive tumor GNPs in either group, which suggested tumor GNPs did not express *Gfap-tk in vitro* and therefore were not susceptible to TK-mediated ablation (Figure A1.3B).

Next, we designed GCV dosing schemes to ablate tumor astrocytes at all stages of tumor development (Figure A1.4A). Tumor mice (n=5 per group) were given 7 daily injections of GCV in three separate groups beginning either at P25, P35, or P45, and dissected 1 week later (Figure A1.4B). Surprisingly, tumor mice with *Gfap-tk* that received GCV had complete tumor regression compared to vehicle-treated and drug control mice (Figure A1.4C-E). In groups that began GCV treatment at P25 and P35, complete tumor regression was achieved with 100% survival up to at least 3 months following treatment (Figure A1.4F). Even mice treated with large tumors at P45 achieved a 75% survival rate after 7 days of GCV treatment.

While the results of the ablation were striking, several critical observations challenged interpretation of the data. First, immunostaining with a different TK antibody revealed low levels of TK protein detection throughout *Math1-GFP*-positive tumor regions (Figure A1.5A). Upon closer investigation, we observed TK immunoreactivity in *Math1-GFP*⁺ tumor GNPs, in addition to tumor astrocytes (Figure A1.5B). Furthermore, many of these TK-positive tumor GNPs were dividing. Tumor GNPs were labeled with the thymidine analog BrdU in a 4-hour period prior to dissection, which suggested tumor GNPs would be susceptible to TK-mediated apoptosis. Also, tumor astrocytes were BrdU-negative and therefore would not have been susceptible to TK-mediated apoptosis. During these experiments, we performed RNA-sequencing on acutely purified tumor GNPs. The analysis revealed a 4-fold increase in *Gfap* expression compared to

pre-transformed GNPs that are *p53*^{-/-}; *Ptch*^{+/-} and collected before tumor formation at postnatal day 7. In later experiments, there was a decrease in *Gfap* expression after culturing tumor GNPs (Figure 2.15B), which would explain why TK ablation was not found to occur *in vitro*. Collectively, it appeared that *in vivo* tumor GNPs were susceptible to GCV-induced apoptosis and precluded a definitive conclusion of the *in vivo* tumor astrocyte ablation experiments.

A few key experiments could have been performed at the beginning of this project to control for potential experimental complexities. First, realtime PCR for *Gfap* and *Tk* in purified GNPs versus the whole tumor tissue, which contains the tumor astrocytes, may have revealed *Gfap* promoter activity in tumor GNPs. Second, detecting TK protein levels with Western blot in purified tumor GNPs may have revealed the low level expression. TK-mediate ablation relies on cell proliferation. Therefore, we should have predicted TK would not successfully ablate tumor astrocytes when we did not detect dividing tumor astrocytes. The initial results were promising, but the expression *Gfap-tk* in tumor GNPs did not allow us to directly test the initial hypothesis by specifically ablating tumor astrocytes. Next, we tried an alternative approach to ablate tumor astrocytes with DT-A^a.

Figure A1.2 GFAP-TK expression in the cerebellum and Bergmann glia ablation.

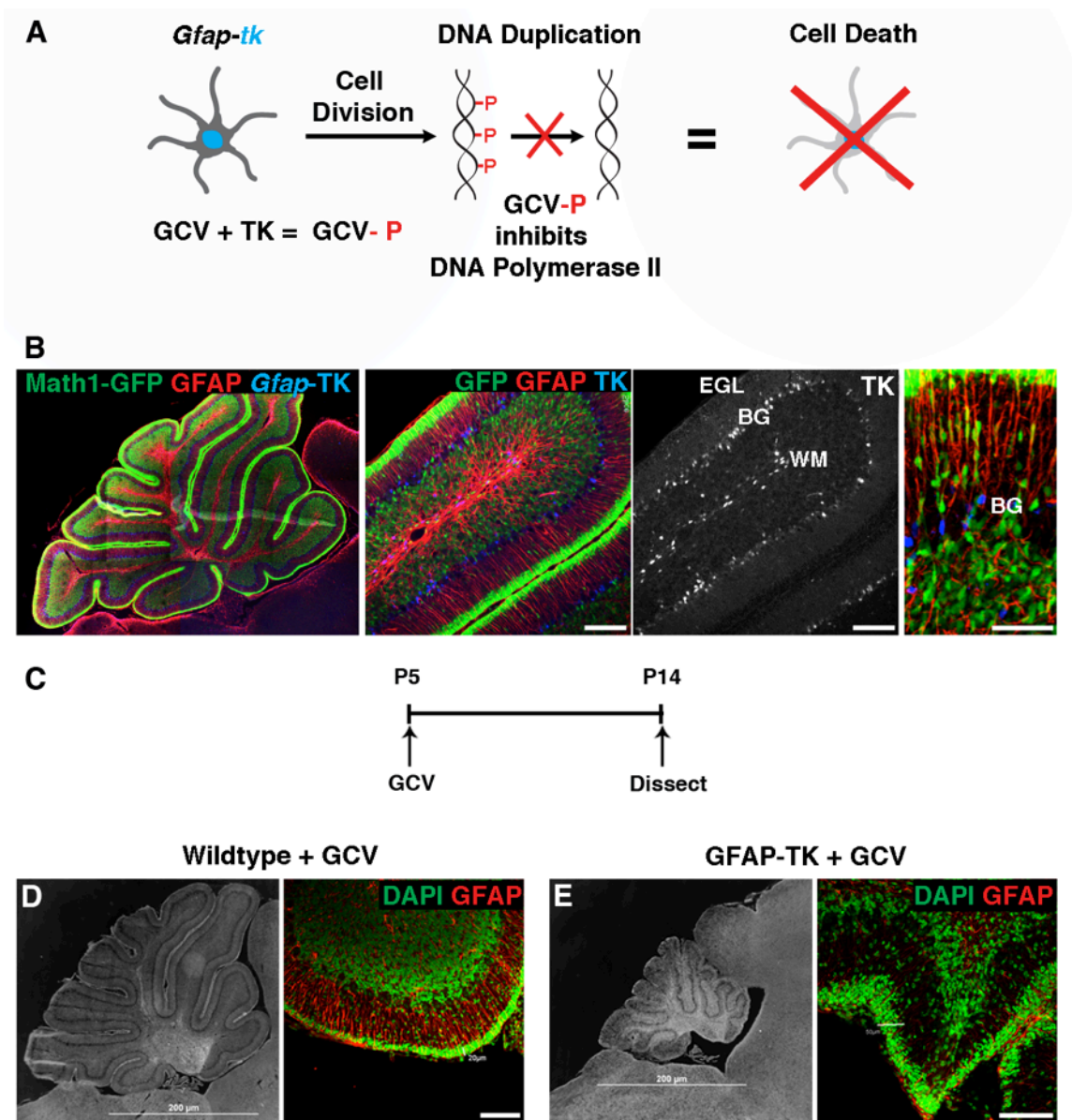


Figure A1.2 GFAP-TK expression in the cerebellum and Bergmann glia ablation.

(A) Thymidine kinase (TK) is a metabolizing enzyme for ganciclovir (GCV), an analog of 2'-deoxy-guanosine. Astrocyte-expressing GFAP-TK phosphorylates GCV, which is further phosphorylated by other cellular kinases. Phosphorylated GCV incorporates into synthesizing DNA during duplication in S-phase. Phosphorylation residues inhibit DNA polymerase activity and apoptosis is induced and subsequently cell death follows.

(B) GFAP-TK is expressed in cerebellar astrocytes. TK⁺ nuclei are present in white matter (WM) astrocytes and in Bergmann glia (BG). No detectable TK expression was observed in the external germinal layer (EGL) where Math1-GFP GNP^s reside.

(C) Dosage scheme for cerebellar astrocyte ablation. GFAP-TK⁺ and littermate wildtype control pups were given one dose of GCV at postnatal day 5 (P5) and analyzed at P14.

(D) GCV treatment of wildtype mice had no overt effects on cerebellar histogenesis. GFAP-TK pups treated with GCV displayed gross defects in tissue structure, as cerebella were half the size of controls.

Scale bars: B= 100 μ m, right panel 50 μ m, D-E= left panel 200 μ m, right panel 100 μ m.

Figure A1.3 GFAP-TK expression in tumor astrocytes.

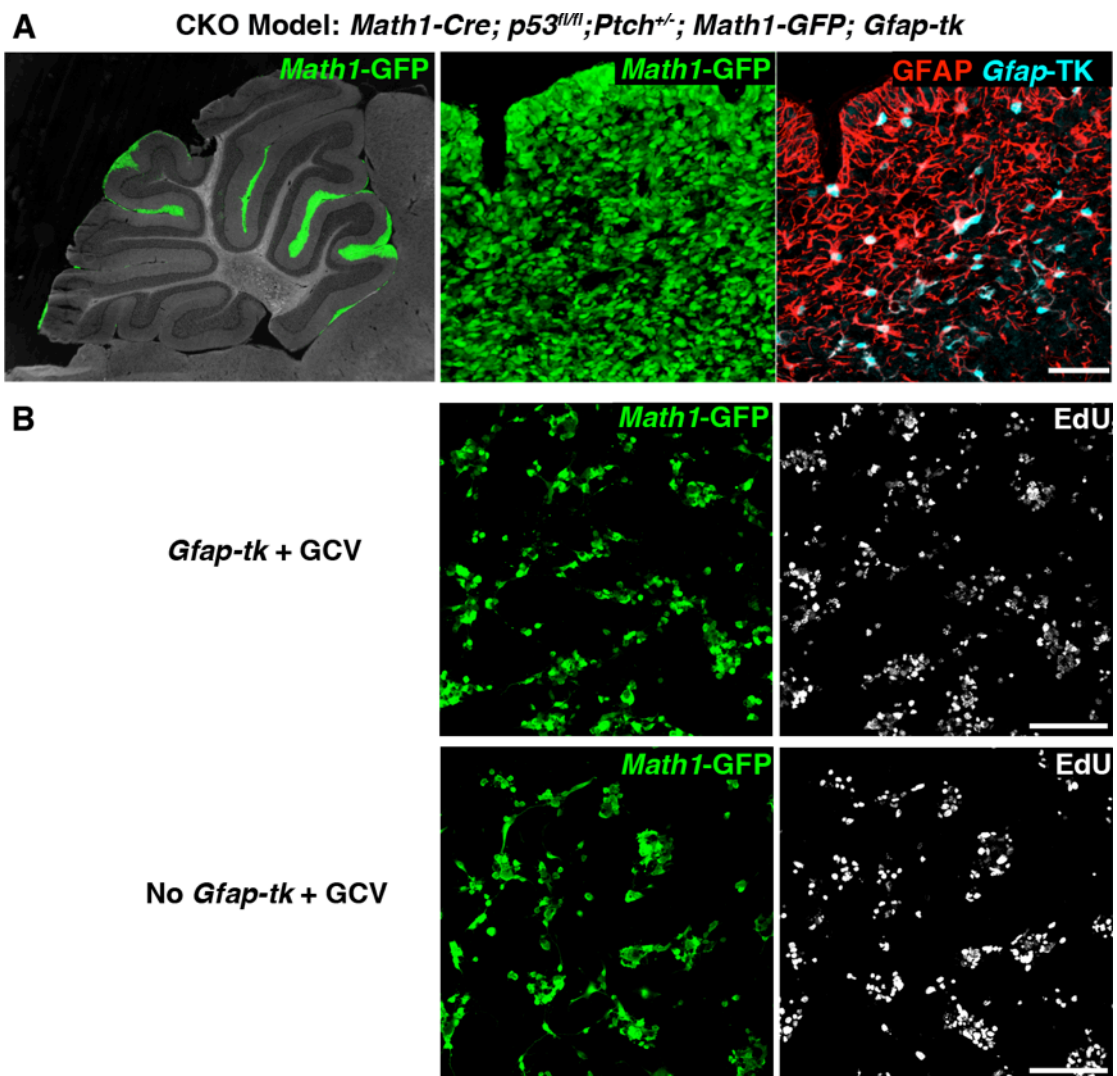


Figure A1.3 GFAP-TK expression in tumor astrocytes.

(A) A conditional knockout model medulloblastoma with Math1-GFP to distinguish tumor GNPs from astrocytes expressing GFAP-TK. GFP+ tumor regions contained astrocytes with TK+ nuclei.

(B) To test whether tumor GNPs were susceptible to GCV-mediated ablation, purified GNPs were cultured for 2DIV in the presence of GCV. There was no obvious difference in proliferation (EdU pulsed 2-hours prior to fixation to label S-phase cycle cells) between GCV-treated TK+ and TK- tumor GNPs, suggesting tumor GNPs did not express GFAP-TK.

Scale bars: A = 50 μ m, B = 100 μ m.

Figure A1.4 GFAP-TK tumor astrocyte ablation.

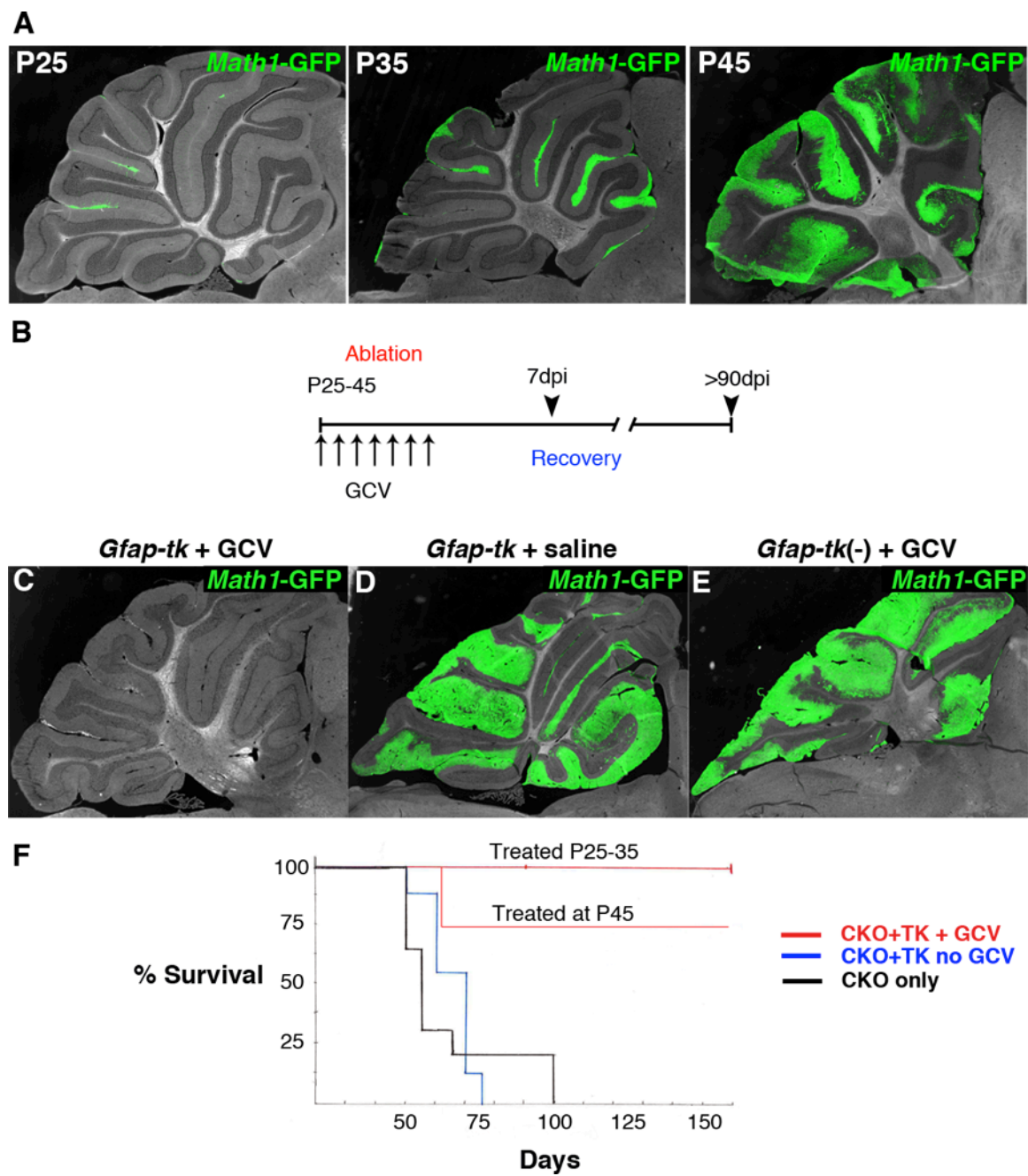


Figure A1.4 GFAP-TK tumor astrocyte ablation.

(A) Conditional knockout medulloblastoma with Math1-GFP (CKO;Math1-GFP) have 3 characteristic sizes based on age (P25 – small, P35 – medium, P45 – large tumors).

(B) CKO;Math1-GFP mice with and without GFAP-TK were treated with GCV or vehicle control. Beginning at 3 tumor size timepoints, GCV or vehicle was administered for daily for 7 days, then allowed to recover and analyzed 7 days or >90 days later (n=5 for each group).

(C-E) Representative outcome of GCV treatment at all timepoints. Tumor mice with GFAP-TK treated with GCV had complete tumor regression (C, absence of Math1-GFP). Vehicle treated (D) and drug control (E) groups had progressive tumor growth (Math1-GFP+ tumor regions) appropriate for endpoint dissection (P35 injected, P50 analysis shown here).

(D) Kaplan-Meier survival analysis of treatment groups. Tumor mice with GFAP-TK treated with GCV between P25-35 (*n=5 per group*) had a 100% survival rate and long-term regression recorded to at least P150, compared to vehicle and drug control which die between P75-100 (*n= 5 per group*). Late-stage tumor treatment of GFAP-TK mice had a 75% survival rate and long-term regression (*n=5*).

Figure A1.5 GFAP-TK is misexpressed in tumor GNPs.

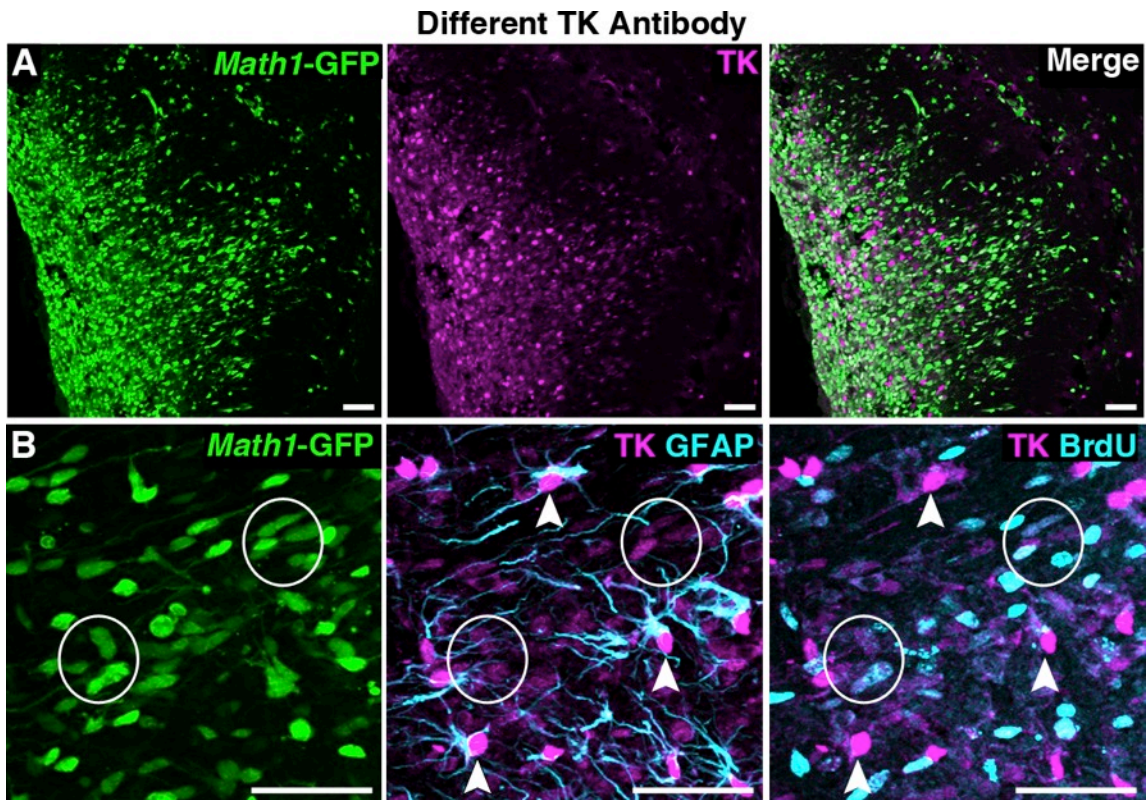


Figure A1.5 GFAP-TK is misexpressed in tumor GNPs.

(A) A different antibody to TK detected low-level expression throughout Math1-GFP tumor regions.

(B) Math1-GFP tumor GNPs express GFAP-TK. There were two expression patterns for TK: 1) strong signal in tumor astrocytes (arrowheads), and 2) weak signal in Math1-GFP+ tumor GNPs (circled). A short 4-hour pulse of BrdU labeled dividing cells prior to dissection. TK was expressed in BrdU+GFP+ tumor GNPs, which suggests they would be susceptible to GCV-mediated cell ablation, while tumor astrocytes were not (BrdU-negative).

Scale bars: A-B = 50 μ m.

A1.3 Diphtheria toxin-mediated astrocyte ablation.

Because the *Gfap-tk* transgene was shown to have had promiscuous expression in tumor GNPs, a different *Gfap* transgene with different genome insertion sites was used to target tumor astrocytes specifically. We chose the drug-inducible tetracycline transactivator (tTA)/ tetO operon system to conditionally express DT-A^a in tumor astrocytes (Lewandoski, 2001). Briefly, using the GNP-lineage traced CKO model, where tumor GNPs and tumor astrocytes are permanently labeled with RFP (Figure A1.6A), transgenes were crossed in the model for the tTA/tetO system (Figure A1.6B). In this model, the tTA protein is sequestered in the cytoplasm of tumor astrocytes expressing *Gfap-tTA* when doxycycline (Dox) is present. When Dox is removed, the tTA enters the nucleus, binds to tetO operons, and promotes expression of the *DT-A^a* transgene. To visualize tumor astrocytes with tetO activation, a tetO-human histone H2B tagged with GFP (*tetO-H2B:GFP*) transgene was included to allow detection of GFP+ nuclei. Tumor astrocyte ablation is accomplished in this system upon Dox removal when the *tetO-DT-A^a* transgene is activated and the astrocytes should undergo cell death.

To characterize the transgene expression patterns in cerebellar astrocytes, control mice with *Gfap-tTA* and *tetO-H2B:GFP* had Dox withdrawn to promote tTA activation of the tetO transgene (*tet ON*) from P0-10 and were analyzed for GFP expression in astrocytes (Figure A1.6C-E). GFP expression levels were relatively low at this time, since the majority of GFAP+ cells were labeled with

H2B:GFP. Decreased tTA activation of *tetO-H2B:GFP* was likely due to residual of Dox sequestration of tTA from Dox deposits that may leach out from tissues that have been exposed to Dox throughout embryonic development, and low levels of Dox delivered through the mother's milk that could arise from Dox also leaching out of her tissues (Gallagher, 2003). Nonetheless, the expression pattern indicated astrocytes were labeled. White matter (WM) astrocytes and some Bergmann glia nuclei at the inner molecular layer (ML) had GFP-positive nuclei (Figure A1.6D). Higher magnification also revealed labeling in the meninges (Figure A1.6E, circled) that cover the brain. However, GNPs in the external germinal layer (EGL) were not labeled, suggesting that *Gfap-tTA* was not being expressed even at low levels in GNP. Given the low expression pattern with this Dox removal scheme, we opted to maintain *tet* ON throughout embryonic and postnatal development by assessing all matings in the absence of Dox to test astrocyte ablation.

Cerebellar astrocyte ablation was tested with constitutive *tet* ON throughout development of mice with *Gfap-tTA* and *tetO-DT-A^a*. Verification that this scheme would drive *Gfap-tTA* expression in the majority of cerebellar astrocytes was confirmed by observing comprehensive coverage with *tetO-H2B:GFP* (Figure A1.7A). When cerebella were analyzed at P16, there was no overt difference in tissue structure or size between control and ablation groups (Figure A1.7B-C, respectively). Closer investigation determined that GFAP+ astrocytes were still present and the NeuN+ granule neuron population seemed

equivalent, indicating that there was no obvious ablation phenotype (Figure A1.7B-C) similar to *Gfap-tk* ablation (Figure A1.2D-E). However, it was formally possible that the DT-A^a transgene was epigenetically silenced and therefore not activated. If this was true, it was also possible that the transgene could be re-activated in cancer cells (Jones and Baylin, 2002). For this reason, we proceeded to assess whether this transgene would ablate tumor astrocytes.

To bypass any potential developmental effects of astrocyte ablation, tumor mice were maintained on Dox food (*tet* OFF) until P18, after which Dox was removed (*tet* ON) until P35 (Figure A1.8A). At P35, small tumor regions were identified on the surface of folia (Figure A1.8A, outlined). Upon closer examination, tumor regions contained GFP-positive cells, and Bergmann glia adjacent to the tumor were also GFP-positive (Figure A1.8B). GFP-positive cells in the tumor region were not proliferating (Figure A1.8C, GFP-positive and KI67-negative). When tumor astrocytes were visualized with GFAP, we did not observe GFP localization to astrocyte bodies (Figure A1.8D). We identified GFP-positive cells in the tumor region as oligodendrocyte precursor cells (Figure A1.8E, PDGFR α -positive and OLIG2-positive). From these observations, there are two interpretations. First, *Gfap-tTA* was misexpressed in the tumor, labeling OPCs instead of astrocytes. Alternatively, the *tetO-DT-A^a* transgene remained silenced or was not strong enough to ablate cells, as we would have expected there to be no GFP-positive cells in the tumor if DT-A^a was effective. In conclusion, neither the driver nor the effector transgenes performed as

anticipated in this model, possibly due to genomic instabilities that resulted in misexpression or silencing of the transgenes in tumor cells.

Figure A1.6 Conditional knockout model with DT-A^a ablation and reporter transgenes.

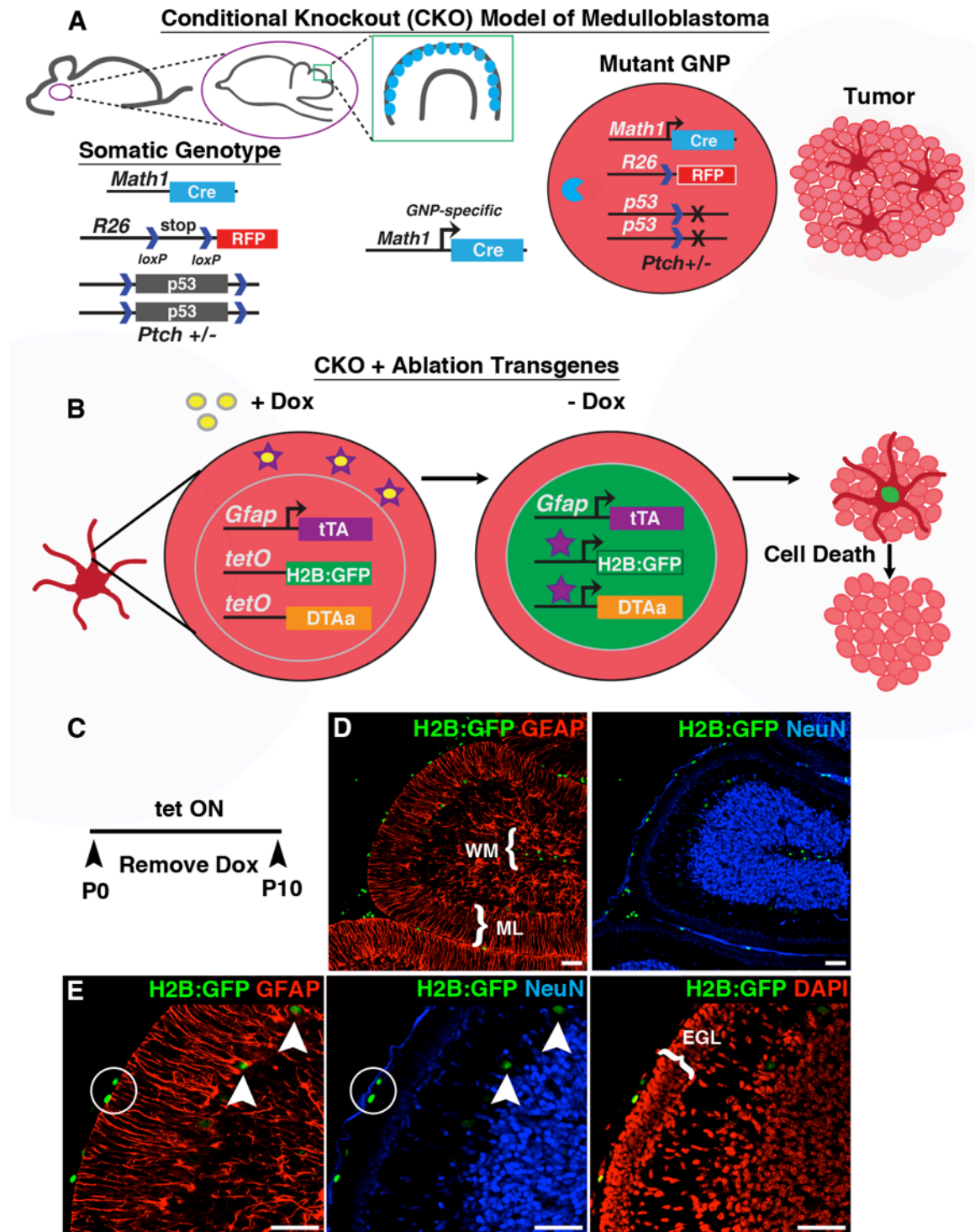


Figure A1.6 Conditional knockout model with DT-A^a ablation and reporter transgenes.

(A) GNP lineage traced model of medulloblastoma. *Math1-Cre* specifically expresses in GNPs, resulting in excision of floxed sequences generating constitutive RFP expression and null *p53* alleles in somatic *Ptch*^{+/-} mice. Both tumor GNPs and astrocytes are RFP+.

(B) Conditional expression of DT-A^a and a reporter in tumor astrocytes. Astrocytes expressing GFAP will drive expression of tTA that is sequestered in the cytoplasm when doxycycline (Dox) is present. When Dox is absent, tTA translocates to the nucleus and binds the tetO operon to drive expression of DT-A^a for ablation and human histone H2B:GFP (H2B:GFP) to visualize cells.

(C) To verify specificity of *GFAP-tTA* expression, Dox was removed at P0 to promote tTA-tetO (tet ON) expression of mice with tetO-H2B:GFP and cerebella were analyzed at P10.

(D) GFP+ cells were seen in the location of white matter (WM) astrocytes, Bergmann glia in the molecular layer (ML), and the outer surface of the cerebellum.

(E) High magnification revealed GFP expression in the meninges (circled) and in Bergmann glia nuclei (arrowheads). Also there was no obvious GFP expression in GNPs in the external germinal layer (EGL).

Scale bars: D-E = 50µm.

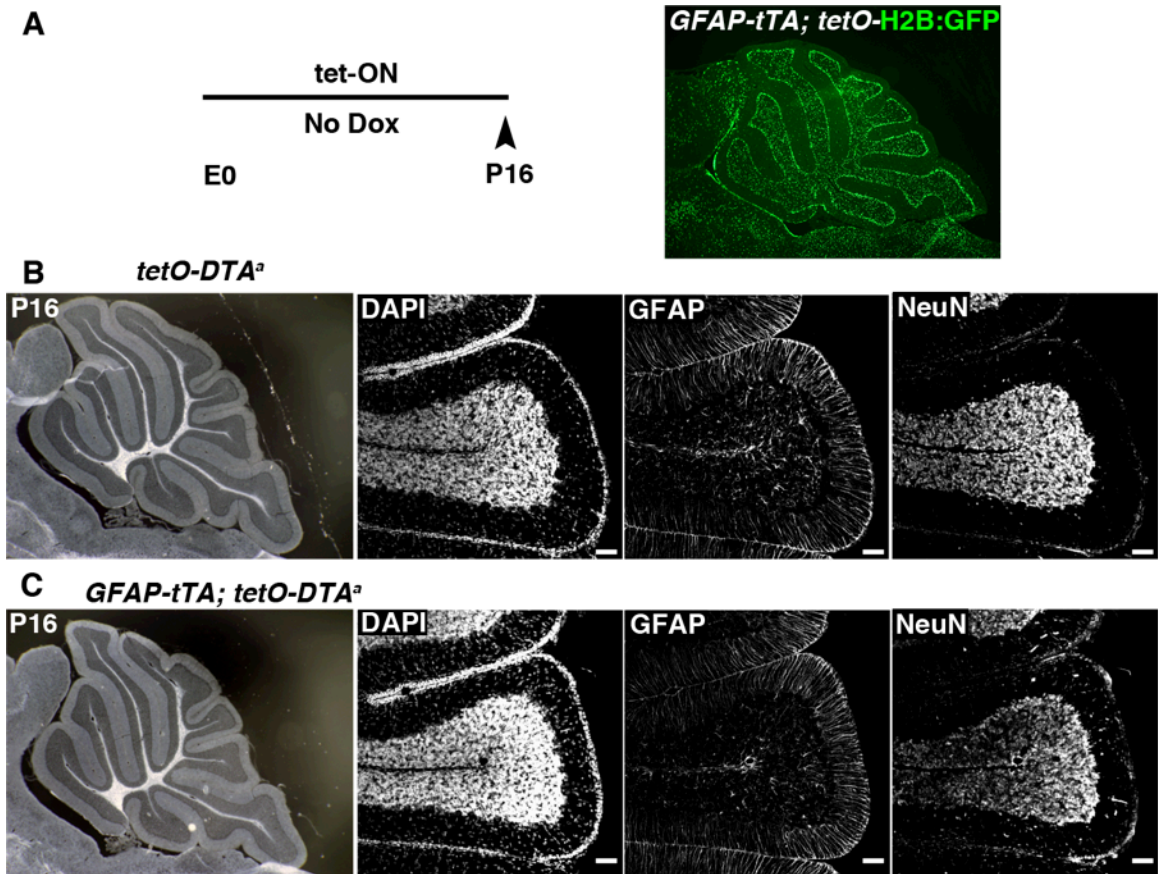
Figure A1.7 Bergmann glia are resistant to DT-A^a ablation.

Figure A1.7 Bergmann glia are resistant to DT-A^a ablation.

(A) To test the extreme limit of DT-A^a ablation, Dox was completely removed through embryonic and postnatal development until P16. First, we examined the extent of *GFAP-tTA* expression level in these mice with tetO-H2B:GFP and observed full expression patterns in all cerebellar astrocytes (right, an image of whole cerebellum).

(B-C) *GFAP-tTA; tetO-DT-A^a* were examined for astrocyte ablation and improper histogenesis. There were no obvious differences in tissue structure or astrocyte population between *tetO-DT-A^a* single transgenic mice (B) and *GFAP-tTA; tetO-DT-A^a* ablation mice (C). This observation suggested DT-A^a was either not robust enough to kill astrocytes or the transgene was epigenetically silenced.

Scale bars: B-C = 50µm.

Figure A1.8 GFAP-tTA transgene is misexpressed in tumor.

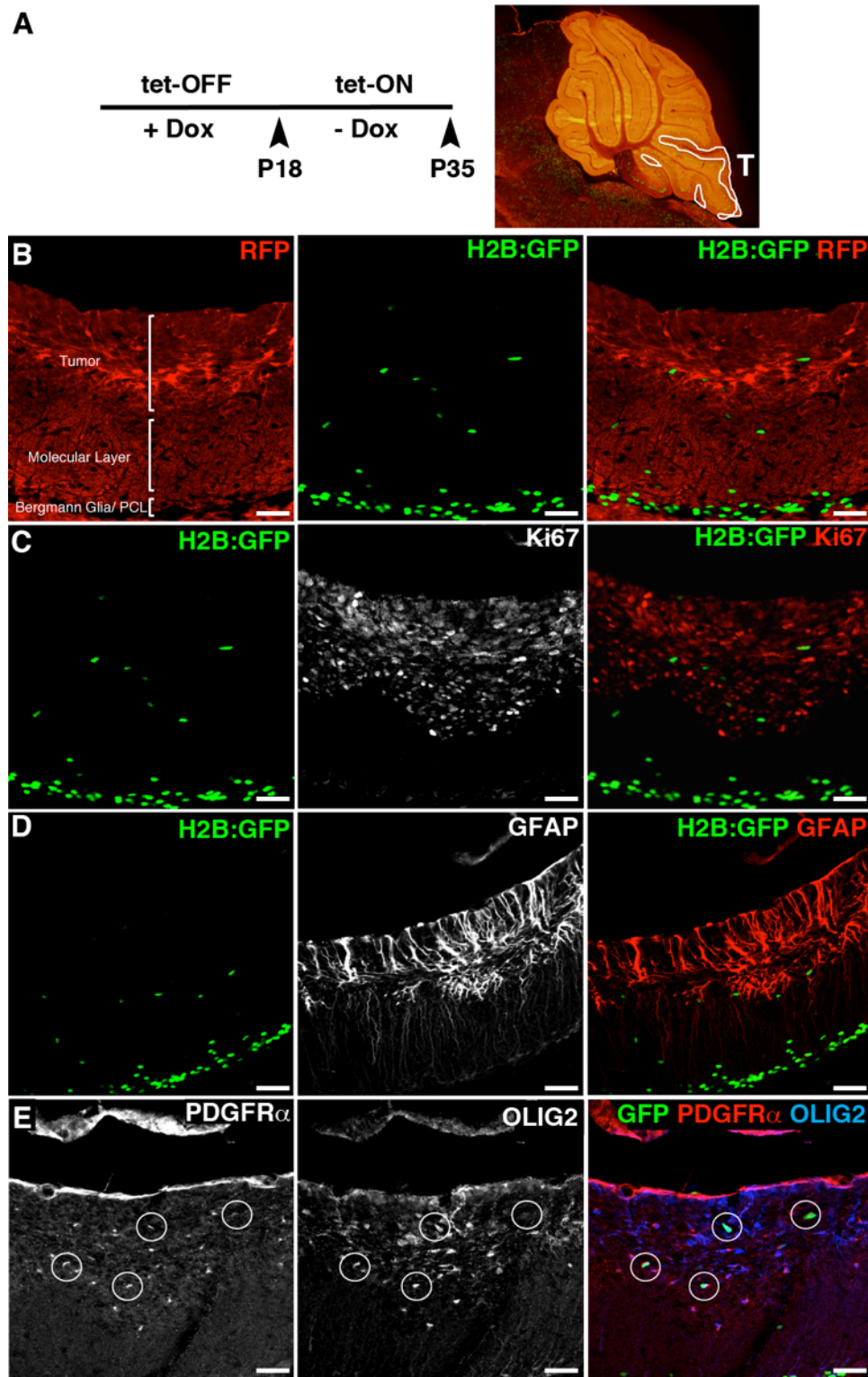


Figure A1.8 GFAP-tTA transgene is misexpressed in tumor.

(A) Tumor astrocyte ablation with *GFAP-tTA*; *tetO-DT-A^a*; *tetO-H2B:GFP*. To bypass any developmental effects of astrocyte ablation, Dox was removed at P18 and tumors (outlined in whole cerebellum image) were analyzed at P35.

(B) GFP+ cells were present in tumors and labeling of adjacent Bergmann glia nuclei were also labeled.

(C) GFP+ cells were not proliferating in the tumor (Ki67-).

(D) GFP+ nuclei did not appear to localize to GFAP+ astrocyte bodies in the tumor.

(E) GFP+ cells in the tumor were oligodendrocyte precursor cells (PDGFR α + and OLIG2+). This observation suggests *GFAP-tTA* did not label astrocytes in the tumor and that DT-A^a is likely silenced since GFP+ cells remained.

Scale bars: B-E = 50 μ m.

A1.4 Intersectional approach with diphtheria toxin for astrocyte ablation.

Transgenes driven by the *Gfap* promoter presented multiple complications, as previously discussed. Therefore, we used a different astrocyte promoter to drive expression of the DT-A^a transgene in a conditional manner. *Aldh1L1* is specifically expressed in astrocytes and could therefore be a viable promoter with which to target tumor astrocytes (Cahoy et al., 2008; Zamanian et al., 2012). We confirmed expression of *Aldh1L1* in tumor astrocytes using *in situ* hybridization during this experiment, and more recently with an *Aldh1L1-GFP* transgene (Figure 2.11B). Using the GNP-lineage traced CKO medulloblastoma model, we crossed in the *Aldh1L1-loxP-GFP-stop-loxP-DT-A^a* transgene (Tsai et al., 2012). *Math1-Cre* expression in tumor GNPs will excise the floxed sequence. If the GNP transdifferentiates into an *Aldh1L1*-expressing tumor astrocyte, then DT-A^a will be expressed and the cell should die (Figure A1.9A). When we assessed tumor formation at P50 in this model, proliferative (KI67-positive) tumor regions were evident (Figure A1.9B). There was a marked absence of GFP signal in regions of the tumor compared to GFP-positive Bergmann glia in folia adjacent to the tumor, indicating that the *Math1-Cre* had removed the floxed sequence (Figure A1.9B, middle). However, when we assessed the presence of tumor astrocytes with BLBP immunostaining, we found that the astrocytes were still present (Figure A1.9B, right). This observation suggested that if *Aldh1L1* was driving expression of DT-A^a, then DT-A^a was not strong enough to induce cell death. Alternatively, the transgene could have been epigenetically silenced in tumor GNPs even

though transgene expression was seen in normal Bergmann glia adjacent to the tumor. Together, all of the experiments with DT-A^a described above indicate that this mode of cell ablation was not an effective means to target tumor astrocytes. Future genetic models designed to accomplish this goal are discussed in Chapter 3.

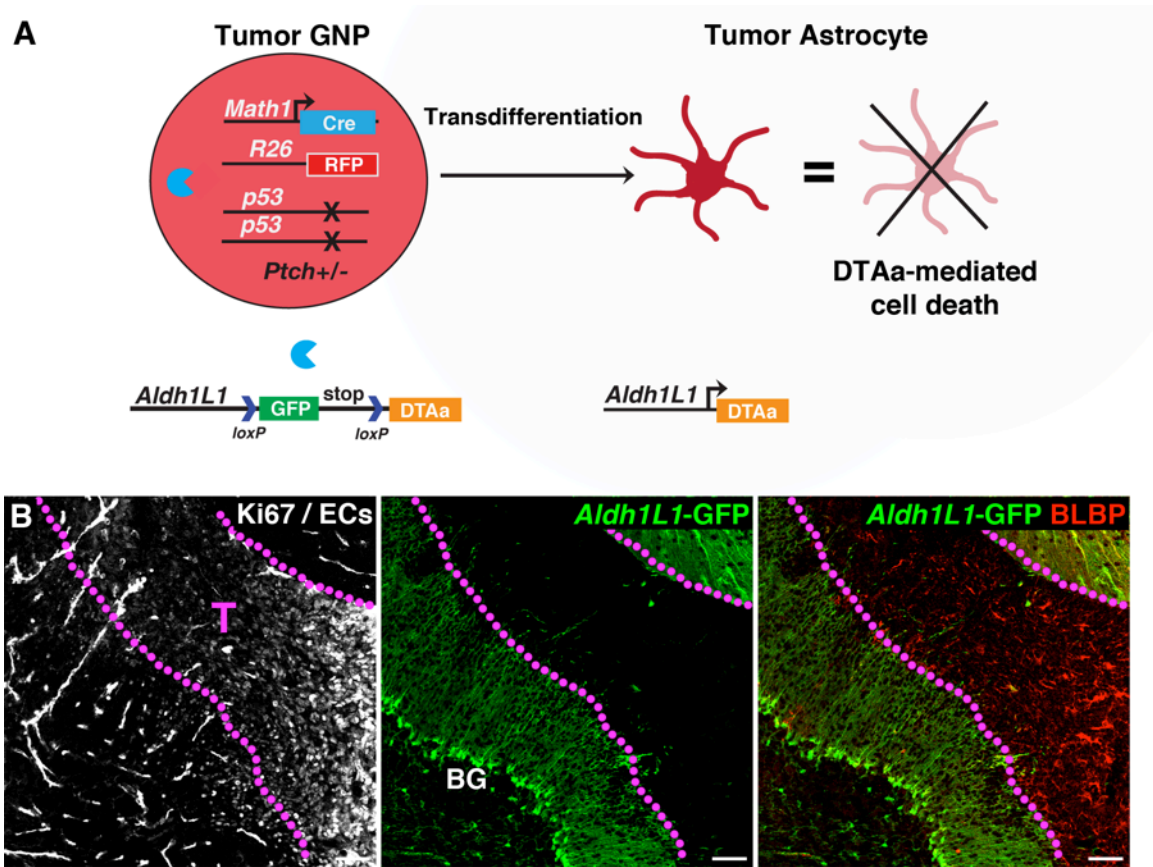
Figure A1.9 DT-A^a does not ablate tumor astrocytes.

Figure A1.9 DT-A^a does not ablate tumor astrocytes.

(A) A conditional DT-A^a transgene driven by *Aldh1L1* expression was crossed into the GNP lineage traced medulloblastoma model. The conditional transgene contains a floxed-GFP-stop sequence that is excised in *Math1-Cre* expressing GNPs. Therefore when a tumor transdifferentiates into an *Aldh1L1*-expressing tumor astrocyte, DT-A^a should be expressed, resulting in astrocyte death.

(B) Tumors were identified by KI67+ proliferating cells (endothelial cells were also labeled from the mouse monoclonal antibody). While tumor regions were GFP-negative, indicating *Math1-Cre* removed the floxed sequence in astrocytes, immunostaining with BLBP revealed that astrocytes were still present in the tumor.

Scale bars: B = 50 μ m.

Literature Cited

- Abbott, N.J., Rönnebeck, L., and Hansson, E. (2006). Astrocyte–endothelial interactions at the blood–brain barrier. *Nat Rev Neurosci* 7, 41–53.
- Adams, N.C., Tomoda, T., Cooper, M., Dietz, G., and Hatten, M.E. (2002). Mice that lack astrotactin have slowed neuronal migration. *Development* 129, 965–972.
- Ajami, B., Bennett, J.L., Krieger, C., Tetzlaff, W., and Rossi, F.M.V. (2007). Local self-renewal can sustain CNS microglia maintenance and function throughout adult life. *Nat Neurosci* 10, 1538–1543.
- Alder, J., Cho, N.K., and Hatten, M.E. (1996). Embryonic precursor cells from the rhombic lip are specified to a cerebellar granule neuron identity. *Neuron* 17, 389–399.
- Algire, G.H., Chalkley, H.W., Legallais, F.Y., and Park, H.D. (1945). Vasculae Reactions of Normal and Malignant Tissues in Vivo. I. Vascular Reactions of Mice to Wounds and to Normal and Neoplastic Transplants. *JNCI J Natl Cancer Inst* 6 (1): 73-85.
- Allavena, P., Sica, A., Solinas, G., Porta, C., and Mantovani, A. (2008). The inflammatory micro-environment in tumor progression: The role of tumor-associated macrophages. *Critical Reviews in Oncology/Hematology* 66, 1–9.
- Alvarez-Buylla, A., García-Verdugo, J.M., and Tramontin, A.D. (2001). A unified hypothesis on the lineage of neural stem cells. *Nat Rev Neurosci* 2, 287–293.
- Alvero, A.B., Fu, H.-H., Holmberg, J., Visintin, I., Mor, L., Marquina, C.C., Oidtman, J., Silasi, D.-A., and Mor, G. (2009). Stem-Like Ovarian Cancer Cells Can Serve as Tumor Vascular Progenitors. *Stem Cells* 27, 2405–2413.
- Appella, E., and Anderson, C.W. (2001). Post-translational modifications and activation of p53 by genotoxic stresses. *Eur. J. Biochem.* 268, 2764–2772.
- Armulik A., Genové G., Mäe, M., Nisancioglu, M.H., Wallgard, E., Niaudet, C., He, L., Norlin, J., Lindblom, P., Strittmatter, K., et al. (2010). Pericytes regulate the blood–brain barrier. *Nature* 468, 557–561.
- Aruga, J. (2004). The role of *Zic* genes in neural development. *Molecular and Cellular Neuroscience* 26, 205–221.
- Ayrault, O., Zindy, F., Rehg, J., Sherr, C.J., and Roussel, M.F. (2009). Two tumor suppressors, p27Kip1 and patched-1, collaborate to prevent medulloblastoma. *Mol Cancer Res* 7, 33–40.

- Bailey, P., and Cushing, H. (1925). Medulloblastoma cerebelli: a common type of midcerebellar glioma of childhood. *Arch Neuropsych* 14, 192.
- Balkwill, F., and Mantovani, A. (2001). Inflammation and cancer: back to Virchow? *Lancet* 357, 539–545.
- Baptista, C.A., Hatten, M.E., Blazeski, R., and Mason, C.A. (1994). Cell-cell interactions influence survival and differentiation of purified Purkinje cells in vitro. *Neuron* 12, 243–260.
- Barnard, R.O.R., and Pambakian, H.H. (1980). Astrocytic differentiation in medulloblastoma. *J Neurol Neurosurg Psychiatry* 43, 1041–1044.
- Baumann, N., and Pham-Dinh, D. (2001). Biology of oligodendrocyte and myelin in the mammalian central nervous system. *Physiol. Rev.* 81, 871–927.
- Behringer, R.R., Mathews, L.S., Palmiter, R.D., and Brinster, R.L. (1988). Dwarf mice produced by genetic ablation of growth hormone-expressing cells. *Genes & Development* 2, 453–461.
- Ben-Arie, N., Bellen, H.J., Armstrong, D.L., McCall, A.E., Gordadze, P.R., Guo, Q., Matzuk, M.M., and Zoghbi, H.Y. (1997). *Math1* is essential for genesis of cerebellar granule neurons. *Nature* 390, 169–172.
- Ben-Neriah, Y., Daley, G.Q., Mes-Masson, A.M., Witte, O.N., and Baltimore, D. (1986). The chronic myelogenous leukemia-specific P210 protein is the product of the *bcr/abl* hybrid gene. *Science* 233, 212–214.
- Bertrand, N., Castro, D.S., and Guillemot, F. (2002). Proneural genes and the specification of neural cell types. *Nat Rev Neurosci* 3, 517–530.
- Bélanger, M., Allaman, I., and Magistretti, P.J. (2011). Brain Energy Metabolism: Focus on Astrocyte-Neuron Metabolic Cooperation. *Cell Metabolism* 14, 724–738.
- Blouw, B., Song, H., Tihan, T., Bosze, J., Ferrara, N., Gerber, H.P., Johnson, R.S., and Bergers, G. (2003). The hypoxic response of tumors is dependent on their microenvironment. *Cancer Cell* 4, 133–146.
- Bode, A.M., and Dong, Z. (2004). Post-translational modification of p53 in tumorigenesis. *Nat Rev Cancer* 4, 793–805.
- Borrelli, E., Heyman, R., Hsi, M., and Evans, R.M. (1988). Targeting of an inducible toxic phenotype in animal cells. *Proc Natl Acad Sci USA* 85, 7572–7576.

Breitman, M.L., Clapoff, S., Rossant, J., Tsui, L.C., Glode, L.M., Maxwell, I.H., and Bernstein, A. (1987). Genetic ablation: targeted expression of a toxin gene causes microphthalmia in transgenic mice. *Science* *238*, 1563–1565.

Breitman, M.L., Rombola, H., Maxwell, I.H., Klintworth, G.K., and Bernstein, A. (1990). Genetic ablation in transgenic mice with an attenuated diphtheria toxin A gene. *Molecular and Cellular Biology* *10*, 474–479.

Buch, T., Heppner, F.L., Tertilt, C., Heinen, T.J.A.J., Kremer, M., Wunderlich, F.T., Jung, S., and Waisman, A. (2005). A Cre-inducible diphtheria toxin receptor mediates cell lineage ablation after toxin administration. *Nat Meth* *2*, 419–426.

Burger, P.C., Grahmann, F.C., Bliestle, A., and Kleihues, P. (1987). Differentiation in the medulloblastoma. *Acta Neuropathol* *73*, 115–123.

Burstein, H.J., Elias, A.D., Rugo, H.S., Cobleigh, M.A., Wolff, A.C., Eisenberg, P.D., Lehman, M., Adams, B.J., Bello, C.L., DePrimo, S.E., et al. (2008). Phase II Study of Sunitinib Malate, an Oral Multitargeted Tyrosine Kinase Inhibitor, in Patients With Metastatic Breast Cancer Previously Treated With an Anthracycline and a Taxane. *J Clin Oncol* *26*, 1810–1816.

Bush, T.G., Puvanachandra, N., Horner, C.H., Polito, A., Ostenfeld, T., Svendsen, C.N., Mucke, L., Johnson, M.H., and Sofroniew, M.V. (1999). Leukocyte infiltration, neuronal degeneration, and neurite outgrowth after ablation of scar-forming, reactive astrocytes in adult transgenic mice. *Neuron* *23*, 297–308.

Bush, T.G., Savidge, T.C., Freeman, T.C., Cox, H.J., Campbell, E.A., Mucke, L., Johnson, M.H., and Sofroniew, M.V. (1998). Fulminant jejuno-ileitis following ablation of enteric glia in adult transgenic mice. *Cell* *93*, 189–201.

Bussolati, B., Bruno, S., Grange, C., Ferrando, U., and Camussi, G. (2008a). Identification of a tumor-initiating stem cell population in human renal carcinomas. *The FASEB Journal* *22*, 3696–3705.

Bussolati, B., Grange, C., Sapino, A., and Camussi, G. (2008b). Endothelial cell differentiation of human breast tumour stem/progenitor cells. *Journal of Cellular and Molecular Medicine* *13*, 309–319.

Cahoy, J.D., Ben Emery, Kaushal, A., Foo, L.C., Zamanian, J.L., Christopherson, K.S., Xing, Y., Lubischer, J.L., Krieg, P.A., Krupenko, S.A., et al. (2008). A transcriptome database for astrocytes, neurons, and oligodendrocytes: a new resource for understanding brain development and function. *J. Neurosci.* *28*, 264–278.

Cajal, S.R.Y., Swanson, N., and Swanson, L.W. (1995). *Histology of the nervous system of man and vertebrates*. Oxford University Press USA.

Cazares, L.H., Adam, B.-L., Ward, M.D., Nasim, S., Schellhammer, P.F., Semmes, O.J., and Wright, G.L. (2002). Normal, benign, preneoplastic, and malignant prostate cells have distinct protein expression profiles resolved by surface enhanced laser desorption/ionization mass spectrometry. *Clin. Cancer Res.* *8*, 2541–2552.

Chapman, P.B., Hauschild, A., Robert, C., Haanen, J.B., Ascierto, P., Larkin, J., Dummer, R., Garbe, C., Testori, A., Maio, M., et al. (2011). Improved Survival with Vemurafenib in Melanoma with BRAF V600E Mutation. *New England Journal of Medicine* *364*, 2507–2516.

Choi, N., Zhang, B., Zhang, L., Ittmann, M., and Xin, L. (2012). Adult Murine Prostate Basal and Luminal Cells Are Self-Sustained Lineages that Can Both Serve as Targets for Prostate Cancer Initiation. *Cancer Cell* *21*, 253–265.

Chow, J., Ogunshola, O., Fan, S.Y., Li, Y., Ment, L.R., and Madri, J.A. (2001). Astrocyte-derived VEGF mediates survival and tube stabilization of hypoxic brain microvascular endothelial cells in vitro. *Brain Res Dev Brain Res* *130*, 123–132.

Collier, R.J. (1975). Diphtheria toxin: mode of action and structure. *Bacteriol Rev* *39*, 54–85.

de Klein, A., van Kessel, A.G., Grosveld, G., Bartram, C.R., Hagemeijer, A., Bootsma, D., Spurr, N.K., Heisterkamp, N., Groffen, J., and Stephenson, J.R. (1982). A cellular oncogene is translocated to the Philadelphia chromosome in chronic myelocytic leukaemia. *Nature* *300*, 765–767.

Delaney, C.L., Brenner, M., and Messing, A. (1996a). Conditional ablation of cerebellar astrocytes in postnatal transgenic mice. *J Neurosci* *16*, 6908–6918.

Delaney, C.L., Brenner, M., and Messing, A. (1996b). Conditional ablation of cerebellar astrocytes in postnatal transgenic mice. *J. Neurosci.* *16*, 6908–6918.

Delpech, B., Delpech, A., Vidard, M.N., Girard, N., Tayot, J., Clement, J.C., and Creissard, P. (1977). Glial fibrillary acidic protein in tumours of the nervous system. *Br J Cancer* *37*, 33–40.

Denny, M., and Gaines, S. (2011). *Chance in Biology* (Princeton University Press).

DeSouza, L., Diehl, G., Rodrigues, M.J., Guo, J., Romaschin, A.D., Colgan, T.J., and Siu, K.W.M. (2005). Search for Cancer Markers from Endometrial Tissues Using Differentially Labeled Tags iTRAQ and cICAT with Multidimensional Liquid Chromatography and Tandem Mass Spectrometry. *J. Proteome Res.* 4, 377–386.

Dings, R.P.M., Loren, M., Heun, H., McNeil, E., Griffioen, A.W., Mayo, K.H., and Griffin, R.J. (2007). Scheduling of Radiation with Angiogenesis Inhibitors Anginex and Avastin Improves Therapeutic Outcome via Vessel Normalization. *Clinical Cancer Research* 13, 3395–3402.

Dong, H., Strome, S.E., Salomao, D.R., Tamura, H., Hirano, F., Flies, D.B., Roche, P.C., Lu, J., Zhu, G., Tamada, K., et al. (2002). Tumor-associated B7-H1 promotes T-cell apoptosis: A potential mechanism of immune evasion. *Nature Medicine*.

Druker, B.J., Talpaz, M., Resta, D.J., Peng, B., Buchdunger, E., Ford, J.M., Lydon, N.B., Kantarjian, H., Capdeville, R., Ohno-Jones, S., et al. (2001). Efficacy and safety of a specific inhibitor of the BCR-ABL tyrosine kinase in chronic myeloid leukemia. *N Engl J Med* 344, 1031–1037.

Druker, B.J., Tamura, S., Buchdunger, E., Ohno, S., Segal, G.M., Fanning, S., Zimmermann, J., and Lydon, N.B. (1996). Effects of a selective inhibitor of the Abl tyrosine kinase on the growth of Bcr-Abl positive cells. *Nature Medicine* 2, 561–566.

Dvorak, H.F. (1986). Tumors: wounds that do not heal: similarities between tumor stroma generation and wound healing. *N Engl J Med* 315, 1650–1659.

Ebos, J.M.L., Lee, C.R., Cruz-Munoz, W., Bjarnason, G.A., Christensen, J.G., and Kerbel, R.S. (2009). Accelerated Metastasis after Short-Term Treatment with a Potent Inhibitor of Tumor Angiogenesis. *Cancer Cell* 15, 232–239.

Edlundh-Rose, E., Egyházi, S., Omholt, K., Månsson-Brahme, E., Platz, A., Hansson, J., and Lundeberg, J. (2006). NRAS and BRAF mutations in melanoma tumours in relation to clinical characteristics: a study based on mutation screening by pyrosequencing. *Melanoma Res* 16, 471–478.

Elion, G.B., Furman, P.A., Fyfe, J.A., de Miranda, P., Beauchamp, L., and Schaeffer, H.J. (1977). Selectivity of action of an antiherpetic agent, 9-(2-hydroxyethoxymethyl) guanine. *Proc Natl Acad Sci USA* 74, 5716–5720.

Ellison, D. (2002). Classifying the medulloblastoma: insights from morphology and molecular genetics. *Neuropathol Appl Neurobiol* 28, 257–282.

Ellison, D.W., Clifford, S.C., and Giangaspero, F. (2006). Medulloblastoma. In Russell & Rubinstein's Pathology of Tumors of the Nervous System, R.E. McLendon, M.K. Rosenblum, and D.D. Bigner, eds. (New York: Oxford University Press, Inc.), pp. 247–264.

Emmert-Buck, M.R., Bonner, R.F., Smith, P.D., Chuaqui, R.F., Zhuang, Z., Goldstein, S.R., Weiss, R.A., and Liotta, L.A. (1996). Laser capture microdissection. *Science* 274, 998–1001.

Eng, L.F., and Rubinstein, L.J. (1978). Contribution of immunohistochemistry to diagnostic problems of human cerebral tumors. *Journal of Histochemistry & Cytochemistry* 26, 513–522.

Feil, R., Wagner, J., Metzger, D., and Chambon, P. (1997). Regulation of Cre recombinase activity by mutated estrogen receptor ligand-binding domains. *Biochem Biophys Res Commun* 237, 752–757.

Ferrara, N. (2010). Cytokine & Growth Factor Reviews. *Cytokine Growth Factor Rev* 21, 21–26.

Folkman, J., Merler, E., Abernathy, C., and Williams, G. (1971). Isolation of a tumor factor responsible for angiogenesis. *J Exp Med* 133, 275–288.

Folkman, J. (2007). Angiogenesis: an organizing principle for drug discovery? *Nat Rev Drug Discov* 6, 273–286.

Foo, L.C. (2013). Purification of Rat and Mouse Astrocytes by Immunopanning. *Cold Spring Harbor Protocols* 2013, pdb.prot074211–pdb.prot074211.

Foo, L.C., Allen, N.J., Bushong, E.A., Ventura, P.B., Chung, W.-S., Zhou, L., Cahoy, J.D., Daneman, R., Zong, H., Ellisman, M.H., et al. (2011). Development of a Method for the Purification and Culture of Rodent Astrocytes. *Neuron* 71, 799–811.

Franco, O.E., Shaw, A.K., Strand, D.W., and Hayward, S.W. (2010). Seminars in Cell & Developmental Biology. *Seminars in Cell and Developmental Biology* 21, 33–39.

Frank, A.J., Hernan, R., Hollander, A., Lindsey, J.C., Lusher, M.E., Fuller, C.E., Clifford, S.C., and Gilbertson, R.J. (2004). The TP53-ARF tumor suppressor pathway is frequently disrupted in large/cell anaplastic medulloblastoma. *Molecular Brain Research* 121, 137–140.

Friedman, D.B., Hill, S., Keller, J.W., Merchant, N.B., Levy, S.E., Coffey, R.J., and Caprioli, R.M. (2004). Proteome analysis of human colon cancer by two-dimensional difference gel electrophoresis and mass spectrometry. *Proteomics* 4, 793–811.

Furman, P.A., Clair, M.H.S., Fyfe, J.A., Rideout, J.L., Keller, P.M., and Elion, G.B. (1979). Inhibition of herpes simplex virus-induced DNA polymerase activity and viral DNA replication by 9-(2-hydroxyethoxymethyl)guanine and its triphosphate. *Journal of Virology* 32, 72–77.

Gabrilovich, D.I., and Nagaraj, S. (2009). Myeloid-derived suppressor cells as regulators of the immune system. *Nat Rev Immunol* 9, 162–174.

Gallagher, A.R. (2003). Use of the Tetracycline System for Inducible Protein Synthesis in the Kidney. *Journal of the American Society of Nephrology* 14, 2042–2051.

Gao, W.O., Heintz, N., and Hatten, M.E. (2009). Gao WQ 1991 - Cerebellar Granule Cell Neurogenesis is regulated by cell-cell interactions. *Neuron* 6, 705–715.

Gao, W.Q., and Hatten, M.E. (1994). Immortalizing oncogenes subvert the establishment of granule cell identity in developing cerebellum. *Development* 120, 1059–1070.

Gay, L., Miller, M.R., Ventura, P.B., Devasthali, V., Vue, Z., Thompson, H.L., Temple, S., Zong, H., Cleary, M.D., Stankunas, K., et al. (2013). Mouse TU tagging: a chemical/genetic intersectional method for purifying cell type-specific nascent RNA. *Genes & Development* 27, 98–115.

Gibson, P., Tong, Y., Robinson, G., Thompson, M.C., Curre, D.S., Eden, C., Kranenburg, T.A., Hogg, T., Poppleton, H., Martin, J., et al. (2010). Subtypes of medulloblastoma have distinct developmental origins. *Nature* 468, 1095–1099.

Gilbertson, R.J., and Ellison, D.W. (2008). The Origins of Medulloblastoma Subtypes. *Annu. Rev. Pathol. Mech. Dis.* 3, 341–365.

Gilhuis, H.J., Laak, J.A.W.M., Pomp, J., Kappelle, A.C., Gijtenbeek, J.M.M., and Wesseling, P. (2006). Three-dimensional (3D) reconstruction and quantitative analysis of the microvasculature in medulloblastoma and ependymoma subtypes. *Angiogenesis* 9, 201–208.

- Ginhoux, F., Greter, M., Leboeuf, M., Nandi, S., See, P., Gokhan, S., Mehler, M.F., Conway, S.J., Ng, L.G., Stanley, E.R., et al. (2010). Fate Mapping Analysis Reveals That Adult Microglia Derive from Primitive Macrophages. *Science* 330, 841–845.
- Ginhoux, F., Lim, S., Hoeffel, G., Low, D., & Huber, T. (2013). Origin and differentiation of microglia. *Frontiers in Cellular Neuroscience*, 7, 45–45.
- Gong, S., Zheng, C., Doughty, M.L., Losos, K., Didkovsky, N., Schambra, U.B., Nowak, N.J., Joyner, A., Leblanc, G., and Hatten, M.E. (2003). A gene expression atlas of the central nervous system based on bacterial artificial chromosomes. *Nature* 425, 917–925.
- Goodrich, L.V., Milenković, L., Higgins, K.M., and Scott, M.P. (1997). Altered Neural Cell Fates and Medulloblastoma in Mouse patched Mutants. *Science* 277, 1109–1113.
- Greaves, M., and Maley, C.C. (2012). Clonal evolution in cancer. *Nature* 481, 306–313.
- Grivennikov, S.I., Greten, F.R., and Karin, M. (2010). Immunity, Inflammation, and Cancer. *Cell* 140, 883–899.
- Grizzi, F., Weber, C., and Di Ieva, A. (2008). Antiangiogenic strategies in medulloblastoma: reality or mystery. *Pediatr Res* 63, 584–590.
- Hanahan, D., and Folkman, J. (1996). Patterns and Emerging Mechanisms of the Angiogenic Switch during Tumorigenesis. *Cell* 86, 353–364.
- Hanahan, D., and Weinberg, R.A. (2011). Hallmarks of Cancer: The Next Generation. *Cell* 144, 646–674.
- Hanisch, U.-K., and Kettenmann, H. (2007). Microglia: active sensor and versatile effector cells in the normal and pathologic brain. *Nat Neurosci* 10, 1387–1394.
- Hatten, M.E. (1985). Neuronal regulation of astroglial morphology and proliferation in vitro. *J Cell Biol* 100, 384–396.
- Hatten, M.E., and Liem, R. (1981). Astroglial Cells Provide a Template for the Positioning of Developing Cerebellar Neurons In Vitro. *J Cell Biol* 90, 622–630.
- Henner, A., Ventura, P.B., Jiang, Y., and Zong, H. (2013). MADM-ML, a Mouse Genetic Mosaic System with Increased Clonal Efficiency. *PLoS ONE* 8.

Heyman, R.A., Borrelli, E., Lesley, J., Anderson, D., Richman, D.D., Baird, S.M., Hyman, R., and Evans, R.M. (1989). Thymidine kinase obliteration: creation of transgenic mice with controlled immune deficiency. *Proc Natl Acad Sci USA* *86*, 2698–2702.

Hoeben, A. (2004). Vascular Endothelial Growth Factor and Angiogenesis. *Pharmacological Reviews* *56*, 549–580.

Huber, H., Eggert, A., Janss, A.J., Wiewrodt, R., Zhao, H., Sutton, L.N., Rorke, L.B., Phillips, P.C., and Grotzer, M.A. (2001). Angiogenic profile of childhood primitive neuroectodermal brain tumours/medulloblastomas. *Eur. J. Cancer* *37*, 2064–2072.

Hughes, E.G., Kang, S.H., Fukaya, M., and Bergles, D.E. (2013). Oligodendrocyte progenitors balance growth with self-repulsion to achieve homeostasis in the adult brain. *Nat Neurosci* *16*, 668–676.

Iadecola, C., and Nedergaard, M. (2007). Glial regulation of the cerebral microvasculature. *Nat Neurosci* *10*, 1369–1376.

Jacks, T., Remington, L., Williams, B.O., Schmitt, E.M., Halachmi, S., Bronson, R.T., and Weinberg, R.A. (1994). Tumor spectrum analysis in p53-mutant mice. *Current Biology* *4*, 1–7.

Janes, K.A., Wang, C.-C., Holmberg, K.J., Cabral, K., and Brugge, J.S. (2010). Identifying single-cell molecular programs by stochastic profiling. *Nat Meth* *7*, 311–317.

Jones, D.T.W., Jäger, N., Kool, M., Zichner, T., Hutter, B., Sultan, M., Cho, Y.-J., Pugh, T.J., Hovestadt, V., Stütz, A.M., et al. (2012). Dissecting the genomic complexity underlying medulloblastoma. *Nature* *488*, 100–105.

Jones, M.B., Krutzsch, H., Shu, H., Zhao, Y., Liotta, L.A., Kohn, E.C., and Petricoin, E.F. (2002). Proteomic analysis and identification of new biomarkers and therapeutic targets for invasive ovarian cancer. *Proteomics* *2*, 76–84.

Jones, P.A., and Baylin, S.B. (2002). The fundamental role of epigenetic events in cancer. *Nature Reviews Genetics* *3*, 415–428.

Kang, S.H., Fukaya, M., Yang, J.K., Rothstein, J.D., and Bergles, D.E. (2010). CNS Glial Progenitors Remain Committed to the Oligodendrocyte Lineage in Postnatal Life and following Neurodegeneration. *Neuron* *68*, 668–681.

Kenney, A.M. (2003). Nmyc upregulation by sonic hedgehog signaling promotes proliferation in developing cerebellar granule neuron precursors. *Development* *130*, 15–28.

Leach, D.R., Krummel, M.F., and Allison, J.P. (1996). Enhancement of antitumor immunity by CTLA-4 blockade. *Science* 271, 1734–1736.

Lee, P., Morley, G., Huang, Q., Fischer, A., Seiler, S., Horner, J.W., Factor, S., Vaidya, D., Jalife, J., and Fishman, G.I. (1998). Conditional lineage ablation to model human diseases. *Proc Natl Acad Sci USA* 95, 11371–11376.

Lem, J., Applebury, M.L., Falk, J.D., Flannery, J.G., and Simon, M.I. (1991). Tissue-specific and developmental regulation of rod opsin chimeric genes in transgenic mice. *Neuron* 6, 201–210.

Lewandoski, M. (2001). Conditional control of gene expression in the mouse. *Nature Reviews Genetics* 2, 743–755.

Lewandoski, M. (2014). *Mouse Molecular Embryology: Methods and Protocols*. Springer USA.

Lim, D.A., and Alvarez-Buylla, A. (1999). Interaction between astrocytes and adult subventricular zone precursors stimulates neurogenesis. *Proc Natl Acad Sci USA* 96, 7526–7531.

Lindahl, P. (1997). Pericyte Loss and Microaneurysm Formation in PDGF-B-Deficient Mice. *Science* 277, 242–245.

Liu, C., Sage, J.C., Miller, M.R., Verhaak, R.G.W., Hippenmeyer, S., Vogel, H., Foreman, O., Bronson, R.T., Nishiyama, A., Luo, L., et al. (2011). Mosaic Analysis with Double Markers Reveals Tumor Cell of Origin in Glioma. *Cell* 146, 209–221.

Liu, Z.-R., Shi, M., Hu, Z.-L., Zheng, M.-H., Du, F., Zhao, G., and Ding, Y.-Q. (2010). A refined map of early gene expression in the dorsal rhombomere 1 of mouse embryos. *Brain Research Bulletin* 82, 74–82.

Liu, Z., Li, H., Hu, X., Yu, L., Liu, H., Han, R., Colella, R., Mower, G.D., Chen, Y., and Qiu, M. (2008). Control of precerebellar neuron development by Olig3 bHLH transcription factor. *J Neurosci* 28, 10124–10133.

Loges, S., Mazzone, M., Hohensinner, P., and Carmeliet, P. (2009). Silencing or Fueling Metastasis with VEGF Inhibitors: Antiangiogenesis Revisited. *Cancer Cell* 15, 167–170.

Louis, D.N., Cavenee, W.K., Ohgaki, H., and Wiestler, O.D. (2007). *WHO Classification of Tumours of the Central Nervous System (WHO Regional Office Europe)*.

Lowell, B.B., S-Susulic, V., Hamann, A., Lawitts, J.A., Himms-Hagen, J., Boyer,

- B.B., Kozak, L.P., and Flier, J.S. (1993). Development of obesity in transgenic mice after genetic ablation of brown adipose tissue. *Nature* *366*, 740–742.
- Lu, P., Weaver, V.M., and Werb, Z. (2012). The extracellular matrix: A dynamic niche in cancer progression. *J Cell Biol* *196*, 395–406.
- Lugo, T.G., Pendergast, A.-M., Muller, A.J., and Witte, O.N. (1990). Tyrosine Kinase Activity and Transformation Potency of bcr-abl Oncogene Products. *Science* *247*, 1079–1082.
- Lumpkin, E.A., Collisson, T., Parab, P., Omer-Abdalla, A., Haeberle, H., Chen, P., Doetzelhofer, A., White, P., Groves, A., Segil, N., et al. (2003). Math1-driven GFP expression in the developing nervous system of transgenic mice. *Gene Expression Patterns* *3*, 389–395.
- MacDonald, T.J., Aguilera, D., and Castellino, R.C. (2013). The rationale for targeted therapies in medulloblastoma. *Neuro-Oncology* *16*, 9–20.
- Machold, R., and Fishell, G. (2005). Math1 is expressed in temporally discrete pools of cerebellar rhombic-lip neural progenitors. *Neuron* *48*, 17–24.
- Machold, R.R., Klein, C.C., and Fishell, G.G. (2011). Genes expressed in Atoh1 neuronal lineages arising from the r1/isthmus rhombic lip. *Gene Expression Patterns* *11*, 349–359.
- Mancuso, M.R., Davis, R., Norberg, S.M., O'Brien, S., Sennino, B., Nakahara, T., Yao, V.J., Inai, T., Brooks, P., Freemark, B., et al. (2006). Rapid vascular regrowth in tumors after reversal of VEGF inhibition. *J Clin Invest* *116*, 2610–2621.
- Mannoji, H.H., Takeshita, I.I., Fukui, M.M., Ohta, M.M., and Kitamura, K.K. (1981a). Glial fibrillary acidic protein in medulloblastoma. *Acta Neuropathol* *55*, 63–69.
- Mannoji, H., Takeshita, I., Fukui, M., Ohta, M., and Kitamura, K. (1981b). Glial fibrillary acidic protein in medulloblastoma. *Acta Neuropathol* *55*, 63–69.
- Mantovani, A., Sozzani, S., Locati, M., Allavena, P., and Sica, A. (2002). Macrophage polarization: tumor-associated macrophages as a paradigm for polarized M2 mononuclear phagocytes. *Trends Immunol.* *23*, 549–555.
- Marino, S., Vooijs, M., van Der Gulden, H., Jonkers, J., and Berns, A. (2000). Induction of medulloblastomas in p53-null mutant mice by somatic inactivation of Rb in the external granular layer cells of the cerebellum. *Genes & Development* *14*, 994–1004.

Marshall, C.A.G. (2005). Olig2 Directs Astrocyte and Oligodendrocyte Formation in Postnatal Subventricular Zone Cells. *J Neurosci* 25, 7289–7298.

Matei, V., Pauley, S., Kaing, S., Rowitch, D., Beisel, K.W., Morris, K., Feng, F., Jones, K., Lee, J., and Fritsch, B. (2005). Smaller inner ear sensory epithelia in Neurog1 null mice are related to earlier hair cell cycle exit. *Dev. Dyn.* 234, 633–650.

Maxwell, F., Maxwell, I.H., and Glode, L.M. (1987). Cloning, sequence determination, and expression in transfected cells of the coding sequence for the tox 176 attenuated diphtheria toxin A chain. *Molecular and Cellular Biology* 7, 1576–1579.

McKnight, S.L. (1980). The nucleotide sequence and transcript map of the herpes simplex virus thymidine kinase gene. *Nucleic Acids Res* 8, 5949–5964.

Mellman, I., Coukos, G., and Dranoff, G. (2011). Cancer immunotherapy comes of age. *Nature* 480, 480–489.

Mesnil, M., and Yamasaki, H. (2000). Bystander effect in herpes simplex virus-thymidine kinase/ganciclovir cancer gene therapy: role of gap-junctional intercellular communication. *Cancer Research* 60, 3989–3999.

Mesnil, M., Piccoli, C., Tiraby, G., Willecke, K., and Yamasaki, H. (1996). Bystander killing of cancer cells by herpes simplex virus thymidine kinase gene is mediated by connexins. *Proceedings of the National Academy of Sciences* 93, 1831.

Mildner, A., Schmidt, H., Nitsche, M., Merkler, D., Hanisch, U.-K., Mack, M., Heikenwalder, M., Brück, W., Priller, J., and Prinz, M. (2007). Microglia in the adult brain arise from Ly-6ChiCCR2+ monocytes only under defined host conditions. *Nat Neurosci* 10, 1544–1553.

Mitamura, T., Umata, T., Nakano, F., Shishido, Y., Toyoda, T., Itai, A., Kimura, H., and Mekada, E. (1997). Structure-function analysis of the diphtheria toxin receptor toxin binding site by site-directed mutagenesis. *J. Biol. Chem.* 272, 27084–27090.

Miyata, T., Maeda, T., and Lee, J.E. (1999). NeuroD is required for differentiation of the granule cells in the cerebellum and hippocampus. *Genes & Development* 13, 1647–1652.

Morantz, R.A., Wood, G.W., Foster, M., Clark, M., and Gollahon, K. (1979). Macrophages in experimental and human brain tumors. Part 2: studies of the macrophage content of human brain tumors. *J Neurosurg* 50, 305–311.

- Naglich, J.G., Metherall, J.E., Russell, D.W., and Eidels, L. (1992). Expression cloning of a diphtheria toxin receptor: identity with a heparin-binding EGF-like growth factor precursor. *Cell* *69*, 1051–1061.
- Nedergaard, M., Ransom, B., and Goldman, S.A. (2003). New roles for astrocytes: Redefining the functional architecture of the brain. *Trends in Neurosciences* *26*, 523–530.
- Nimmerjahn, A., Kirchhoff, F., and Helmchen, F. (2005). Resting microglial cells are highly dynamic surveillants of brain parenchyma in vivo. *Science* *308*, 1314–1318.
- Northcott, P.A., Korshunov, A., Pfister, S.M., and Taylor, M.D. (2012). The clinical implications of medulloblastoma subgroups. *Nature Reviews Neurology* *8*, 340–351.
- Nowell, P.C. (1976). The clonal evolution of tumor cell populations. *Science* *194*, 23–28.
- Okano-Uchida T., Himi, T., Komiya, Y., and Ishizaki, Y. (2004). Cerebellar granule cell precursors can differentiate into astroglial cells. *Proc Natl Acad Sci USA* *101*, 1211–1216.
- Oliver, T.G., Read, T.A., Kessler, J.D., Mehmeti, A., Wells, J.F., Huynh, T.T.T., Lin, S.M., and Wechsler-Reya, R.J. (2005). Loss of patched and disruption of granule cell development in a pre-neoplastic stage of medulloblastoma. *Development* *132*, 2425–2439.
- Packer, R.J., and Vezina, G. (2008). Management of and prognosis with medulloblastoma: therapy at a crossroads. *Arch Neurol* *65*, 1419–1424.
- Pàez-Ribes, M., Allen, E., Hudock, J., Takeda, T., Okuyama, H., Viñals, F., Inoue, M., Bergers, G., Hanahan, D., and Casanovas, O. (2009). Antiangiogenic therapy elicits malignant progression of tumors to increased local invasion and distant metastasis. *Cancer Cell* *15*, 220–231.
- Palmiter, R.D., Behringer, R.R., Quaife, C.J., Maxwell, F., Maxwell, I.H., and Brinster, R.L. (1987). Cell lineage ablation in transgenic mice by cell-specific expression of a toxin gene. *Cell* *50*, 435–443.
- Pan, N., Jahan, I., Lee, J.E., and Fritsch, B. (2009). Defects in the cerebella of conditional Neurod1 null mice correlate with effective Tg(Atoh1-cre) recombination and granule cell requirements for Neurod1 for differentiation. *Cell Tissue Res* *337*, 407–428.

Pietras, K., and Östman, A. (2010). Hallmarks of cancer: Interactions with the tumor stroma. *Exp Cell Res* 316, 1324–1331.

Pietsch, T., Waha, A., Koch, A., Kraus, J., Albrecht, S., Tonn, J., Sörensen, N., Berthold, F., Henk, B., Schmandt, N., et al. (1997). Medulloblastomas of the desmoplastic variant carry mutations of the human homologue of *Drosophila* patched. *Cancer Research* 57, 2085–2088.

Plate, K.H., Breier, G., Weich, H.A., and Risau, W. (1992). Vascular endothelial growth factor is a potential tumour angiogenesis factor in human gliomas in vivo. *Nature* 359, 845–848.

Pollock, P.M., and Meltzer, P.S. (2002). A genome-based strategy uncovers frequent BRAF mutations in melanoma. *Cancer Cell* 2, 5–7.

Presta, L.G., Chen, H., O'Connor, S.J., Chisholm, V., Meng, Y.G., Krummen, L., Winkler, M., and Ferrara, N. (1997). Humanization of an anti-vascular endothelial growth factor monoclonal antibody for the therapy of solid tumors and other disorders. *Cancer Research* 57, 4593–4599.

Pugh, C.W., and Ratcliffe, P.J. (2003). Regulation of angiogenesis by hypoxia: role of the HIF system. *Nature Medicine* 9, 677–684.

Pugh, T.J., Weeraratne, S.D., Archer, T.C., Krummel, D.A.P., Auclair, D., Bochicchio, J., Carneiro, M.O., Carter, S.L., Cibulskis, K., Erlich, R.L., et al. (2012). Medulloblastoma exome sequencing uncovers subtype-specific somatic mutations. *Nature* 488, 106–110.

Pyonteck, S.M., Akkari, L., Schuhmacher, A.J., Bowman, R.L., Sevenich, L., Quail, D.F., Olson, O.C., Quick, M.L., Huse, J.T., Teijeiro, V., et al. (2013). CSF-1R inhibition alters macrophage polarization and blocks glioma progression. *Nature Medicine* 19, 1264–1272.

Quail, D.F., and Joyce, J.A. (2013). Microenvironmental regulation of tumor progression and metastasis. *Nature Medicine* 19, 1423–1437.

Ricci-Vitiani, L., Pallini, R., Biffoni, M., Todaro, M., Invernici, G., Cenci, T., Maira, G., Parati, E.A., Stassi, G., Larocca, L.M., et al. (2010). Tumour vascularization via endothelial differentiation of glioblastoma stem-like cells. *Nature* 468, 824–828.

Rigolin, G.M. (2006). Neoplastic circulating endothelial cells in multiple myeloma with 13q14 deletion. *Blood* 107, 2531–2535.

Robinson, G., Parker, M., Kranenburg, T.A., Lu, C., Chen, X., Ding, L., Phoenix, T.N., Hedlund, E., Wei, L., Zhu, X., et al. (2012). Novel mutations target distinct subgroups of medulloblastoma. *Nature* 488, 43–48.

Roggendorf, W., Strupp, S., and Paulus, W. (1996a). Distribution and characterization of microglia/macrophages in human brain tumors. *Acta Neuropathol* 92, 288–293.

Roggendorf, W., Strupp, S., and Paulus, W. (1996b). Distribution and characterization of microglia/macrophages in human brain tumors. *Acta Neuropathol* 92, 288–293.

Rossi, M.L., Buller, J.R., Heath, S.A., Carey, M.P., Carboni, P., Koutsoubelis, G., and Coakham, H.B. (1991). The monocyte/macrophage infiltrate in 35 medulloblastomas: a paraffin-wax study. *Tumori* 77, 36–40.

Roussel, M.F., and Hatten, M.E. (2011). Cerebellum development and medulloblastoma. *Curr. Top. Dev. Biol.* 94, 235–282.

Rowley, J.D. (1973). Letter: A new consistent chromosomal abnormality in chronic myelogenous leukaemia identified by quinacrine fluorescence and Giemsa staining. *Nature* 243, 290–293.

Rubsam, L.Z., Davidson, B.L., and Shewach, D.S. (1998). Superior cytotoxicity with ganciclovir compared with acyclovir and 1-beta-D-arabinofuranosylthymine in herpes simplex virus-thymidine kinase-expressing cells: a novel paradigm for cell killing. *Cancer Research* 58, 3873–3882.

Saito, M., Iwawaki, T., Taya, C., Yonekawa, H., Noda, M., Inui, Y., Mekada, E., Kimata, Y., Tsuru, A., and Kohno, K. (2001). Diphtheria toxin receptor-mediated conditional and targeted cell ablation in transgenic mice. *Nature Biotechnology* 19, 746–750.

Salsman, V.S., Chow, K.K.H., Shaffer, D.R., Kadikoy, H., Li, X.-N., Gerken, C., Perlaky, L., Metelitsa, L.S., Gao, X., Bhattacharjee, M., et al. (2011). Crosstalk between Medulloblastoma Cells and Endothelium Triggers a Strong Chemotactic Signal Recruiting T Lymphocytes to the Tumor Microenvironment. *PLoS ONE* 6, e20267.

Schüller, U., Heine, V.M., Mao, J., Kho, A.T., Dillon, A.K., Han, Y.-G., Huillard, E., Sun, T., Ligon, A.H., Qian, Y., et al. (2008). Acquisition of granule neuron precursor identity is a critical determinant of progenitor cell competence to form Shh-induced medulloblastoma. *Cancer Cell* 14, 123–134.

Shekouh, A.R., Thompson, C.C., Prime, W., Campbell, F., Hamlett, J., Herrington, C.S., Lemoine, N.R., Crnogorac-Jurcevic, T., Buechler, M.W., Friess, H., et al. (2003). Application of laser capture microdissection combined with two-dimensional electrophoresis for the discovery of differentially regulated proteins in pancreatic ductal adenocarcinoma. *Proteomics* 3, 1988–2001.

Shen, R., Ye, Y., Chen, L., Yan, Q., Barsky, S.H., and Gao, J.-X. (2008). Precancerous Stem Cells Can Serve As Tumor Vasculogenic Progenitors. *PLoS ONE* 3, e1652.

Shweiki, D., Itin, A., Soffer, D., and Keshet, E. (1992). Vascular endothelial growth factor induced by hypoxia may mediate hypoxia-initiated angiogenesis. *Nature* 359, 843–845.

Sica, A., Allavena, P., and Mantovani, A. (2008). Cancer related inflammation: The macrophage connection. *Cancer Lett* 267, 204–215.

Silbereis, J.J., Heintz, T.T., Taylor, M.M.M., Ganat, Y.Y., Ment, L.R.L., Bordey, A.A., and Vaccarino, F.F. (2010). Astroglial cells in the external granular layer are precursors of cerebellar granule neurons in neonates. *Molecular and Cellular Neuroscience* 44, 12–12.

Sims, D.E. (1986). The pericyte--a review. *Tissue Cell* 18, 153–174.

Sitek, B., Sipos, B., Alkatout, I., Poschmann, G., Stephan, C., Schulenburg, T., Marcus, K., Lüttges, J., Dittert, D.-D., Baretton, G., et al. (2009). Analysis of the Pancreatic Tumor Progression by a Quantitative Proteomic Approach and Immunohistochemical Validation. *J. Proteome Res.* 8, 1647–1656.

Soda, Y., Marumoto, T., Friedmann-Morvinski, D., Soda, M., Liu, F., Michiue, H., Pastorino, S., Yang, M., Hoffman, R.M., and Kesari, S. (2011). Transdifferentiation of glioblastoma cells into vascular endothelial cells. *Proc Natl Acad Sci USA* 108, 4274–4280.

Sofroniew, M.V., and Vinters, H.V. (2010). Astrocytes: biology and pathology. *Acta Neuropathol* 119, 7–35.

Song, H.H., Stevens, C.F.C., and Gage, F.H.F. (2002). Astroglia induce neurogenesis from adult neural stem cells. *Nature* 417, 39–44.

Stone, J., Itin, A., Alon, T., Pe'er, J., Gnessin, H., Chan-Ling, T., and Keshet, E. (1995). Development of retinal vasculature is mediated by hypoxia-induced vascular endothelial growth factor (VEGF) expression by neuroglia. *J. Neurosci.* 15, 4738–4747.

Storm, R., Cholewa-Waclaw, J., Reuter, K., Bröhl, D., Sieber, M., Treier, M., Müller, T., and Birchmeier, C. (2009). The bHLH transcription factor Olig3 marks the dorsal neuroepithelium of the hindbrain and is essential for the development of brainstem nuclei. *Development* *136*, 295–305.

Straussman, R., Morikawa, T., Shee, K., Barzily-Rokni, M., Qian, Z.R., Du, J., Davis, A., Mongare, M.M., Gould, J., Frederick, D.T., et al. (2013). Tumour micro-environment elicits innate resistance to RAF inhibitors through HGF secretion. *Nature* *487*, 500–504.

Streubel, B., Chott, A., Huber, D., Exner, M., Jäger, U., Wagner, O., and Schwarzingler, I. (2004). Lymphoma-specific genetic aberrations in microvascular endothelial cells in B-cell lymphomas. *New England Journal of Medicine* *351*, 250–259.

Su, W.-C., Su, W.-P., Cheng, Shieh, and Yeh (2012). PLGA nanoparticles codeliver paclitaxel and Stat3 siRNA to overcome cellular resistance in lung cancer cells. *Ijn* 4269.

Swann, J.B., and Smyth, M.J. (2007). Immune surveillance of tumors. *J Clin Invest* *117*, 1137–1146.

Takano, T., Tian, G.-F., Peng, W., Lou, N., Libionka, W., Han, X., and Nedergaard, M. (2005). Astrocyte-mediated control of cerebral blood flow. *Nat Neurosci* *9*, 260–267.

Taylor, M.D., Liu, L., Raffel, C., Hui, C.-C., Mainprize, T.G., Zhang, X.Y., Agatep, R., Chiappa, S., Gao, L.Z., Lowrance, A., et al. (2002). Mutations in SUFU predispose to medulloblastoma. *Nat Genet* *31*, 306–310.

Tsai, H.H., Li, H., Fuentealba, L.C., Molofsky, A.V., Taveira-Marques, R., Zhuang, H., Tenney, A., Murnen, A.T., Fancy, S.P.J., Merkle, F., et al. (2012). Regional Astrocyte Allocation Regulates CNS Synaptogenesis and Repair. *Science* *337*, 358–362.

Tumbar, T., Guasch, G., Greco, V., Blanpain, C., Lowry, W.E., Rendl, M., and Fuchs, E. (2004). Defining the epithelial stem cell niche in skin. *Science* *303*, 359–363.

Uziel, T., Zindy, F., Xie, S., Lee, Y., Forget, A., Magdaleno, S., Rehg, J.E., Calabrese, C., Solecki, D., Eberhart, C.G., et al. (2005). The tumor suppressors Ink4c and p53 collaborate independently with Patched to suppress medulloblastoma formation. *Genes & Development* *19*, 2656–2667.

Wang, J., Lin, W., Popko, B., and Campbell, I.L. (2004). Inducible production of interferon- γ in the developing brain causes cerebellar dysplasia with activation of the Sonic hedgehog pathway. *Molecular and Cellular Neuroscience* 27, 489–496.

Wang, V.Y., Rose, M.F., and Zoghbi, H.Y. (2005). Math1 Expression Redefines the Rhombic Lip Derivatives and Reveals Novel Lineages within the Brainstem and Cerebellum. *Neuron* 48, 31–43.

Wechsler-Reya, R.J., and Scott, M.P. (1999). Control of neuronal precursor proliferation in the cerebellum by Sonic Hedgehog. *Neuron* 22, 103–114.

Wetmore, C., Eberhart, D.E., and Curran, T. (2001). Loss of p53 but not ARF accelerates medulloblastoma in mice heterozygous for patched. *Cancer Research* 61, 513–516.

Willett, C.G., Boucher, Y., di Tomaso, E., Duda, D.G., Munn, L.L., Tong, R.T., Chung, D.C., Sahani, D.V., Kalva, S.P., Kozin, S.V., et al. (2004). Direct evidence that the VEGF-specific antibody bevacizumab has antivascular effects in human rectal cancer. *Nature Medicine* 10, 145–147.

Wilson, C.W., and Chuang, P.T. (2010). Mechanism and evolution of cytosolic Hedgehog signal transduction. *Development* 137, 2079–2094.

Wright, J.H. (1910). Neurocytoma or neuroblastoma, a kind of tumor not generally recognized. *J Exp Med* 12, 556–561.

Xie, J., Murone, M., Luoh, S.-M., Ryan, A., Gu, Q., Zhang, C., Bonifas, J.M., Lam, C.-W., Hynes, M., and Goddard, A. (1998). Activating Smoothed mutations in sporadic basal-cell carcinoma. *Nature* 391, 90–92.

Yamaizumi, M., Mekada, E., Uchida, T., and Okada, Y. (1978). One molecule of diphtheria toxin fragment A introduced into a cell can kill the cell. *Cell* 15, 245–250.

Yang, Z.-J., Ellis, T., Markant, S.L., Read, T.-A., Kessler, J.D., Bourbonoulas, M., Schüller, U., Machold, R., Fishell, G., Rowitch, D.H., et al. (2008). Medulloblastoma Can Be Initiated by Deletion of Patched in Lineage-Restricted Progenitors or Stem Cells. *Cancer Cell* 14, 11–11.

Yeh, J.E., Toniolo, P.A., and Frank, D.A. (2013). Targeting transcription factors. *Current Opinion in Oncology* 25, 652–658.

Yin, D., Li, Y., Lin, H., Guo, B., Du, Y., Li, X., Jia, H., Zhao, X., Tang, J., and Zhang, L. (2013). Functional graphene oxide as a plasmid-based Stat3 siRNA carrier inhibits mouse malignant melanoma growth in vivo. *Nanotechnology* 24, 105102.

- Yue, T. (2006). A Critical Role for Dorsal Progenitors in Cortical Myelination. *J Neurosci* *26*, 1275–1280.
- Zamanian, J.L., Xu, L., Foo, L.C., Nouri, N., Zhou, L., Giffard, R.G., and Barres, B.A. (2012). Genomic Analysis of Reactive Astroglia. *J Neurosci* *32*, 6391–6410.
- Zhao, H., Desai, V., Wang, J., Epstein, D.M., Miglarese, M., and Buck, E. (2012). Epithelial-Mesenchymal Transition Predicts Sensitivity to the Dual IGF-1R/IR Inhibitor OSI-906 in Hepatocellular Carcinoma Cell Lines. *Molecular Cancer Therapeutics* *11*, 503–513.
- Zhukov, T.A., Johanson, R.A., Cantor, A.B., Clark, R.A., and Tockman, M.S. (2003). Discovery of distinct protein profiles specific for lung tumors and pre-malignant lung lesions by SELDI mass spectrometry. *Lung Cancer* *40*, 267–279.
- Zhukova, N., Ramaswamy, V., Remke, M., Pfaff, E., Shih, D.J.H., Martin, D.C., Castelo-Branco, P., Baskin, B., Ray, P.N., Bouffet, E., et al. (2013). Subgroup-Specific Prognostic Implications of TP53 Mutation in Medulloblastoma. *J Clin Oncol* *31*, 2927–2935.
- Zong, H., Espinosa, S., Su, H.H., Muzumdar, M.D., and Luo, L.Q. (2005). Mosaic analysis with double markers in mice. *Cell* *121*, 479–492.
- Zuniga, R.M., Torcuator, R., Jain, R., Anderson, J., Doyle, T., Schultz, L., and Mikkelsen, T. (2010). Rebound tumour progression after the cessation of bevacizumab therapy in patients with recurrent high-grade glioma. *J Neurooncol* *99*, 237–242.